THE ROLE OF IRON AS A MICRONUTRIENT IN THE ANTARCTIC SEA ICE ENVIRONMENT

By

Pier van der Merwe, BSc (Hons)

Submitted in fulfilment of the

requirements for the Degree of

Doctor of Philosophy

University of Tasmania November, 2010

DECLARATION OF ORIGINALITY

This thesis contains no material which has been accepted for a degree or diploma by the University or any other institution, except by way of background information and duly acknowledged in the thesis, and to the best of the candidate's knowledge and belief no material previously published or written by another person except where due acknowledgement is made in the text of the thesis, nor does the thesis contain any material that infringes copyright.

Pier van der Merwe November 2010

STATEMENT OF AUTHORITY OF ACCESS

The publishers of the papers comprising Chapters 3 and 4 hold the copyright for that content, and access to the material should be sought from the respective journals. The remaining non published content of the thesis may be made available for loan and limited copying in accordance with the Copyright Act 1968

Pier van der Merwe November 2010

THESIS ABSTRACT

It is now understood that the Southern Ocean is a high-nutrient, low-chlorophyll zone; production being limited by the micronutrient iron (Fe). The seasonal formation and subsequent melt of Antarctic sea ice covers an area of approximately 17 million km^2, an area roughly twice the size of the Australian continent. Sea ice has the ability to store Fe at concentrations two orders of magnitude higher than in the underlying water column. Its formation can negatively influence the concentration of dissolved Fe in surface waters surrounding the continent by entrainment within the sea ice. However, during its melt, it can release this stored reserve of Fe into the underlying water column at a time that is coincidentally ideal for algal growth. During the winter, light-limited conditions prevail, however, during spring and into summer, stratification of the water column due to increased meltwater and shallowing of the mixed layer, combine with increased solar radiation, seeding of the water column with sea ice algae and the release of Fe. The result is large algal blooms that may significantly affect the regional carbon cycle with possible flow-on effects to global climate. However, considerable variability in the estimates of the size and relative contribution of these ice edge blooms exists.

Fe can be sourced to Southern Ocean surface waters from sediment resuspension, aeolian dust deposition, hydrothermal plume waters or from extraterrestrial dust. However, there is growing evidence that sea-ice-entrained Fe may be one of the most bioavailable due to abundant organic complexation coupled with photo-oxidation either *in situ* or upon release into strongly-stratified melt waters. This work adds significantly to our understanding of the distribution and concentration of Fe in Antarctic sea ice; and is coupled with measurements of physical and biogeochemical variables. It is based on two independent research voyages into the Antarctic sea ice environment including one spatial study during the transition from winter to early spring, sampling pack and fast ice (SIPEX, Sept-Oct 2007) and one temporal study in fast ice off the

coast of East Antarctica (Oct-Dec 2009). Before this thesis less than a handful of studies had sampled Antarctic sea ice in dedicated studies. In an area of 17 million km^2 with characteristically high heterogeneity, this makes for an extremely patchy data set requiring more validation.

Aside from adding to the global data set for Antarctic sea ice, brines, underlying sea water and snow, with measurements of dissolved, particulate and total dissolvable Fe, salinity, temperature, Chlorophyll *a* (Chl *a*), ice texture, stable oxygen isotope, exopolysaccharides, particulate and dissolved organic carbon and nitrogen and macronutrient variables, the main findings of this work are: 1) Validation that sea ice can concentrate Fe up to two orders of magnitude higher than in the underlying water column. 2) Exopolysaccharides are not directly correlated with proportional concentrations of Fe within sea ice however they can be with Chl *a* and particulate organic carbon. 3) Apparent dissolved Fe (dFe × brine volume fraction) and estimates of cellular carbon to Fe ratios suggest that during SIPEX, the sea ice microbial biota were not limited by dissolved Fe but rather may have been by nitrogen (NO_2+NO_3) or silicate ($Si(OH)_4$). 4) Conversely, under-ice seawater algal communities may have been limited by dissolved Fe and/or light and grazing by zooplankton during SIPEX. 5) A significant inverse correlation between dissolved Fe and Chl *a* in the basal layers of pack ice, most likely indicates the active drawdown of dissolved Fe by the sea ice biota, combined with some fraction lost to the water column or converted to the particulate fraction. 6) During SIPEX, a markedly higher concentration of particulate Fe was observed at our fast ice site (0.96 – 214 $nmol.L^{-1}$) relative to several pack ice sites (0.87 – 77.7 $nmol.L^{-1}$) and comparison of particulate leachable Fe (plFe) with particulate Fe (pFe) indicated the highly refractory nature and therefore most likely sedimentary origin of this enrichment. 7) A high particulate-to-dissolved Fe ratio was observed at the fast ice site during SIPEX (285:1) relative to the highest observed in pack ice (23:1). This suggests a decoupling between the sources and/or sinks of the dissolved and particulate

fractions, which is closely linked to the proximity of the continent and a release of shelf-derived pFe. 8) Preferential release of dissolved Fe (and not particulate Fe) into brines at all sites sampled with the sack-hole method (and therefore indicative of brine drainage), indicates the diffuse nature of the dissolved fraction. Furthermore, this indicates that there may be a temporal decoupling between the release of the dissolved and particulate fractions into the water column as sea ice becomes more permeable during the seasonal melt. 9) During a temporal study of fast ice off the coast of East Antarctica, we observed in high temporal resolution the release of each of the size fractions of Fe into the underlying water column. This information coupled with high-quality meteorological data gives valuable insight into the processes involved in the seasonal melt of sea ice and its release of Fe.

ACKNOWLEDGEMENTS

This thesis is based on two field studies in Antarctica and as such would not have been possible without the help and support of numerous Australian Antarctic Division staff. I gratefully acknowledge the officers and crew of R.S.V. Aurora Australis, as well as colleagues and support personnel involved in the SIPEX and Casey time series expeditions.

Thank you to my three supervisors, Dr Andrew Bowie, Dr Klaus Meiners and Dr. Carol Mancuso-Nichols for their untiring support and enthusiasm throughout this project. Thank you to Dr Delphine Lannuzel for your help and mentoring in every aspect of this project, including shivering on the ice for hours on end!

I would like to thank Dr Ashley Townsend for his invaluable mentoring and support with the ICP-MS analyses. I would like to thank Dr Tony Worby for his support and training during SIPEX. I am indebted to the Commonwealth Scientific and Industrial Research Organization, Marine Research division for providing a clean container for iron concentration enumeration during SIPEX. I am greatly indebted to Dr Christopher Krembs for providing valuable insight during the method development stage of chapter 3. To Dianna Davis for her training in processing the POC samples. Thank you to all the staff and students at IASOS and then IMAS for providing a fantastic work environment and support.

This work was sponsored by an Australian Antarctic Science project (#3026) and through a scholarship top-up from the Antarctic Climate and Ecosystems Cooperative Research Centre. Further acknowledgement for work carried out by other researchers that has been included in this thesis is listed in the acknowledgements section after each chapter.

PUBLICATIONS RESULTING FROM RESEARCH COMPLETED DURING CANDIDATURE

van der Merwe, P., Lannuzel, D., Mancuso Nichols, C., Meiners, K., Heil, P., Norman, L., Thomas, D.N. and Bowie, A., 2009. Biogeochemical observations during the winter-spring transition in East Antarctic sea ice: evidence of iron and exopolysaccharide controls. Marine Chemistry, 115, 163-175.

van der Merwe, P., Lannuzel, D., Bowie, A., Mancuso Nichols, C. and Meiners, K., In Press. Iron fractionation in pack and fast ice in East Antarctica: temporal decoupling between the release of dissolved and particulate iron during spring melt. Deep-Sea Research Part II Oceanographic Research Papers.

van der Merwe, P., Lannuzel, D., Bowie, A., Meiners, K., Submitted. High temporal resolution observations of spring fast-ice melt and seawater iron enrichment in East Antarctica. JGR-Biogeosciences

Bowie, A., Townsend, A. T., Lannuzel, D., Remenyi, T., & **van der Merwe, P.** (2010). Modern sampling and analytical methods for the determination of trace elements in marine particulate material using magnetic sector ICP-MS. Analytica Chimica Acta, 676(1-2), 15-27.

Lannuzel, D., Schoemann, V., de Jong, J., Pasquer, B., Masson, F., **van der Merwe, P.,** et al. (2010). What controls the distribution of dissolved iron in Antarctic sea ice: spatial, seasonal or inter-annual variability? Journal of Geophysical Research-Biogeosciences, 115(3), G03022.

Lannuzel, D., Bowie, A., van der Merwe, P., Townsend, A. T., & Schoemann, V. (accepted). Distribution of dissolved and particulate metals in Antarctic sea ice. Marine Chemistry.

Nicol, S., Bowie, A., Jarman, S., Lannuzel, D., Meiners, K. and **van der Merwe, P**., 2010. Southern Ocean iron fertilization by baleen whales and Antarctic krill. Fish and Fisheries (Oxford), 11 (2), 203-209

Norman, L., Thomas, D.N., Stedmon, C.A., Granskog, M.A., Papadimitriou, S., Krapp, R.H., Meiners, K., Lannuzel, D., **van der Merwe, P**. and Dieckmann, G., In Press. The characteristics of dissolved organic matter (DOM) and chromophoric dissolved organic matter (CDOM) in Antarctic sea ice. Deep-Sea Research Part II Oceanographic Research Papers.

Aslam S.N., Norman, L., **van der Merwe, P.,** Meiners, K., Thomas, D.N., Underwood, G.J.C. Submitted, Characterisation of exopolymeric substances (EPS) from East Antarctic sea ice during winter–spring transition, Marine Chemistry.

STATEMENT OF CO-AUTHORSHIP

The following people and institutions contributed to the publication of the work undertaken as part of this thesis:

1/ van der Merwe, P., Lannuzel, D., Mancuso Nichols, C., Meiners, K., Heil, P., Norman, L., Thomas, D.N. and Bowie, A., 2009. Biogeochemical observations during the winter-spring transition in East Antarctic sea ice: evidence of iron and exopolysaccharide controls. Marine Chemistry, 115, 163-175.

van der Merwe, P., 70% *Lannuzel, D. 11%, Mancuso Nichols, C. 5%, Meiners, K. 4%, Heil, P. 1%, Norman, L. 1%, Thomas, D.N. 1% and Bowie A. 7%,*

2/ van der Merwe, P., Lannuzel, D., Bowie, A., Mancuso Nichols, C. and Meiners, K., In Press. Iron fractionation in pack and fast ice in East Antarctica: temporal decoupling between the release of dissolved and particulate iron during spring melt. Deep-Sea Research Part II Oceanographic Research Papers.

van der Merwe, P. 80%, *Lannuzel, D. 10%, Bowie, A. 7.5%, Mancuso Nichols, C 0.5%. and Meiners, K. 2%.*

3/ van der Merwe, P., Lannuzel, D., Bowie, A., Meiners, K., Submitted. High temporal resolution observations of spring fast-ice melt and seawater iron enrichment in East Antarctica. JGR- Biogeosciences

van der Merwe, P. 80%, *Lannuzel, D. 10%, Bowie, A. 7.5%, Meiners, K. 2.5%,*

First author papers contributions

Author van der Merwe, P. designed and implemented the experiment, collected, processed and analysed the samples for dFe, TDFe, PSA EPS, AB EPS, Chl *a*, salinity, temperature, brine volume fraction and ice texture. van der Merwe, P. also collected and processed ready for analysis, macro nutrient, DOC, POC, oxygen isotope. All data analysis, statistics and manuscript writing by van der Merwe, P.

Author Lannuzel, D. aided in experiment design, collection, processing and analytical analysis of samples as well as manuscript drafting.

Author Bowie, A. aided in experimental design, analytical analysis, proposal funding and manuscript drafting.

Author Meiners, K. aided in experimental design, analytical analysis and manuscript drafting.

Author Mancuso Nichols, C. aided in experimental design, analytical analysis and manuscript drafting.

Author Heil, P. aided in analytical analysis of oxygen isotope samples and manuscript drafting.

Author Norman, L. aided in analytical analysis of macro-nutrient samples and manuscript drafting.

Author Thomas, D.N. aided in manuscript drafting.

Co-Authored papers contributions

4/ Bowie, A., Townsend, A. T., Lannuzel, D., Remenyi, T., & van der Merwe, P. (2010). Modern sampling and analytical methods for the determination of trace elements in marine particulate material using magnetic sector ICP-MS. Analytica Chimica Acta, 676(1-2), 15-27.

van der Merwe, P*., 8 % Aiding in the method development of the particulate digestion and the CRM recovery experiment design, digestion, measurement and analysis as well as manuscript drafting.*

5/ Lannuzel, D., Schoemann, V., de Jong, J., Pasquer, B., Masson, F., **van der Merwe, P.**, Tison, J.L. and Bowie, A., Accepted. What controls the distribution of dissolved iron in Antarctic sea ice: spatial, seasonal or inter-annual variability? Journal of Geophysical Research-Biogeosciences.

***van der Merwe, P**., 8 % Sea ice core collection, processing, Chl a, POC and dFe analysis on the FIA for the SIPEX data set and manuscript drafting.*

6/ Lannuzel, D., Bowie, A., van der Merwe, P., Townsend, A. T., & Schoemann, V. (accepted). Distribution of dissolved and particulate metals in Antarctic sea ice. Marine Chemistry.

***van der Merwe, P**., 10 % Sea ice core collection, processing, Chl a, POC and dFe analysis on the FIA for the SIPEX data set and manuscript drafting.*

7/ Nicol, S., Bowie, A., Jarman, S., Lannuzel, D., Meiners, K. and **van der Merwe, P**., 2010. Southern Ocean iron fertilization by baleen whales and Antarctic krill. Fish and Fisheries (Oxford), 11 (2), 203-209

***van der Merwe, P**., 5 % Sample digestion, preparation and measurement on the ICP-MS as well as manuscript drafting.*

8/ Norman, L., Thomas, D.N., Stedmon, C.A., Granskog, M.A., Papadimitriou, S., Krapp, R.H., Meiners, K., Lannuzel, D., **van der Merwe, P**. and Dieckmann, G., In Press. The characteristics of dissolved organic matter (DOM) and chromophoric dissolved organic matter (CDOM) in Antarctic sea ice. Deep-Sea Research Part II Oceanographic Research Papers.

***van der Merwe, P**., 5 % Sea ice core collection, processing, Chl a, POC, Salinity, temperature, brine volume fraction analysis for the SIPEX "Fe site" data set and manuscript drafting.*

9/ Aslam S.N., Norman, L., **van der Merwe, P.,** Meiners, K., Thomas, D.N., Underwood, G.J.C. Submitted, Characterisation of exopolymeric substances (EPS) from East Antarctic sea ice during winter–spring transition, Marine Chemistry.

***van der Merwe, P**., 5 % Sea ice core collection, processing, Chl a, POC, Salinity, temperature, brine volume fraction analysis for the SIPEX "Fe site" data set and manuscript drafting.*

We the undersigned agree with the above stated "proportion of work undertaken" for each of the above published (or submitted) peer-reviewed manuscripts contributing to this thesis:

Signed: _____ _____

Andrew Bowie
Supervisor
Antarctic Climate & Ecosystems
Cooperative Research Centre
University of Tasmania

Date:_____

Michael Stoddart
Director
Institute for Marine and
Antarctic Studies
University of Tasmania

Date:_____

1. Introduction

Although the Southern Ocean represents only 10% of the world's oceans, it is responsible for sequestering 25% of atmospheric CO_2 (Takahashi et al., 2002). This is primarily through the physical process of CO_2 dissolving into cold Antarctic water which is downwelled via the solubility pump but also through biological uptake of aqueous CO_2 through photosynthesis and the sinking out of a small but significant fraction of the particulate organic carbon to the sea floor via the biological pump (Fig 1.1).

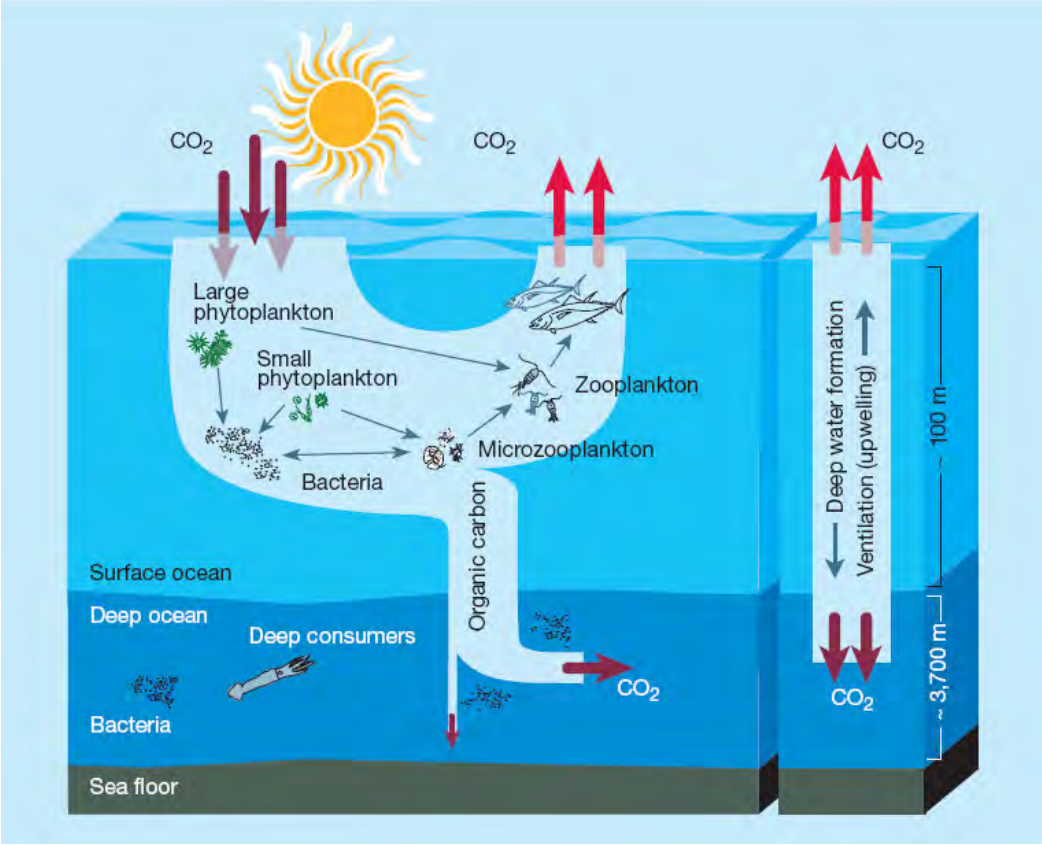

Figure 1.1: Schematic representation of the biological pump (left) and the solubility pump (right). Image source (Chisholm, 2000).

It is now well established via direct measurements (de Baar et al., 1995), bottle enrichment experiments (Martin et al., 1990a), mesoscale enrichment experiments (Bowie et al., 2001; Boyd

et al., 2000) and modelling studies (Tagliabue et al., 2009a), that the Southern ocean is a high nutrient, low chlorophyll region and that the major limiting nutrient is iron (Fe). Fe is an essential element of all known living organisms and is used by phytoplankton in photosynthetic and respiratory electron transport chains among other metabolic uses (Sunda, 2001).

1.1. Role of sea ice in regulating the Earth's Climate

Approximately 17×10^6 km^2 of the Southern Ocean is covered by seasonal sea ice and its formation and subsequent melt is one of the largest seasonal events on Earth (Lowe, 1997) (Fig 1.2). While sea ice chemistry is commonly indicative of the seawater from which it formed (Eicken, 2003), its capacity to concentrate trace metals such as Fe up to two orders of magnitude higher than in the under lying sea water (Grotti et al., 2005; Lannuzel et al., 2008; Lannuzel et al., 2007), makes it a significant temporal storage of this important micronutrient element. The annual melt of sea ice releases this reservoir into the surrounding water column (Lannuzel et al., 2008; Sedwick & Ditullio, 1997). When the released Fe is coupled with the release of ice algae and stratification of the water column (Tagliabue & Arrigo, 2006), vast phytoplankton blooms are triggered (Fitzwater et al., 2000), which are observable by satellite. These large blooms substantially impact the local carbon cycle and the radiative properties of the atmosphere through DMS production (Arrigo et al., 2008b; Boyd, 2007; Legendre et al., 1992) and therefore potentially play a significant role in global climate.

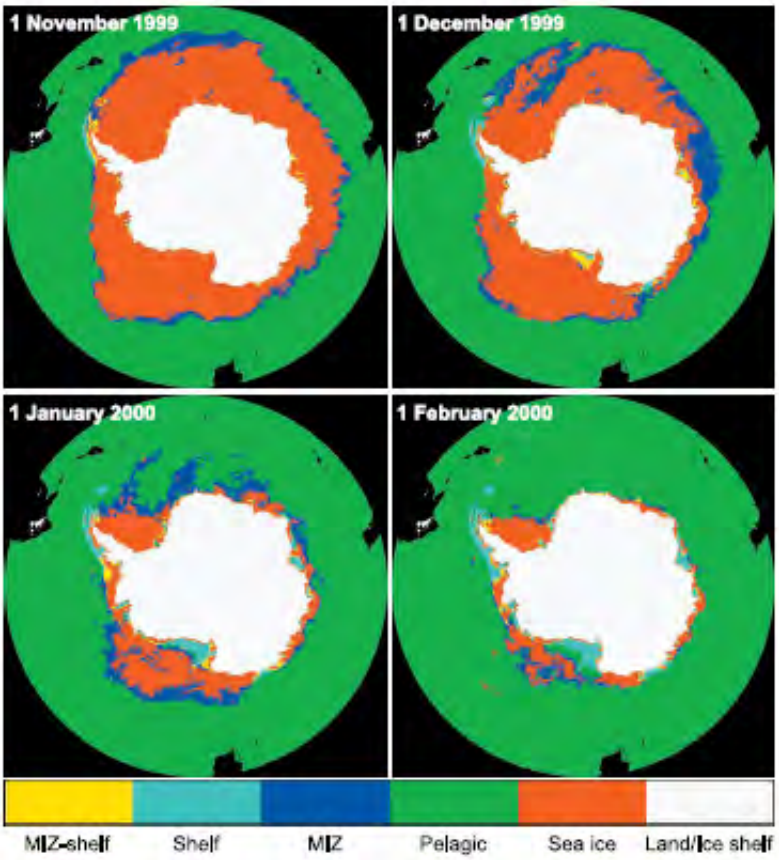

Figure 1.2: Map showing the generalised ecological provinces around Antarctica. Note the distribution of the Marginal Ice Zone (MIZ) at varying stages of sea ice melt. Source: (Arrigo et al., 2008b).

1.2. Background to sea ice Fe measurements

The study of Fe in marine systems requires some operationally defined size fractions to allow meaningful comment. These have somewhat arbitrarily been adopted over the years and now some level of continuity between studies can be expected. Dissolved Fe (dFe) is generally all Fe that passes through a 0.2 or 0.4 µm filter and includes small colloids as well as the smaller soluble fraction. Conversely, particulate Fe (pFe) is all Fe that remains on a 0.2 or 0.4 µm filter and can include large particles of biological or lithogenic origin and a range of colloids. Total dissolvable Fe is generally a sub-sample of unprocessed sample which is acidified to pH 1.8 and

stored for at least 6 months. Therefore, TDFe includes all easily exchangeable fractions but not the highly refractory lithogenic fraction. Particulate leachable Fe (plFe) is the difference between TDFe and dFe and is therefore all non-lithogenic particles. Soluble Fe is regarded as the truly dissolved Fe fraction below 0.02 μm in size and is not widely used in sea ice research due to technical difficulties associated with the small pore size in samples with high organic loading. It is through these operationally defined size fractions that comparisons can be drawn between independent research.

Work by El-Sayed and Taguchi (1981) as well as Smith and Nelson (1985) identified dense phytoplankton blooms that occur in conjunction with the receding ice edge (Fig 1.3). Smith and Nelson (1985) noted the unusually high biogenic silica to carbon ratio of these blooms indicating dominance by diatoms. In these early studies, regulation of the blooms was attributed to several factors including, the increased freshening and therefore stratification of the water column leading to a shallower mixed layer, grazing control, macronutrient drawdown, seeding of the water column with sea ice algae and proximity to land masses (a somewhat indirect link to nutrient supply). It was not until the seminal work of Martin (1990) that the role of the micronutrient Fe was brought into the limelight and the paradox of apparent underutilisation of the major macronutrients in areas such as the Southern Ocean could begin to be resolved.

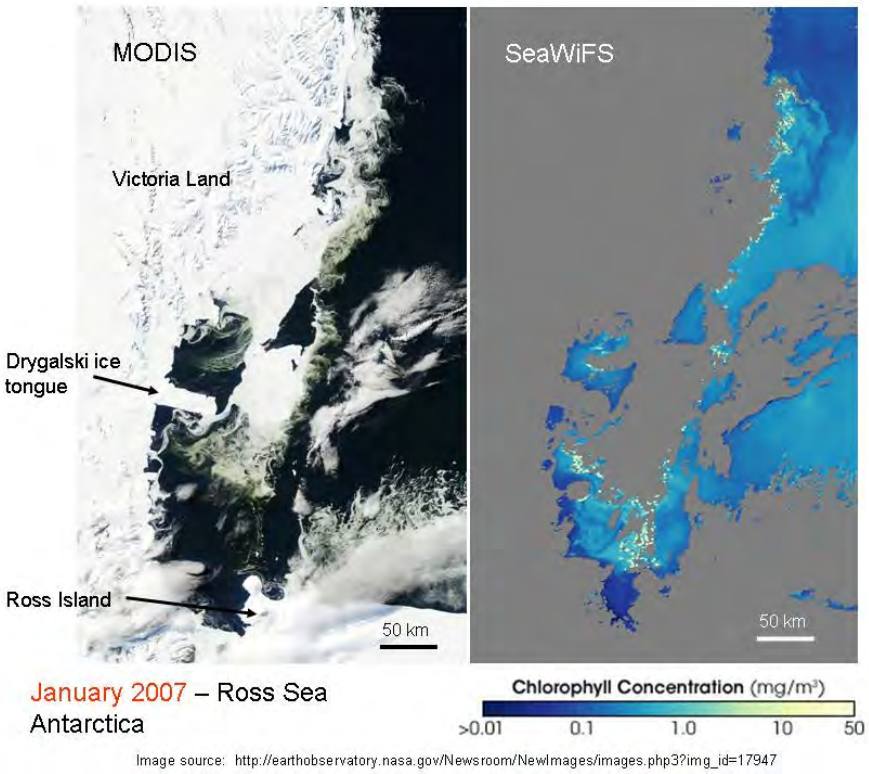

Figure 1.3. MODIS and SeaWiFS ocean colour satellite images that show phytoplankton blooms associated with the receding sea ice edge during January in the Ross Sea, Antarctica.

With this new understanding came new insight and research started to focus on the sources of Fe to the Southern Ocean including the role of sea ice in delivering Fe to the surface waters during the annual sea ice melt. Martin et al (1990) noted that one of the important sources of Fe to surface waters around Antarctica must be sea ice. One of the first research papers to publish data on a seasonal water column enrichment in the central Ross sea and attribute this to sea ice melting was Sedwick and Ditullio (1997), however they could only surmise that sea ice was the source as they did not directly measure sea ice. Regardless, their data showed that surface waters in the proximity of melting sea ice resulted in elevated dissolved and total dissolvable Fe concentrations relative to surface waters removed from melting sea ice. In the 17 days between their initial measurement and their subsequent visit, they observed a decrease in Fe back to

typical, sub-nM, limiting dissolved Fe concentrations. Although they noted horizontal advection and vertical mixing could also be responsible for the observed deficit, they concluded that a combination of vertical mixing and biological activity, including particle scavenging, was responsible for the drawdown of Fe, nitrate + nitrite, phosphate and silicate. Bottle incubation experiments verified the Fe limited state of the primarily diatom dominated phytoplankton assemblage. Fitzwater et al (2000) also observed blooming phytoplankton, particularly diatoms, in the presence of elevated total Fe (dissolved and particulate) concentrations in the Ross Sea in the austral summer of 1990. By looking at Fe:Al (aluminium) and Al:Mn (manganese) ratios and comparing these with known crustal elemental ratios, they attributed the source of the Fe to be from both directly resuspended sediments and sediments incorporated into sea ice and subsequently released into the surface layer upon melting. At this stage there were many questions about the sources of Fe to sea ice, with another theory suggesting that one of the primary sources could have been aeolian dust incorporated into the sea ice throughout the winter growth season and then released upon melting (Martin et al., 1991). However, uncertainty exists over the importance of this source for the majority of Antarctic sea ice due primarily to the distance from ice free land masses and therefore the extremely low reported Fe-dust fluxes.

1.3. Full sea ice Fe profiling studies and major findings

Martin et al (1990b) measured a fragment of floating sea ice and was followed several years later by two similar repeat measurements (Boye et al. 2001, de Baar and de Jong 2001) to prove that sea ice contained significant quantities of Fe relative to surface sea water. However, since then, there exist only a few research papers that have directly measured the concentration of Fe in Antarctic sea ice by removing cores *in situ*. These comprise of two papers by Grotti et al (2001, 2005) in Terra Nova Bay in the Western Ross Sea and 3 papers by Lannuzel et al (2007, 2008, 2009) and more detailed studies of iron speciation in Antarctic sea ice by our group are

presented in chapters 3, 4 and 5 and have been published in 2009 and 2010. Together this work represents only five field studies. Technically, of the two Grotti et al papers, only the 2005 paper presents a full data set on sea ice trace metals as the 2001 paper was focused on the underlying water column, with only one sea ice core analysed. Their study was inspired by the findings of several of the papers already mentioned, including (Fitzwater et al., 2000; Martin et al., 1990a; Sedwick & Ditullio, 1997; Sedwick et al., 2000) which either observed or proposed Fe enrichment within the water column from melting sea ice.

During a research study at a near shore station inside the Gerlache Inlet (Terra Nova Bay, Western Ross Sea), Grotti et al. (2001) sampled the water column for various biogeochemical parameters over the course of 100 days from 13th Nov until the 21st of Feb. Although Grotti et al. (2001, 2005) believed that they were sampling pack ice, a recent study using composite MODIS satellite images revealed that between Cook Ice Shelf to Cape Adare (152˚ E to 172˚ E) there is an approximately 50 km wide strip of reoccurring fast ice located parallel to the coast (A. Fraser pers. comm.). Grotti et al. (2001) were one of the first to document a full sea ice Fe profile and noted basal ice particulate Fe concentrations of more than 7 μmol L^{-1} on the single core collected during this study. Furthermore, they also attributed the observed sea water enrichment to melting sea ice, and noted that the maximum dissolved and particulate sea water Fe fraction occurred independently, indicating temporally distinct processes involved with the release of these different phases from melting sea ice.

The work of Grotti et al. (2001) during Austral spring 1997/1998 inspired the researchers to return to sample the coastal land fast ice in a dedicated study during the austral summer of 2000/2001 (Grotti et al., 2005). Grotti et al. (2005) was the first dedicated study of coastal fast ice for Fe distribution and their sample site was in an area of approximately 400 m water depth. They conducted a time series from 5th of November 2000 until the 11th of January 2001

sampling approximately every two weeks. They sampled for a range of biogeochemical variables and trace metals including dissolved and particulate Fe. They observed high spatial and temporal variability but also the characteristic "L" shaped profile of particulate metals, showing maximum concentrations at the ice water interface. The temporal resolution of their study was one sampling station approximately every 15 days, therefore this study may have lacked the resolution that we now know is required to truly document the melting process that can induce significant change in the sea ice metal concentrations on the order of <10 days (Lannuzel et al., 2008). Furthermore there was no mention of how surface air or water temperatures affected this process.

However, Grotti et al. (2005) clearly showed that indeed there was sufficient storage of trace metals within sea ice to explain the enrichment in the underlying water column. They also deduced from the absolute concentration of particulate trace metals as well as the speciation pattern (based on a sequential extraction of increasingly strong acids and oxidants) that the primary source of Fe to this coastal sea ice was resuspended sediments entrained into the ice during winter ice formation. They observed, by way of a principal component analysis, that the particulate Fe fraction was associated with organic matter, a result supported by several subsequent studies (Hassler & Schoemann, 2009; Schoemann et al., 2001).

1.4. The link between physical and biogeochemical properties

The Grotti et al (2005) results highlight one of the fascinating processes that occur within sea ice once a healthy algal and bacteria assemblage has formed at the skeletal layer (ice-water interface). Sea ice serves as a floating substrate for microbes that colonise various microhabitats at the surface, the interior and particularly within the basal layer of sea ice. Sea ice consists of

solid ice and liquid brine inclusions which form during ice formation as salt ions are rejected from the growing ice crystal lattices. Sea ice microhabitats are semi-enclosed environments: exchange of nutrients with sea water is controlled by brine volume which is a function of bulk-salinity and temperature. Therefore, for any sea ice algae assemblage, growth is limited by the starting concentrations of macro and trace nutrients unless some exchange with the outside seawater or atmosphere occurs (Thomas & Papadimitriou, 2003). Thus, through the process of warming of sea ice and the associated fluctuations in permeability (Golden et al., 1998) an influx of nutrients occurs. During these times, nutrient uptake and possibly luxury uptake (the process of storing excess nutrients intercellularly) can occur as well as increasing the interstitial nutrient concentrations within the brine channels. Recent research has shown the important process of convection in the lowermost 5-10 cm (skeletal layer) in replenishing nutrients in this layer (Vancoppenolle et al., 2010). When cooler conditions are encountered and the permeability decreases, these assemblages are essentially isolated. These nutrients then become part of the internal biological pool or associated with acid polysaccharide particulates and can only be returned to the water column through brine drainage or melting (Vancoppenolle et al., 2010). However, due to the affinity of particulate and dissolved organics such as acid polysaccharides for absorbing metals (Morillo Perez et al., 2008), the flow of nutrients is primarily into the sea ice and thus would explain the concentrating effect that sea ice exhibits when there is a high standing stock of biology within. Indeed the ability of biofilms to concentrate metals has long been established (Loaec et al., 1997; Morillo Perez et al., 2008; Muñoz et al., 2006).

Lannuzel et al. (2007) sampled pack ice in the 112˚ – 119˚ E section of East Antarctica for dissolved and total dissolvable Fe together with a range of physical and biogeochemical variables. This study was the first to sample pack ice as apposed to coastal fast ice and therefore gave new insight into the larger scale spatial distribution of Fe in Antarctic sea ice. They found

that ice thermodynamics and biological activity were important in determining the distribution of Fe within the sea ice profiles. They observed that although underlying seawater dFe and TDFe concentrations were elevated relative to published concentrations in ice-free surface waters, they did not see sea water Fe profiles characteristic of obvious enrichment from above. Given the water column depth below the study sites were between 500 and 3000 m, vast dilution makes such water column enrichment difficult to observe. Lannuzel et al (2007) also found that snow Fe concentrations were lower than those observed in the immediately underlying sea ice and suggested that snow accumulation and then subsequent melting and concentration in the low-permeability cold, surface-sea ice, over an extended timeframe, implied that aerosol deposition on pack ice may concentrate in this upper layer. They noted that due to the fact that when seawater freezes, impurities are concentrated into the brines they should see higher concentrations of particulate Fe (particulate leachable Fe (plFe) was used as a proxy in this case) in the brines than in the sea ice. In fact, the opposite was observed and it was suggested to be due to the affinity of Fe for particles and organic matter attached to the sea ice matrix. However the study did not expand on how this fact affects the release of Fe during the sea ice melt, an idea expanded on more thoroughly in later research (see chapters 3, 4 and 5).

Ice texture, as observed on thin sea ice sections observed under cross-polarised light, gives an indication of the process that led to its formation. Small ice crystals are an indication of frazil ice formation under turbulent conditions, while long columnar ice crystals suggest ice growth under quiescent conditions. Interestingly, Lannuzel et al. (2007) found no clear relationship between sea ice texture and Fe concentration, a finding supported again in later research (chapter 3). The reason for this lack of correlation may be due to the processes involved in the entrainment of Fe into sea ice during its growth. Exopolysaccharides (EPS) are a range of organic materials produced by benthic and free floating bacteria, diatoms and other autotrophs that can either form encapsulating coatings surrounding cells or be released into the water

column in a colloidal phase (Mancuso Nichols et al., 2004; Meiners et al., 2004). During sea ice formation, frazil ice can form down to 30 m (Thomas & Papadimitriou, 2003). These small frazil ice crystals form when cold, turbulent conditions lead to supercooled underlying seawater. Cells, EPS or detrital material from the water column often become attached to the ice crystals (Garrison et al., 1983). Once turbulent conditions calm, the frazil ice rises to the surface, or underside of newly formed frazil ice, bringing with it the algae and organics entrained lower in the water column. This "scavenging" or "harvesting" process can concentrate biomass, EPS and nutrients in the sea ice. It is interesting to note that when frazil ice is rising to the surface with algal cells attached, the EPS on the outside of the cells would be in contact with constantly recirculating water. Due to the fact that EPS can bind dissolved Fe from the water column, this could concentrate Fe in the EPS and also strip it out of the water column. This process could also operate when EPS rich particles sink out of the water column in the open ocean. This may well be occurring, but then we would expect to see distinct differences in the nutrients, biomass, and organic concentrations coinciding with the changes in ice texture. However, this process would only act initially upon formation of sea ice, as once the sea ice is formed, algae continues to grow particularly in the basal ice where nutrient exchange with the underlying seawater can occur. Therefore, what we see when we study the profiles of Fe within sea ice is both this allocthonous concentrated Fe and "fossil" organics in the background and then autochthonous growth, nutrient drawdown and production of organic material superimposed over the top (Meiners et al., 2003). To further complicate the picture, a process of convective overturning controlled by both the density of the brines and the permeability of the ice occurs in conjunction with wave field pumping through porous columnar ice (Lannuzel et al., 2008). Indeed, Lannuzel et al. (2007) observed this dynamic system at some unknown stage of these co-occurring processes and somewhat unsurprisingly did not see clear distinctions in Fe concentrations at ice texture boundaries. However, their calculations of Fe into and from pack ice resulted in estimates of 90% of Fe into the forming sea ice being from upwelled Fe rich deep

water and furthermore, 70% of the (implied) enrichment in spring surface waters (i.e relative to ice-free surface waters) could be derived from this melting temporal storage of Fe.

In Lannuzel et al (2008), a time series was conducted in a single pack ice floe in the Western Weddell Sea. As well as physical and biogeochemical variables, particulate, dissolved and total dissolvable Fe was measured every 5 days between November 2004 and January 2005. One very striking feature to arise out of this research was the observation of a rapid loss of Fe to the water column over the course of approximately 10 days during which convective overturning of the highly saline brine with the relatively less salty underlying seawater helped mediate this rapid loss. However once the melting progressed and brine salinities were diluted with both fresh meltwater and sea water, convective overturning was shut off and molecular diffusion was the only means by which further loss of Fe could occur, therefore after this point Fe loss to the water column was greatly reduced.

This thesis adds significantly to our understanding of the distribution and concentration of Fe in Antarctic sea ice; and is coupled with measurements of physical and biogeochemical variables. It is based on two independent research voyages into the Antarctic sea ice environment including one spatial study during the transition from winter to early spring, sampling pack and fast ice (SIPEX, Sept-Oct 2007) (chapters 3 and 4) and one temporal study in fast ice off the coast of East Antarctica (Oct-Dec 2009) (chapter 5). Before this thesis, only three dedicated sea ice research studies had sampled Antarctic sea ice for trace metals together with requisite biogeochemical variables. Given that Antarctic sea ice encompasses an area of 17 million km^2 and is characterised by high spatial and temporal heterogeneity, more validation is thus required.

1.5. Aims

1/ To document the spatial distribution and concentration of EPS in first year sea ice. This information was then related to physical (temperature, ice texture) and biogeochemical [salinity, stable oxygen isotope, dFe, macronutrients, POC, dissolved organic carbon (DOC) and Chlorophyll *a* (Chl a) concentrations] variables to elucidate some of the relationships within this complex environment. The sampling was carried out during the dynamic transition from austral winter to early spring.

2/ To investigate the fractionation of Fe observed in several sea ice locations both above and removed from the continental shelf within the 110˚ – 130˚ E region of East Antarctica during the onset of sea ice melting from September – October 2007. The data set collected is the first to quantify both the particulate and dissolved Fe fractions within land fast and pack ice in a single study and thus allows a direct comparison. Snow, brines and under ice seawater were also sampled to investigate if there is a preferential release of specific Fe fractions during melting/brine drainage. Our results are compared to the available data in the literature for Fe in Antarctic pack and fast ice. The possible effect of this release on the subsequent phytoplankton blooms is discussed.

3/ To investigate with high temporal resolution, the release of Fe and organics into the underlying water column of first year coastal fast ice in East Antarctica. This data was compared with high quality meteorological data to elucidate the intertwined processes of ice melting and release of Fe, macronutrients, algae and organics. This research could be used as an analogue for more general processes of Fe release in relation to increasing air temperature during the spring melt.

2. Methodology

2.1. Sampling

The reason so few studies have documented the distribution of trace metals is due mainly to the technical difficulties in sampling sea ice in a trace metal clean manner. It can be difficult to access both by ship or land based operations and once the melt progresses it may become dangerous to land personnel on the sea ice with leads opening in the ice between personnel and the ship not uncommon. Once on the ice, full trace metal clean room gear must be worn (TYVEK) over suitable insulating layers (Fig. 2.1a) and care must be taken to distance the sampling site from the ship, vehicle and/or dirty equipment including the generator (situating yourself both up-wind and up-current). When working around the sampling site, personnel must remain downwind of the work area. All equipment must be precleaned in a clean room or laminar flow hood and transported to the ice double bagged. All metal equipment must be dried in front of a laminar flow hood before bagging to minimise the possibility of corrosion.

a 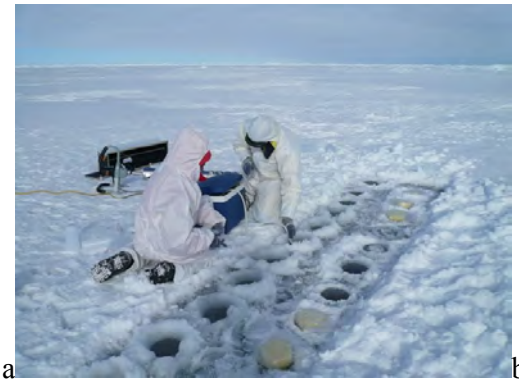 b 

Figure 2.1: a) Sampling site showing full core holes on the left and brine holes on the right. Note the brine hole plugs used to stop contamination of the brines while waiting for them to

infiltrate into the sack hole. b) Snow sampling site. Note the polyethylene (PE) snow shovel used to collect snow.

Sampling overlying snow is relatively easy, as loose snow can be collected using an acid cleaned PE shovel and transferred into a acid cleaned low density polyethylene (LDPE) container (Fig 2.1b) however, sea ice is not so straight forward. Whereas with sea water, a clean plastic water sampler (for example Glo-Flo or Niskin-X water samplers, General Oceanics) can collect water from the water column with relative ease, with sea ice, some sort of cutting and sectioning implements are required, which due to the strength of sea ice, need to be made of metal and therefore pose a contamination risk. Teflon corers were tried without success due to rapid wearing of their components in the highly abrasive sea ice environment (pers comm. Bowie, A.). Titanium (Ti) is a good choice, although large custom made corers can become prohibitively expensive. High grade, electropolished stainless steel has also been used with success and can be cheaper to fabricate due both to its outright cost and malleability relative to Ti (Lannuzel et al., 2006). In the case of the Grotti et al (2001 and 2005) papers, a manually driven, Ti corer (8 cm internal diameter) was employed. Every core was then "decontaminated" by sub-sampling the inner core ice using a separate custom made 25 mm diameter Ti corer. No mention was made of the implement used to section the core lengths into the 400 or 100 mm sections used for the interior or bottom ice sections respectively, although natural breaks in the sea ice may have sufficed. After this, the melted sample was filtered under standard trace metal conditions. Issues arising using this methodology include the fact that sub-sampling with a tiny 25 mm corer down the length of a 400mm core would be incredibly difficult, time consuming and require a great deal of manual handling. Furthermore, the resulting melted core would have a very low volume and therefore push the detection limits of some of the analytical methods employed.

The method employed by Lannuzel et al (2006) was to use an electropolished, high grade, stainless steel corer with a 140mm internal diameter, driven by an electric, high torque drill. They tested for contamination during the coring process by "decontaminating" the core by removing the outer ice of one core, on a custom made polyethylene lathe with titanium cutting chisels (Fig. 2.2a and b).

Figure 2.2a: Anne Trevena and Delphine Lannuzel remove an ice layer using the Ti chisels and PE lathe under trace metal conditions at -27˚ C (Brussels, Belgium).

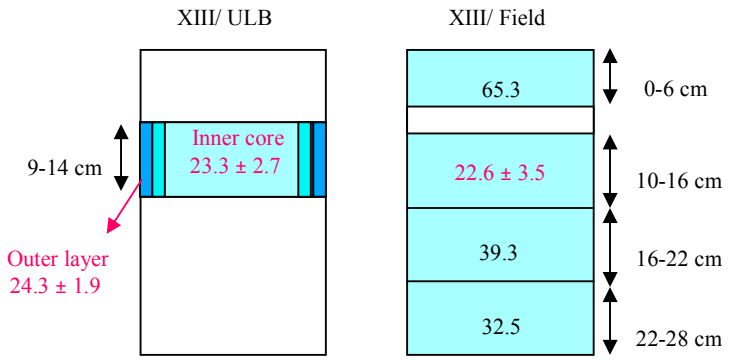

Figure 2.2b: Schematic representation of the ice sections processed and measured TDFe concentrations. TDFe concentrations measured in the field and at the home laboratory (ULB) revealed no significant difference.

The comparison of this "decontaminated core" with one simply drilled and bagged, revealed that no significant contamination occurred during the drilling process using the strict trace metal clean techniques employed during this study (Fig 2.2b). The larger internal diameter of the corer resulted in higher sample volume but sectioning using the lathe was arduous and required many one off custom pieces of equipment. Furthermore, increased sample handling also added to the possibility of sample contamination.

Figure 2.3: Pier van der Merwe and Delphine Lannuzel sampling sea ice using a custom made, electropolished sea ice corer coupled to an electric, high torque drill.

In our studies, it was realised that the ice station itself could be treated as a pseudo-clean room due to the extremely low dust deposition rate characteristic of Antarctica so long as the aforementioned precautions were followed (Fig. 2.3). Furthermore, sectioning of the core using a high grade stainless steel saw immediately on the ice was the most efficient and clean method for sub-sampling trace metal clean sea ice cores. Both the sea ice corer and the stainless steel saw were checked for contamination by soaking them in Ultra High Purity (UHP) water for several hours and then acidifying this water and running it on a suitable analytical device such as the FIA-CL. After several cleaning rinses the Fe values were below the detection limit of the method. To test for sampling contamination, Grotti et al (2005) performed their whole coring and sub-coring method on an artificial core made of UHP water and found that no significant contamination was observed. Tests in other labs however (Lannuzel pers comm.), revealed that in practice, an artificial core made entirely of UHP water is incredibly hard and difficult to sample using traditional sea ice coring equipment. Due to the vast difference in relative

hardness of the frozen matrix, this decontamination step is somewhat unrealistic, as if contamination was found, it could simply be due to the much higher friction and force required to cut pure ice and may very well not pose a contamination risk for sea ice. Ultimately the most important step is standard trace metal clean techniques during sampling but after that, minimal handling is vital for maintaining trace metal clean conditions, and therefore methods that require many manual handling steps should be avoided.

Sea ice coring is inherently destructive in nature and when a core is removed a relatively warm, low-salinity cylinder of sea water is left in the cavity created. The effect of this warm water on the surrounding sea ice is difficult to determine, indeed no sea ice sampling study has fully identified the consequences. Possible effects include increased melting and increases in brine volume fraction in the sea ice surrounding the cored ice. However, as the sea ice is warmed by the infiltrating sea water, it's brine is simultaneously diluted and therefore the freezing temperature is also simultaneously decreased. Thus, the distance from this hole that surrounding sea ice would be affected is highly debatable. What is obvious however, is that the core cavity with infiltrated sea water quickly refreezes at the surface and eventually closes up entirely. Indeed during SIPEX, cores holes drilled at the beginning of sampling would be refrozen on the surface within an hour. During the Casey time series, the warmer air temperatures resulted in the cores not refreezing as quickly. The effect of coring on the surrounding sea ice is only really an issue for time series experiments like the one presented in chapter 5 as the spatial studies (chapters 3 and 4) remove cores so quickly that coring artefacts would be insignificant. To limit coring artefacts during the research presented in chapter 5, we carefully chose our site so that a large area of flat, uniform, and seemingly homogenous ice was used. Successive coring locations were approximately 3m apart which limited both between core heterogeneity and possible coring artefacts.

A final issue arising from the coring method is brine drainage from the core after it has been removed from the ice and before it is sectioned and placed into sealed containers. This is only an issue for the basal ice where brine can be observed to drip from the core if left for approximately a minute. This is why we take special care to immediately section the highly permeable basal ice section first and then subsequently the remaining core. This way, no significant loss of brine will occur.

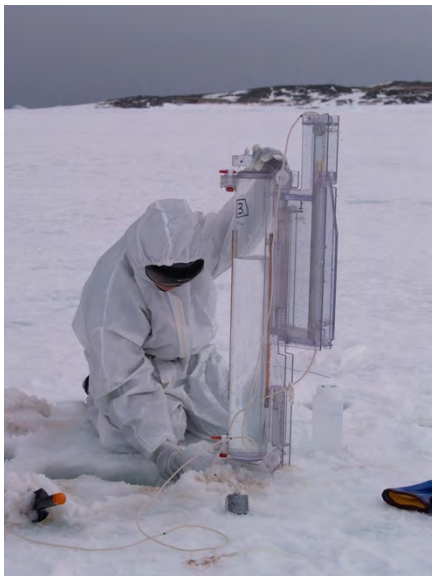

Figure 2.4: Sampling the underlying water column with a Helmond-Byrne water sampler. A sampler of this size could be lowered through 3 overlapping holes drilled through the ice and triggered by the Teflon messenger at any water depth while suspended on Kevlar spectra.

Sampling the water column under the ice can be performed either with a weighted, acid-cleaned peristaltic tubing and pump (as used in chapter 3 and 4) or with a dedicated water sampler such as the custom made Helmond-Byrne (HB) sampler (Fig 2.4) as used in chapter 5. The latter is advantageous due to the fact that you can precisely control the depth of collection. Furthermore, the peristaltic pump can be problematic due to ice formation in the tube and eventual clogging that ensues. The HB sampler is entirely PC in construction except for several titanium fulcrum

pins. Deploying it through the ice requires drilling at least 3 linked core holes and care must be taken to clear the hole of as much organic matter (basal ice fragments) as possible to limit contaminating the sampler on the way down. Once triggered, seven litres of seawater are available to decant on the surface.

2.2. Method development

Aside from the methods detailed in the following chapters (see methods section in chapters 3, 4 and 5) several novel methods were trialled.

2.2.1. Instrumental development

1/ Development of integrated peak analyser software within the FIA-CL Labview .VI files (Fig 2.5a and b). This was several pieces of stand-alone code that were written to find, measure and record each peak height accurately and without the need for the user to constantly be watching the instrument, as was the practice prior to this development. The code uses timing parameters (that can be fine tuned on the front screen of the Labview VI (Fig. 5b)) to narrow down the analysis window to each peak. Then it uses a max value sub-VI to find the peak height index. Then any number of points before and after the peak can be used to find the average peak height. Thus getting an accurate and reproducible measurement of peak height without errors associated with internal instrument noise. This also allows for the VI to be fine tuned for the rapid Fe(II) reaction or for the slower Fe(III) reaction. Simultaneously, the baseline is recorded for every peak and subtracted from the displayed peak height, thus reducing error associated with analytical drift. The final 3 or 4 replicate peak heights are then displayed for the user. This update to the system greatly reduces the time required for post-processing peak heights or areas and enables the user to proceed with other tasks while the instrument is running. The VI can also be easily adapted to return peak area rather than peak height if required.

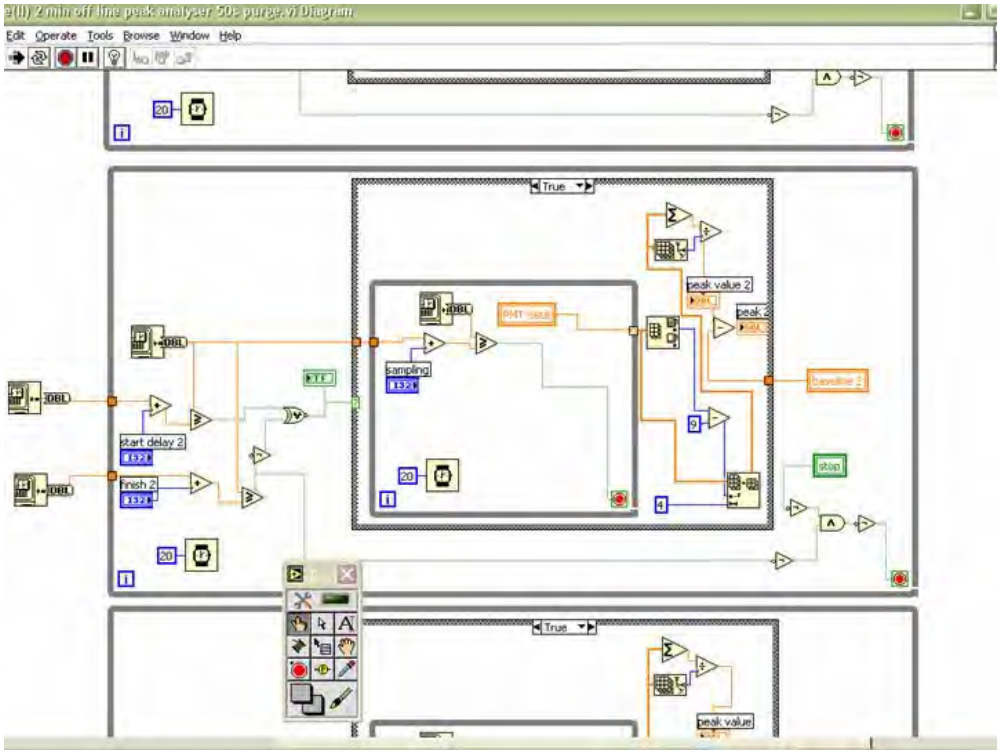

Figure 2.5a: One of the pieces of code for each peak height contained within several "while loops". Separate code is written for the baseline measurements.

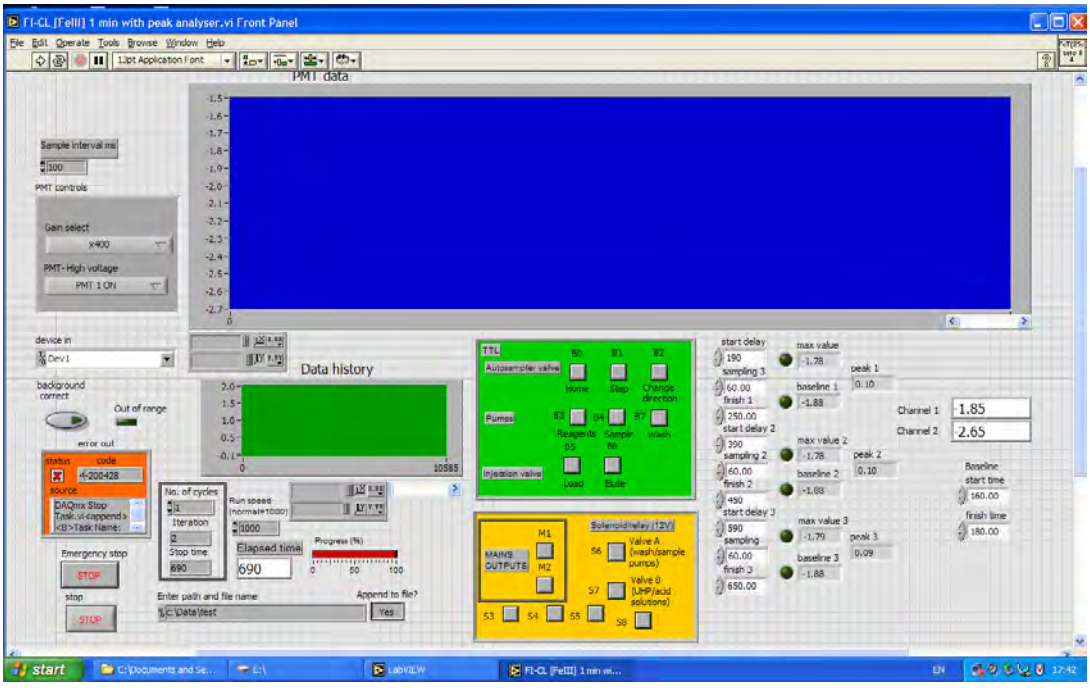

Figure 2.5b: Front screen of the LabView Fe(III) FIA protocol with peak analyser timing parameters and triplicate peak heights at the bottom right.

2/ Fine tuning of the FIA-CL manifold for maximum sensitivity. This included the customisation of the manifold to expose the maximum reaction intensity in front of the PMT detector. Furthermore, electronic heat packs were developed and heavily insulated to limit analytical fluctuations between replicate peak heights due to temperature fluctuations within the reagents. The manifold was installed in conjunction with a portable laminar flow hood to allow trace metal clean reagent and sample manipulation.

3/ Trouble shooting a new FIA-CL manifold and USB computer interface. A separate FIA manifold was successfully built and used that made use of a USB interface between the separate instruments within the manifold (pumps, injection valves, solenoid valves) and the computer (controlled by LabView). In addition to building and fine tuning the manifold, this required modifying the data acquisition code within LabView to allow the computer to read the signal and control the instruments.

2.2.2. Sample processing

4/ A safe and trace metal clean method was developed for the heated digestion of particulate samples using hydrofluoric (HF), hydrochloric and nitric acid. This involved the customisation of a trace metal clean extraction hood (Fig 2.6) to allow sample manipulation within the clean space without exposing the users to highly dangerous HF fumes. Tests were carried out together with a certified extraction hood technician to ensure efficient extraction.

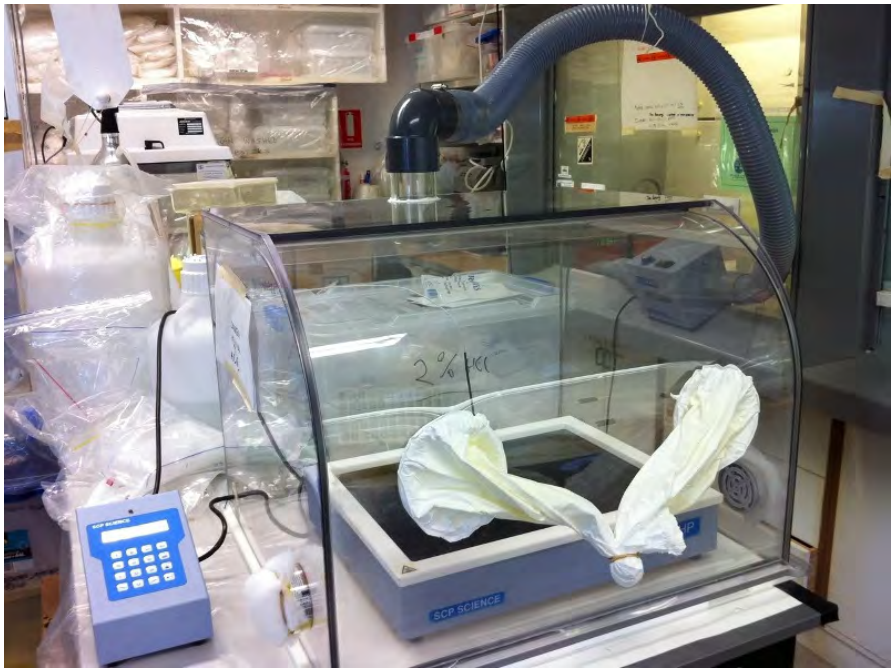

Figure 2.6 Trace metal clean digestion hood. The hood supplied by SCP scientific includes fume extraction via the supplied vacuum pump and flexible hose. The air entering the hermetic space is filtered via two hepa filters (Protector brand RC80A) fitted to the intake ports. These high quality hepa filters are not supplied with the system and must be bought separately (low quality paper filters are supplied instead). The system was modified by drilling holes in the front Perspex screen and fitting hermetically sealed Tyvek sleeves that allow sample manipulation within the clean space while dangerous fumes are being extracted.

5/ Freeze dry protocol for concentrating dissolved samples for subsequent PSA analysis. This protocol was developed to increase the detection limit of the PSA carbohydrate assay by concentrating down a 10 ml sample through freeze drying and then resuspending the residue for analysis. This method was developed but the PSA assay still lacked the required sensitivity for the dissolved fraction of the SIPEX sample set and therefore was not used.

6/ A heated, melting tray for sectioning ice cores in a trace metal clean manner within the laboratory was developed (Fig 2.7). Water was heated in a water bath and pumped along the

section dividers to melt through each section, thereby sectioning the cores in a completely metal free manner. The heating tray was built and trialled on sea ice cores but brine drainage, within the core, between sections made the resulting melted sub-samples of dubious origin. Also the highly sticky nature of the bottom ice algal assemblage resulted in this fraction being slowly transferred to the wrong section recess as the ice core melted.

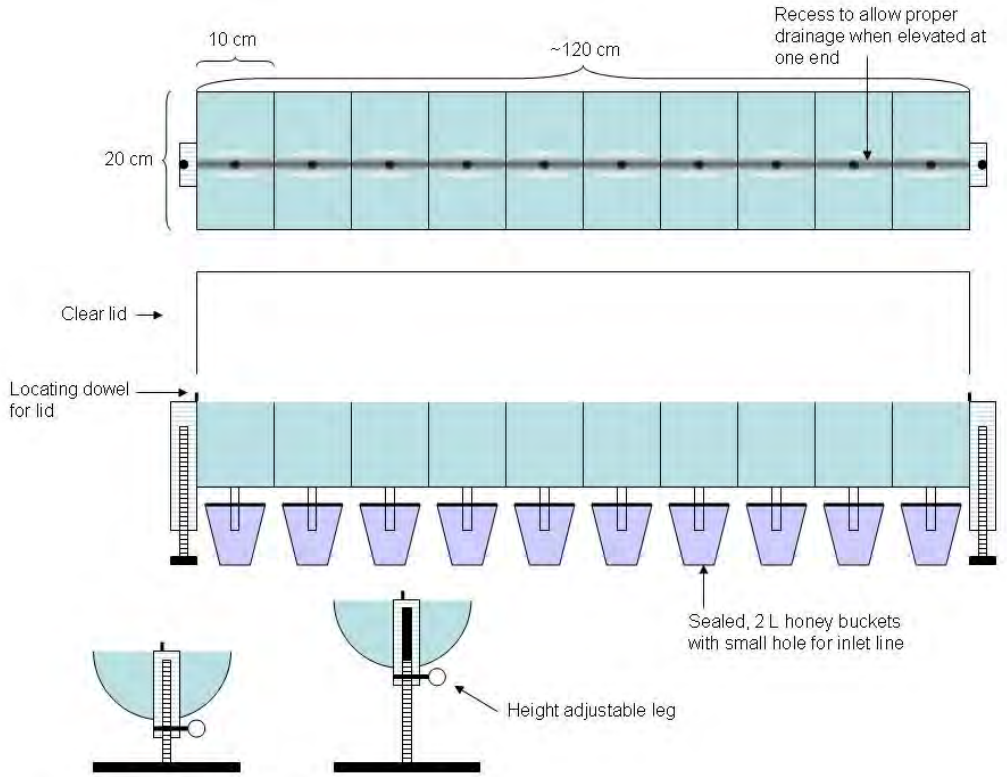

Figure 2.7: Melting tray trialled for the trace metal sectioning of sea ice cores.

2.2.3. Analytical method development

7/ CLE-CSV analysis of sea ice samples was conducted on several samples, however, due to time constraints has not yet been run on a full data set.

8/ Exopolysaccharide measurement intercalibration between Phenol Sulfuric Acid method and Alcian Blue as described in Chapter 3.

9/ During the ICP-MS analysis of particulates the method for both digestion and analysis was fine tuned to obtain the best recovery of the highly refractory transition row metals (see paper 4, Bowie et al. (2010) in publication list).

3. Biogeochemical observations during the winter-spring transition in East Antarctic sea ice: evidence of iron and exopolysaccharide controls.

This chapter has been published:

van der Merwe, P., Lannuzel, D., Mancuso Nichols, C., Meiners, K., Heil, P., Norman, L., et al. (2009). Biogeochemical observations during the winter-spring transition in East Antarctic sea ice: evidence of iron and exopolysaccharide controls. Marine Chemistry, 115, 163-175.

3.1. Abstract

This paper documents the spatial distribution and concentration of exopolysaccharides at 9 discrete sea ice sites, consisting of first year sea ice, and relates this information to physical (ice temperature, texture) and biogeochemical (oxygen stable isotopic composition of the ice, salinity, macronutrients, dissolved iron, particulate organic carbon, dissolved organic carbon and Chlorophyll *a*) variables. The sampling was carried out over a transition from austral winter to early spring conditions as part of the Sea Ice Physics and Ecosystems eXperiment (SIPEX), during September/October 2007 in the 110˚ – 130˚ E region off East Antarctica. Exopolysaccharide concentrations in sea ice varied by 3 orders of magnitude from 2.8 to 2690 µg xanthan equivalent (xeq.) l^{-1}; basal ice mean 493 µg xeq. l^{-1}. Exopolysaccharides correlated significantly with particulate organic carbon and chlorophyll *a* but not with dissolved iron, dissolved organic carbon or macronutrient data, indicating that exopolysaccharides are most likely produced *in situ* by autotrophic sea ice biota, superimposed over fossil organics. We observed increased exopolysaccharide per unit biomass in the colder surface to intermediate ice

at three stations, supporting the theory that exopolysaccharides may be used as a cryoprotectant. Mean bulk ice dissolved iron (depth integrated) across all ice cores was 2.37 nM (range 0.23 to 14.4 nM). Sea ice dissolved iron concentration was always elevated relative to seawater. Apparent dissolved iron and estimates of cellular carbon to iron ratios suggest that the sea ice microbial biota was not limited by dissolved iron but may have been by NO_2+NO_3 or $Si(OH)_4$. Conversely, under ice seawater algal communities may have been limited by dissolved iron and/or light and grazing at the time of sampling. We observed a significant inverse correlation between dissolved Fe and Chlorophyll *a* in the basal layers of the ice, most likely indicating the active drawdown of dissolved Fe by the sea ice biota, combined with some fraction lost to the water column or converted to the particulate fraction.

3.2. Introduction

The formation of sea ice is one of the largest seasonal events on Earth (Lowe, 1997). Its formation is important to climate as sea ice forms at the boundary between the surface ocean and the lower atmosphere, affecting energy, moisture and gas fluxes. Sea ice also supports high levels of primary production which contributes to air-sea carbon dioxide (CO_2) exchanges. Sea ice provides a substrate for dense populations of sea ice algae that can be several orders of magnitude higher than in ice-free seawater (Thomas & Dieckmann, 2002). During the spring/summer melt, sea ice can seed the water column with algae and essential micro-nutrients such as iron (Fe) (Lannuzel et al., 2008; Leventer, 2003; Sedwick & Ditullio, 1997). Coupled with vertical stratification of the water column (Alexander & Niebauer, 1981), vast phytoplankton blooms develop when light and macro-nutrient conditions are favourable. Legendre et al (1992) estimated ice-edge algae blooms to account for 1.41×10^{14} g C year $^{-1}$ in the Antarctic, or approximately 48 - 49 % of Antarctic ice-covered ocean productivity. This biological process acts to draw down CO_2 from the atmosphere, less heterotrophic respiration,

by consuming dissolved inorganic carbon in surface waters and transports a small but significant fraction towards the seafloor as particulate organic carbon (POC) (Arrigo et al., 1997; Gibson & Trull, 1999; Shanks & Trent, 1980). In this way, Southern Ocean sea ice mediate CO_2 induced global warming.

It is now well established that the Southern Ocean is a high nutrient, low chlorophyll (HNLC) region, and that the major limiting nutrient is Fe (Boyd et al., 2000; Martin et al., 1990a). Studies have shown that Fe can be concentrated in sea ice up to 2 orders of magnitude higher than in the underlying seawater (Grotti et al., 2005; Lannuzel et al., 2008; Lannuzel et al., 2007; Loscher et al., 1997). In seawater, Fe is almost entirely (99%) complexed by organic ligands (Boye et al., 2001; Geider, 1999; Gledhill et al., 1998) and such binding may also occur in sea ice. High concentrations of exopolysaccharides (EPS) have been observed in Arctic (Krembs et al., 2002a) and Antarctic sea ice (Dumont et al., 2009). EPS are a group of complex organic material that are primarily high molecular weight polysaccharides with carbon backbones (Krembs & Deming, 2008). EPS can contribute to the dissolved, colloidal and particulate fractions in aquatic systems, however, cationic bridging can drive coalescence of dissolved and colloidal EPS into particulate fractions (Wells, 1998). EPS are secreted by sea ice algae and bacteria (McConville et al., 1985; Meiners et al., 2004) to perform a multitude of functions including acting as a cryoprotectant, enabling cell locomotion and adhesion to surfaces, and buffering pH and salinity fluctuations (Krembs et al., 2002a). The negatively charged EPS may also bind selectively to dissolved Fe (dFe) (Fe^{3+} and Fe^{2+}), and therefore act as an organic ligand (Loaec et al., 1997; Mancuso Nichols et al., 2005b). In the sometimes hyperoxic sea ice environment (Thomas & Dieckmann, 2002), this complexation would be very important as it would slow the oxidation of dissolved iron to iron hydroxide and iron oxide complexes (Sunda, 2003), and therefore, increase the bioavailability of this important trace micronutrient in the sea ice environment.

The aim of this study was to document the spatial distribution and concentration of EPS in first year sea ice. This information was then related to physical (temperature, ice texture) and biogeochemical (salinity, stable oxygen isotope, dFe, macronutrients, POC, dissolved organic carbon (DOC) and Chlorophyll *a* (Chl *a*) concentrations) variables to elucidate some of the relationships within this complex environment. The sampling was carried out during the dynamic transition from austral winter to early spring.

3.3. Material and Methods

3.3.1. Sampling area

Sampling was undertaken as part of a multidisciplinary sea ice research study, SIPEX, during September/October 2007 onboard RV Aurora Australis in the 110˚ – 130˚ E region off East Antarctica (Fig. 3.1). All sampling was conducted up wind and at the greatest feasible distance from the vessel with trace metal clean sampling techniques to allow for the reliable determination of dFe concentrations (see Lannuzel et al., 2006).

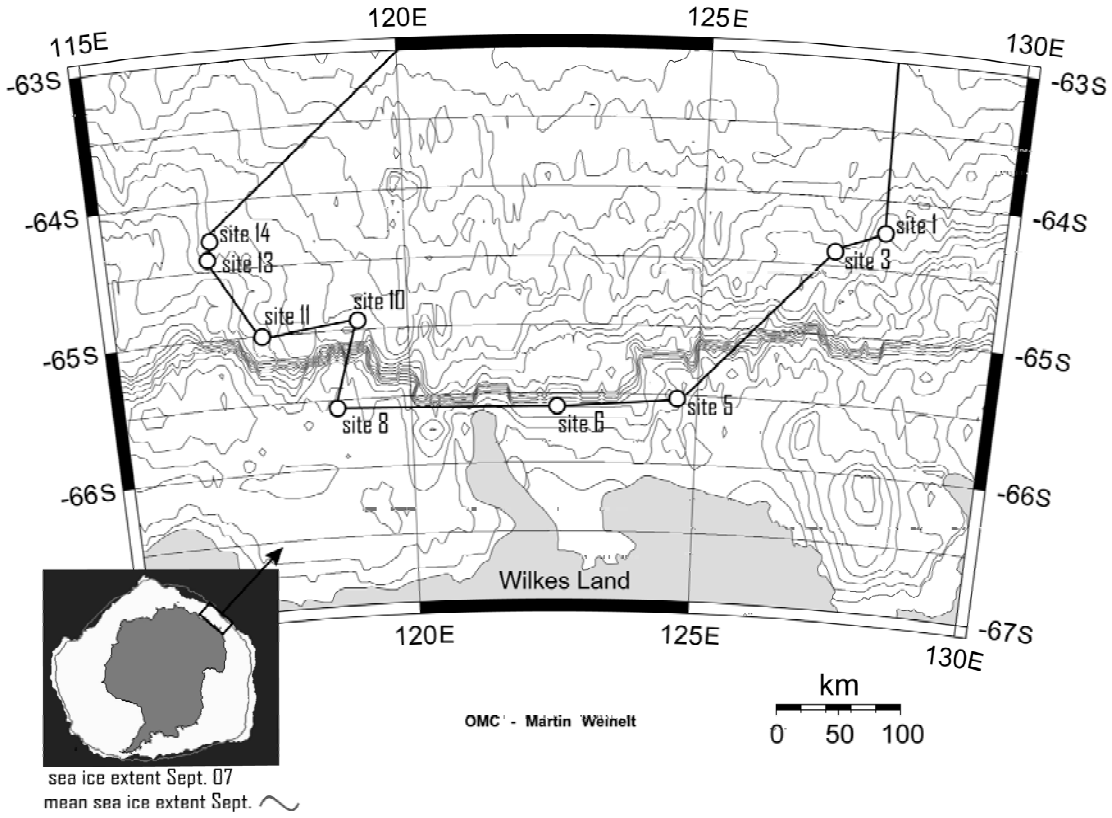

Figure 3.1: SIPEX sampling site locations. Bathymetry contours represent 200 m increments. Image created using Online Map Creation (OMC) (Weinelt, 2006). Inset adapted from Russell (2007).

3.3.2. Sampling methods

All sampling bottles and equipment were decontaminated using trace metal clean techniques according to Lannuzel et al. (2006). Care was taken at each site to select level ice with homogeneous snow thickness. Firstly, snow was collected using acid cleaned low density polyethylene (LDPE) shovels and transferred into acid-cleaned 3.8 l LDPE containers (Nalgene). Ice cores were collected using a non-contaminating, electropolished, stainless steel sea ice corer (140 mm internal diameter, Lichtert Industry, Belgium) driven by an electric power drill. Ice cores were collected about 10 cm away from each other to minimise between-core heterogeneity. Five sections were taken from each core. The five sections were chosen so that a

top, two intermediate and two basal sections were included from every core. The sections were 6 cm which gave a melted volume of approximately 1 l. Cores were sectioned using a stainless steel saw, starting with the highly permeable basal sections. Brine samples (1 l per analyses if time allowed) were collected by drainage from "sack holes" drilled above and below the -5 ˚C sea ice isotherm. This was done to collect brines from both the colder, higher salinity and warmer, lower salinity niches within sea ice. Brines (> -5 ˚C and < -5 ˚C) and under ice seawater (0 and 1 m deep) were collected in 1 l Nalgene LDPE bottles using an insulated peristaltic pump and acid cleaned C-flex tubing (Cole Palmer). All samples were then transported to the ship as quickly as possible to prevent further freezing.

3.3.3. Measured Variables

3.3.3.1. Physical variables

Sea ice and brine temperatures were measured on site on a separate dedicated core. A temperature probe (Testo, ± 0.1 °C accuracy) was inserted in holes freshly drilled along the core every 5 to 10 cm, depending on its length. Bulk salinity was measured for melted ice sections and for brines using a TPS AQUA-C conductivity meter. Where salinity and temperature profiles had different depth resolution, temperature was linearly interpolated to match salinity. Brine volume fraction (Vb/V) was calculated from temperature and salinity data according to Cox and Weeks (1988) and Eicken (2003). Full core length, ice core slices (2-3 mm thickness) were examined under cross-polarised light to identify ice texture (i.e., columnar vs granular) according to the method of Langway (1958). Snow ice was differentiated from frazil ice using $\delta^{18}O$ analysis, where $\delta^{18}O$ values < 0 were interpreted as snow ice and values > 0 as frazil ice (Jeffries & Adolphs, 1997; Toyota et al., 2004).

3.3.3.2. Biogeochemical variables

Melted ice, brine, snow and seawater samples were vacuum filtered under low light conditions onto 25 mm Whatman GF/F filters for Chl *a* determination. Volume filtered depended on visual organic content and available sample volume (range 310 – 2300 ml). The filters were placed into 1.5 ml sealable cuvettes, wrapped in aluminium foil, and stored at -20 ºC for no longer than 1 week. Filters were extracted in 10 ml of 100% methanol for 12 h in the dark at 4˚ C. Chl *a* concentration was then determined following the method of Holm-Hansen et al. (1965) using a Turner Designs, 10AU fluorometer (*in vitro* detection limit 0.02 μg l^{-1}).

3.3.3.3. Exopolysaccharides

Alcian Blue (AB) and Phenol Sulfuric Acid (PSA) assays were used to quantify EPS concentrations. This was done to allow inter-comparison (noting methodological differences) and to test the applicability of these two methods in the sea ice environment. The AB method is technically a semi-quantitative assay, based on the affinity of Alcian Blue stain for acid-polysaccharides (Passow & Alldredge, 1995). It does not penetrate cells and operationally targets particulates >0.4 μm in diameter. The PSA method on the other hand penetrates cells and quantifies simple sugars, oligosaccharides, polysaccharides and their derivatives (Dubois et al., 1956). We have operationally defined the PSA fraction as that which remains on a 0.2 μm PC filter. Care was taken to collect cores for both the AB and PSA assays that were in close proximity to one another (~10 cm separation) and the sections were matched throughout all assays. Melting of ice samples was not carried out in filtered seawater as tests revealed that it did not significantly alter the final EPS yield (van der Merwe, data not shown) and further dilution was undesirable due to the already low concentrations within the samples. Furthermore, the input of intracellular dissolved chemicals during cell rupture of fragile biota is believed to be insignificant relative to the external pools (Thomas & Papadimitriou, 2003) and therefore would not effect the results presented here. The detection limit (3 × the standard deviation of the filter

blank) for the AB and PSA methods was 2.1 μg xeq. L^{-1} and 2.8 μg glucose eq. L^{-1} respectively. However, in practice, standard deviation between replicates in samples below approximately 10 μg L^{-1}, in either method, were quite high. This is most likely due to heterogeneity of particle distribution when filtering onto replicate filters.

3.3.3.3.1. Phenol Sulfuric Acid method

Brine, snow and seawater PSA samples were filtered onboard. Sea ice cores were stored in the dark at -20 ˚C and processed less than 3 months later in the home laboratory. Sea ice cores were melted in the dark at ambient laboratory temperature (18 ˚C) for 18 hours. Melting core sections were monitored so that they were filtered immediately after the ice had melted. Therefore, the liquid sample itself did not reach ambient temperature (~18 ˚C) for longer than 1 hour, if at all, before filtering. All samples were homogenised by gentle stirring before triplicates of 20-500 ml were filtered through polycarbonate membrane filters (47 mm diameter, 0.2 μm pore size).

The PSA analysis was performed as per Dubois et al. (1956) with the following modifications. Calibration for the PSA analysis was achieved by preparing standard additions of 20 – 100 μl of D(+)-glucose (Sigma), added to triplicate 15 ml borosilicate tubes with Teflon-lined screw caps. Filters loaded with samples were removed from the freezer and placed in identical borosilicate tubes and 2 ml of Ultra High Purity (UHP) water (> 18.2 MΩ cm^{-1}) (Barnstead Nanopure Diamond TM) was added to all samples including standards and blanks (filter and test tube). These solutions were then vortex mixed for 15 sec and 50 μL of 80% (w/w) phenol solution (Merck) added. Five ml of 99% sulfuric acid (Univar) was then added directly to the liquid surface of the sample and vortex mixed. The samples were then placed in a water bath set at 30˚C for 30 min and then mixed again. Finally, 3 ml of solution was transferred to 4.5 ml disposable polystyrene (PS) spectrophotometer cuvettes (Kartell) and the absorption was recorded at 485 nm.

3.3.3.3.2. Alcian Blue method

Melted sea ice, snow, seawater and brine samples were homogenised and 4 replicates were filtered at low pressure (< 0.13 bar) onto 25 mm diameter, 0.4 µm pore size Whatman Polycarbonate (PC) filters. The sample volume ranged from 20-500 ml and depended on the visible organic content. Care was taken not to filter too much organic matter and clog the filters. Then, 500 µl of 0.2 µm pre-filtered 0.02% Alcian Blue GX8 (w/v) (Sigma) in 0.06% acetic acid (v/v) (Univar) was added directly onto the filter and drawn through under low vacuum (< 0.13 bar). Filters retaining the stained EPS were then rinsed with 2 ml of UHP water to remove excess dye, placed in 10 ml polypropylene (PP) vials and stored in the dark at -20 °C before analysis in the home laboratory. Blank filters were also stained and kept frozen until further analysis.

The EPS AB analysis was performed as per Passow and Alldredge (1995) with the following modifications. Pre loaded filters were removed from the freezer and transferred to clean, borosilicate tubes with Teflon-lined screw caps. Filters were then extracted for 2 hours in 5 ml 80% (v/v) sulfuric acid (Univar) with gentle agitation (3-5 times). Finally, 3 ml of solution was transferred into 4.5 ml polystyrene disposable cuvettes and absorbance at 787 nm was recorded.

Calibration of the AB method was achieved by cross calibration with the PSA method since the standard gravimetric method of Passow and Alldredge (1995) yielded poor results in our experiments (data not shown and C. Krembs, pers. comm.). To do this, stock solutions of D(+)-glucose (Merck) and xanthan gum (Sigma) were inter-calibrated with the PSA method. Then the same dilution series of xanthan gum was used and 6 replicates were filtered through 0.4 µm (PC, 25 mm diameter) filters under low vacuum (< 0.13 bar). Three of these filters were stained and analysed as per the AB method described above and the remaining three were analysed as per the PSA method.

Filtrate collected through non-stained filters was also recovered and analysed with the PSA method. Filter and test tube blanks were also analysed. PSA analysis of the filters and filtrate

gave the filter capture efficiency and allowed for the determination of the mass of xanthan gum retained on the filter. Then the actual concentration of retained xanthan gum/filter was plotted against its absorption and a model II regression used to determine a calibration relationship (R^2 = 0.99) (C. Krembs, pers comm.). The inter-calibration allowed PSA values (μg glucose eq. l^{-1}) to be converted to AB units (μg xeq. l^{-1}) by the following model II regression equation:

μg xeq.l^{-1} = 0.975 × μg glucose eq.l^{-1} + 0.879, (R^2 = 0.99)

AB units were converted to EPS-C according to a modification of that reported in Engel and Passow (2001) for pelagic, transparent exopolymer particles (TEP):

μg C l^{-1} = 0.75 × μg xeq. l^{-1}.

3.3.3.4. Macro-nutrients, POC/PON and DOC

Macro-nutrient ($Si(OH)_4$, PO_4^{3-} and NO_3 + NO_2) samples were filtered through pre-combusted Whatman GF/F filters and stored frozen until analysis at University of Wales (Bangor, UK) within 8 months after the cruise. Dissolved inorganic nutrients were determined using standard colorimetric methodology (Grasshoff et al., 1983) as adapted for flow injection analysis on a 5 channel LACHAT Quik-Chem 8000 auto-analyser (Hales et al., 2004). The slope of the theoretical dilution line (TDL) was calculated by taking the mean of the ratios of nutrient concentration to salinity from 18 separate measurements of under ice seawater (0 and 1 m depth at 9 sites). Dissolved organic carbon was determined by high-temperature catalytic oxidation (HTCO) using a MQ 1001 TOC analyser (Qian & Mopper, 1996).

All glassware in contact with POC samples was pre-combusted prior to the cruise (450 °C for 12 h). Melted sea ice, seawater and brines were filtered (100 -1000 ml depending on organic matter content) onto pre-combusted (550 °C for 12 h), 25 mm, GF/F filters. Filters were then removed and placed into individual, sterile filter holders and wrapped in aluminium foil to limit light exposure. Filters were stored at -20 ˚C until analysis (< 3 months). The analysis for total nitrogen, carbon and hydrogen was determined at the Central Science Laboratory, University of

Tasmania, using a Thermo Finnigan EA 1112 Series Flash Elemental Analyser (estimated precision ~1%).

3.3.3.5. Iron

Dissolved Fe samples (sea ice, brine, snow and seawater) were processed according to Lannuzel et al. (2006), and was analysed using flow injection analysis with luminol chemiluminescence detection (FIA-CL) with in-line preconcentration onto a 8-hydroxiquinoline (8-HQ) resin (FeIII method), adapted from de Jong et al. (1998) and Obata et al. (1993). This method has been recommended by the new international program GEOTRACES (Bowie & Lohan, 2009). The mean detection limit (3 × blank standard deviation) of the FIA-CL method with 1 minute preconcentration was 0.19 ± 0.06 nM (n = 7). Analysis of SAFe (Sampling and Analysis of Fe) deep water reference seawater samples D2 was 0.88 ± 0.05 nM (n = 9), which was in excellent agreement with the D2 consensus value of 0.91 ± 0.17 nM.

3.3.3.6. Property-property relationships

All variables were plotted to identify trends. As sea ice data is commonly non-normally distributed, the non-parametric Spearman's rank correlation, was used to compare variables that were non-normal. Alternatively, log transformed data was analysed using the Pearsons product moment correlation.

3.4. Results

3.4.1. Sea ice types and thermal regime

Sea ice cores collected ranged between 34.5 and 103 cm (mean 68 cm) in thickness and represented both first year fast ice (site 5) and pack ice (all other) (Fig. 3.1). Most sites exhibited frazil ice underlain by columnar ice (Fig. 3.2). Most cores displayed snow ice

formation at the ice-snow interface (i.e., a frozen mixture of snow and infiltrated seawater). The exceptions were sites 8 and 10 where a thin layer of snow was followed entirely by columnar ice. Sites 6, 13 and 14 showed evidence of rafting processes with superposition of columnar and frazil ice layers. Snow thickness ranged from 2 – 30 cm, mean 15 cm. Several sites (i.e., 1, 11 and 14) showed evidence of deformation of columnar ice crystals, identified as "deformation zone" (Fig. 3.2). Deformed ice has been associated with nearby leads and turbulent hydrodynamic regimes (Eicken & Lange, 1989).

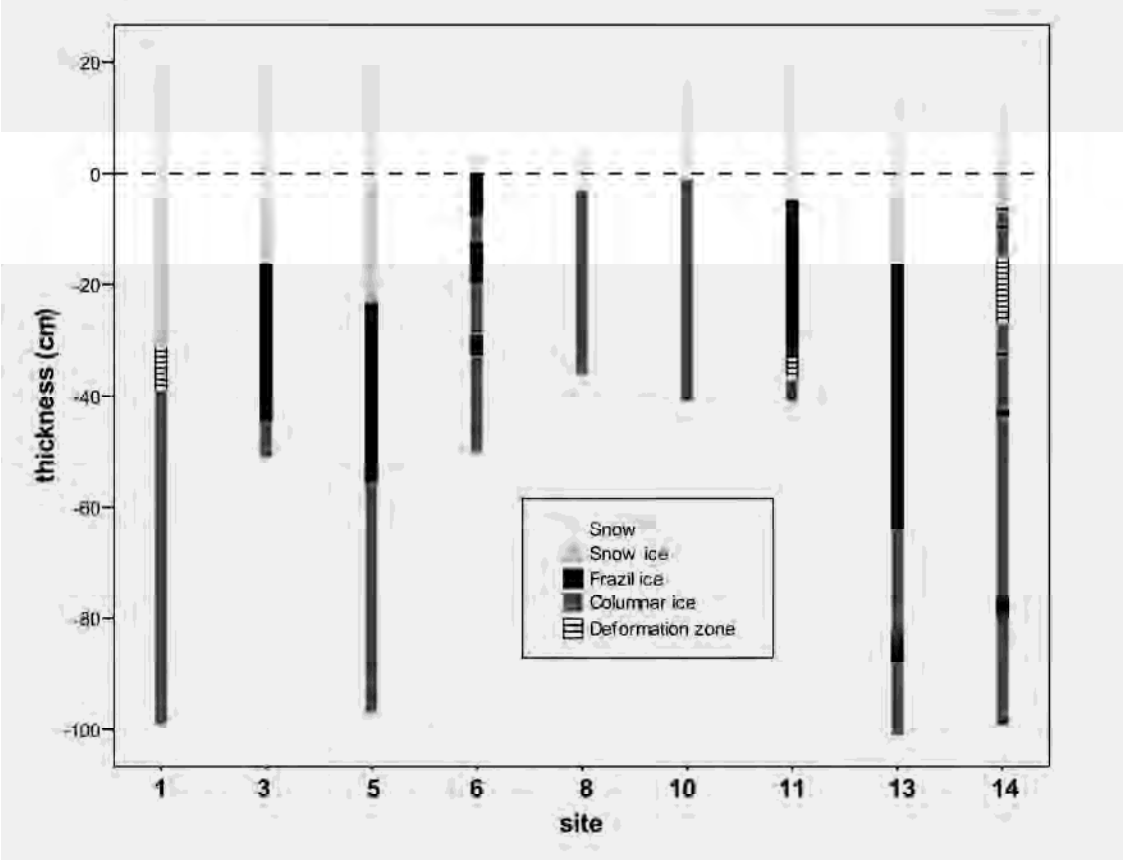

Figure 3.2: Ice texture and snow thickness at all sites sampled. Thickness > 0 indicates loose snow, < 0 indicates compacted snow or ice.

Based on ice temperature and Vb/V there was a clear distinction between cold winter sites (1-5), transition regime (sites 6-10) and the warmer spring-like sites (11-14) (Fig. 3.3). A one-way ANOVA was used to test separately, both mean sea ice temperature and Vb/V between the cold,

transition and warm sites. Lavene's statistic revealed significant homogeneity of variances for both temperature and Vb/V. The null hypothesis that the cold, transition and warm sites came from populations with statistically similar mean temperatures returned a significant result ($P < 0.05$) and therefore the H_0 was rejected. The post-hoc test, Tukey HSD, revealed that the cold and warm sites were significantly different while the transition regime sites were not significantly different from either the cold or warm. The mean ice temperature increased from -6.5 ˚C at the cold winter sites, to -4.4 ˚C at the transition regime, and up to -3.2 ˚C at the warmer sites. Likewise, mean air temperature was observed to increase from -18.8 to -12.4 to -10.0 at the cold, transition and warm sites, respectively. Mean Vb/V was significantly different between the cold and warm but not the transition regime, with 7.8, 11.4 and 14.6 % at the cold, transition and warm sites respectively. With the exception of site 6, there is a general increasing trend in mean bulk ice salinity, although no significant difference is present between the cold, transition and warm sites. Thus, the increase in mean brine volume appears to be driven primarily by an increase in mean temperature but also probably by a slight increase in bulk ice salinity. The transition from cold to warmer sites occurred over just less than a month (11/9/07 site 1; 7/10/07 site 14) at a time when Antarctic sea ice was warming, prior to a rapid pack-ice disintegration in November-December (Worby et al., 1998).

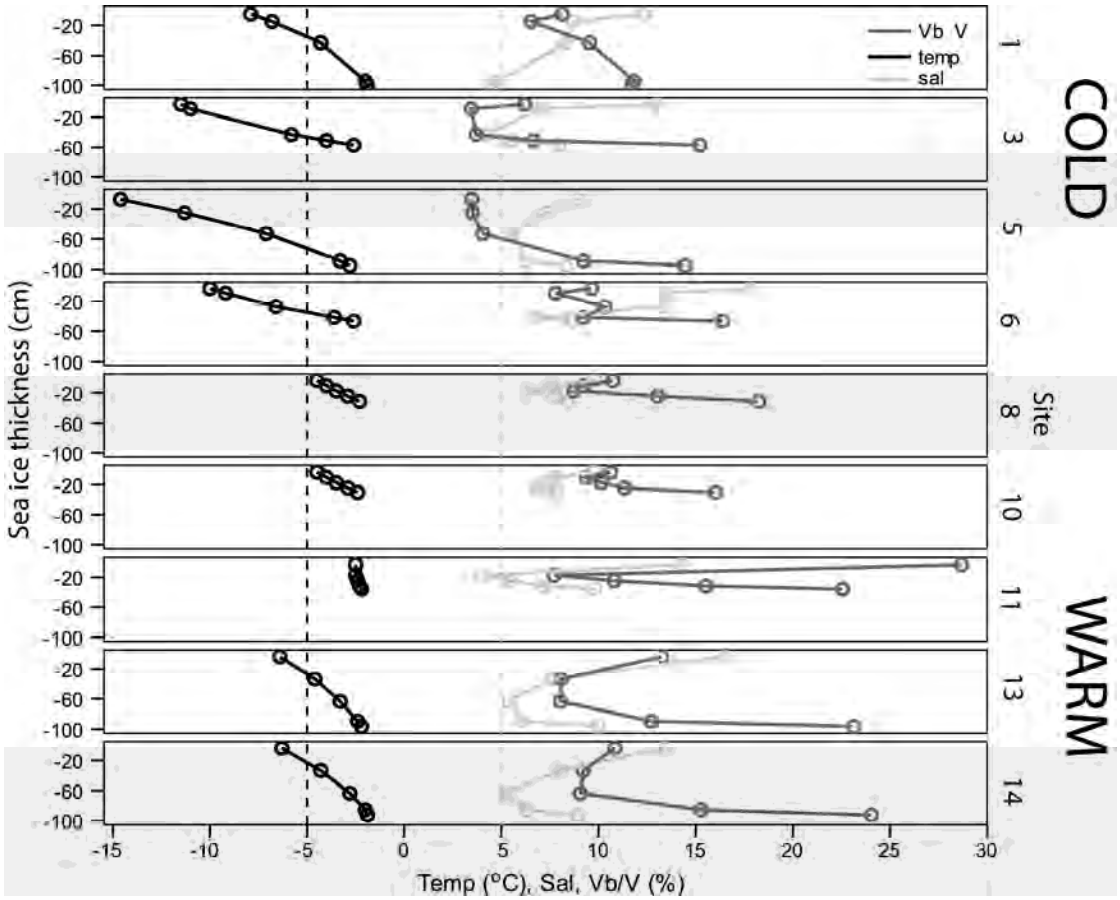

Figure 3.3: Sea ice thermodynamics at each site investigated. Temperature (temp., ˚C), salinity (sal.) and relative brine volume (Vb/V, %). The critical -5˚ C ice temperature (black), bulk salinity 5 (light grey) and 5% Vb/V (dark grey) horizon are highlighted (Golden et al., 1998). Cold and warm labels highlight significantly different mean temperature and associated brine volumes at these sites.

Sites 3 and 5 had ice core sections below the critical 5% Vb/V, indicating the impermeable nature of these sections (Golden et al., 1998). Possible evidence for rafting of site 6 can be observed in its "double C" salinity and brine-volume profile (Fig. 3.3), although the oxygen stable isotope results did not indicate any snow ice layers within the profile. Site 6 also has the highest mean bulk ice salinity.

3.4.2. Biogeochemical variables

3.4.2.1. Chl *a*, nutrients, DOC, POC, PON and EPS

The Chl *a* concentration data illustrated the onset of the growth season by ranging from < 0.7 μg Chl *a* l^{-1} in the basal ice at site 1 to > 17 μg Chl *a* l^{-1} at sites 13 and 14 (Fig. 3.4). Mean Chl *a* concentration at sites 1-10 was 0.33 μg Chl *a* l^{-1}, while at the warm sites the mean value was an order of magnitude higher at 3.13 μg Chl *a* l^{-1} (Fig. 3.4). At all sites except for site 1, the Chl *a* maxima occurred at the ice water interface, coincident with the highest brine volume fraction and temperature. The profiles also highlighted the relatively high Chl *a* concentrations in the brines (sites 1-5, mean 0.36 μg Chl *a* l^{-1}, sites 11-13, mean 0.87 μg Chl *a* l^{-1}) compared to the extremely low concentrations in the sea water (mean 0.02 μg Chl *a* l^{-1} at all sites).

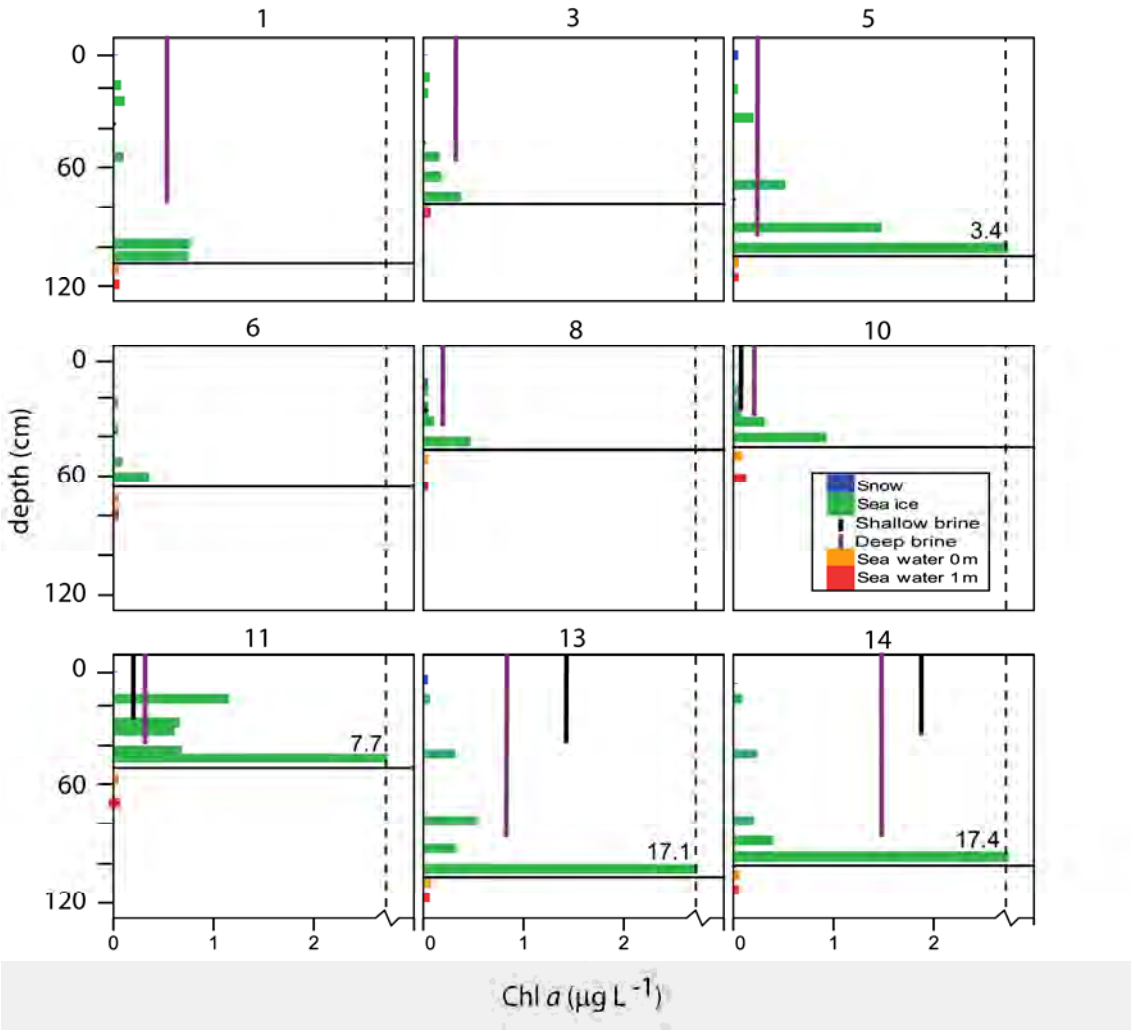

Figure 3.4: Chl *a* concentration (in µg Chl *a* l^{-1}) at each site for sea ice, seawater, brines and snow. Horizontal line indicates ice-water interface. Sites where brines are not visible indicate very low concentrations. Note axis break (dotted line) for high values observed at basal sections at sites 5, 11, 13 and 14.

To highlight the effect that increased biological activity may have on nutrient profiles the sites were divided based on mean Chl *a* concentration into low (sites 1, 3, 6, 8, 10), medium (sites 5 and 11), and high (sites 13 and 14) Chl *a* concentration. A one-way ANOVA revealed significant differences between the means of the high and low but not the medium Chl *a* concentration groups. The distribution of inorganic macronutrients (NO_2+NO_3, PO_4 and $Si(OH)_4$), were separated based on this distinction and plotted versus salinity (Fig. 3.5a - d).

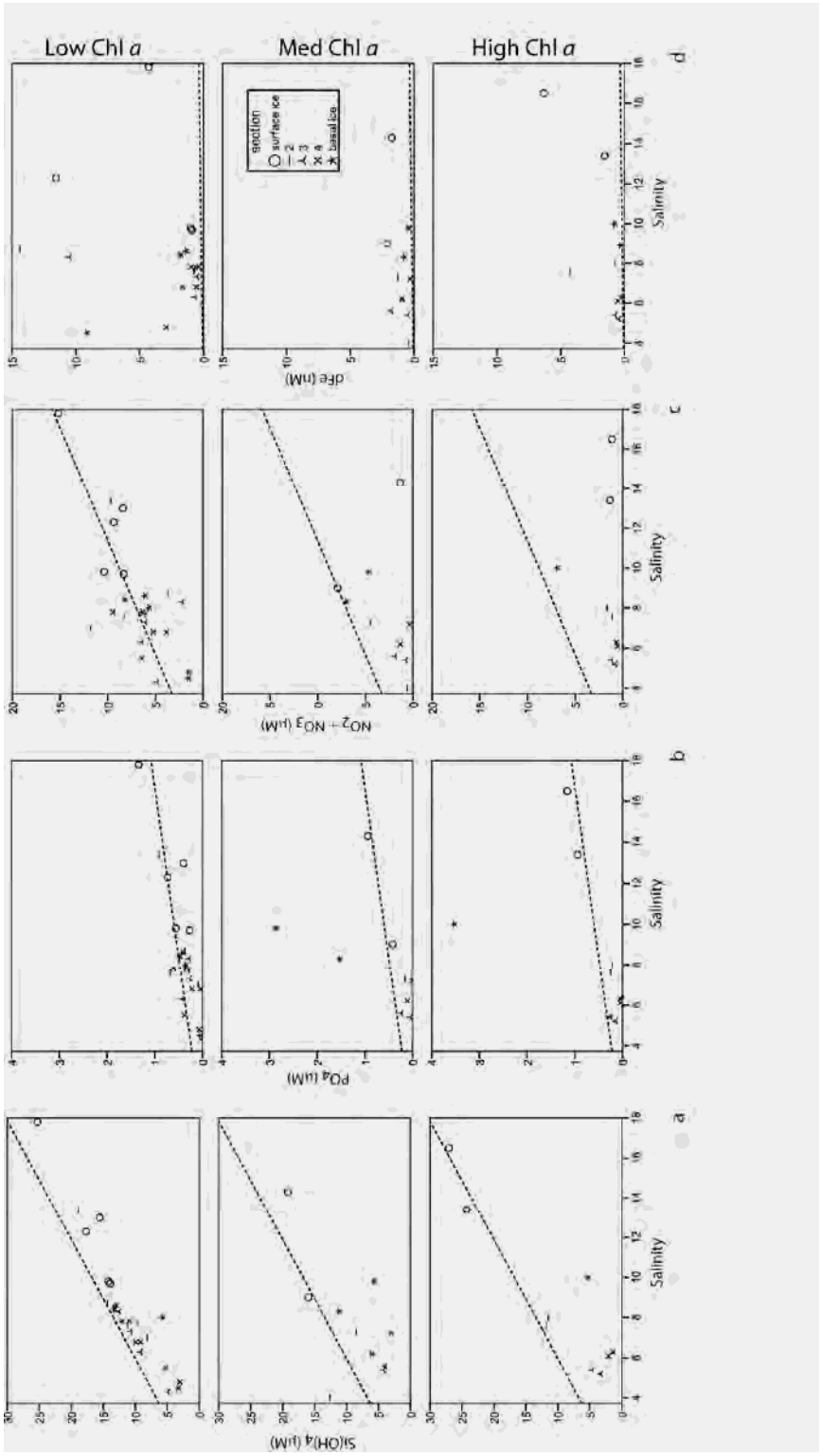

Figure 3.5: Nutrient versus salinity within sea ice: a) $Si(OH)_4$ µM, b) PO_4 µM, c) NO_2+NO_3 µM, d) dFe nM. Dotted line represents the theoretical dilution line (TDL). Sites are divided into high (13 and 14), medium (5 and 11) and low (all remaining) Chl *a* concentration.

In low Chl *a* ice (sites 1, 3, 6, 8, 10), $NO_2 + NO_3$ followed salinity in a conservative manner, whereby it was generally rejected or concentrated together with salts (Fig. 3.5b). Conversely, when biology was more abundant in the system (sites 13 and 14), $NO_2 + NO_3$ was drawn-down, significantly reducing its concentrations relative to the TDL (dashed line, Fig. 3.5c) (one-way ANOVA, $P < 0.01$). Similarly $Si(OH)_4$ at the low Chl *a* sites, followed the TDLs slope although most of the points were slightly below the TDL (Fig. 3.5a). At the high Chl *a* sites, more pronounced decreases relative to the TDL were observed particularly in the lowermost sections, however, overall the means were not significantly different. Conversely, PO_4 followed the TDL at low Chl *a* sites, but at the medium and high Chl *a* sites all of the basal ice sections ($n = 3$) were higher in concentration than the TDL (Fig. 3.5b). Mean sea ice concentrations of $Si(OH)_4$, $NO_2 + NO_3$ and PO_4 were 10.6 ± 6.27, 4.91 ± 3.67 and 0.54 ± 0.71 μM, respectively.

Mean bulk ice dFe was 2.38 nM and ranged from 0.23 – 14.4 nM (Fig. 3.7). Depth integrated (linearly interpolated) mean bulk ice dFe for all ice cores was essentially the same at 2.37 nM. Although highly variable, dFe was found in higher concentrations in the low Chl *a* cores (mean 3.56 nM) than in the medium (mean 1.04 nM) or high (mean 1.59 nM) Chl *a* cores (Fig. 3.5d). In contrast to the macronutrients, dFe was on or above the TDL at all sections for all sites. Within the basal sections only, mean bulk ice dFe was 3.19 nM at the low Chl *a* sites, whereas at the high Chl *a* sites it was 0.55 nM. Mean apparent (brine volume fraction × bulk ice dFe) dFe in the same basal sections was 24.8 nM low Chl *a*, and 2.37 nM high Chl *a*.

Brine dFe ranged from 0.49 – 14.8 nM, mean 2.46 nM. Seawater dFe ranged from <DL – 2.60, mean 0.63 nM. Snow dFe ranged from 0.22 nM at site 11 to 1.14 nM at site 6, mean 0.47 nM. Mean snow values at the cold (0.43 nM), transition (0.72 nM) and warm (0.25 nM) sites were similar. Dissolved Fe concentration in snow did not correlate with snow thickness.

Site
1
3
5
6
8
10
11
13
14
0
20
40
0
-20
-40
-60
-80
-100
Sea Ice thickness (cm)
POC : PON (μM : μM)

Figure 3.6: The POC:PON molar ratio at each site investigated. Dotted line represents the Redfield C:N molar ratio of 6.6.

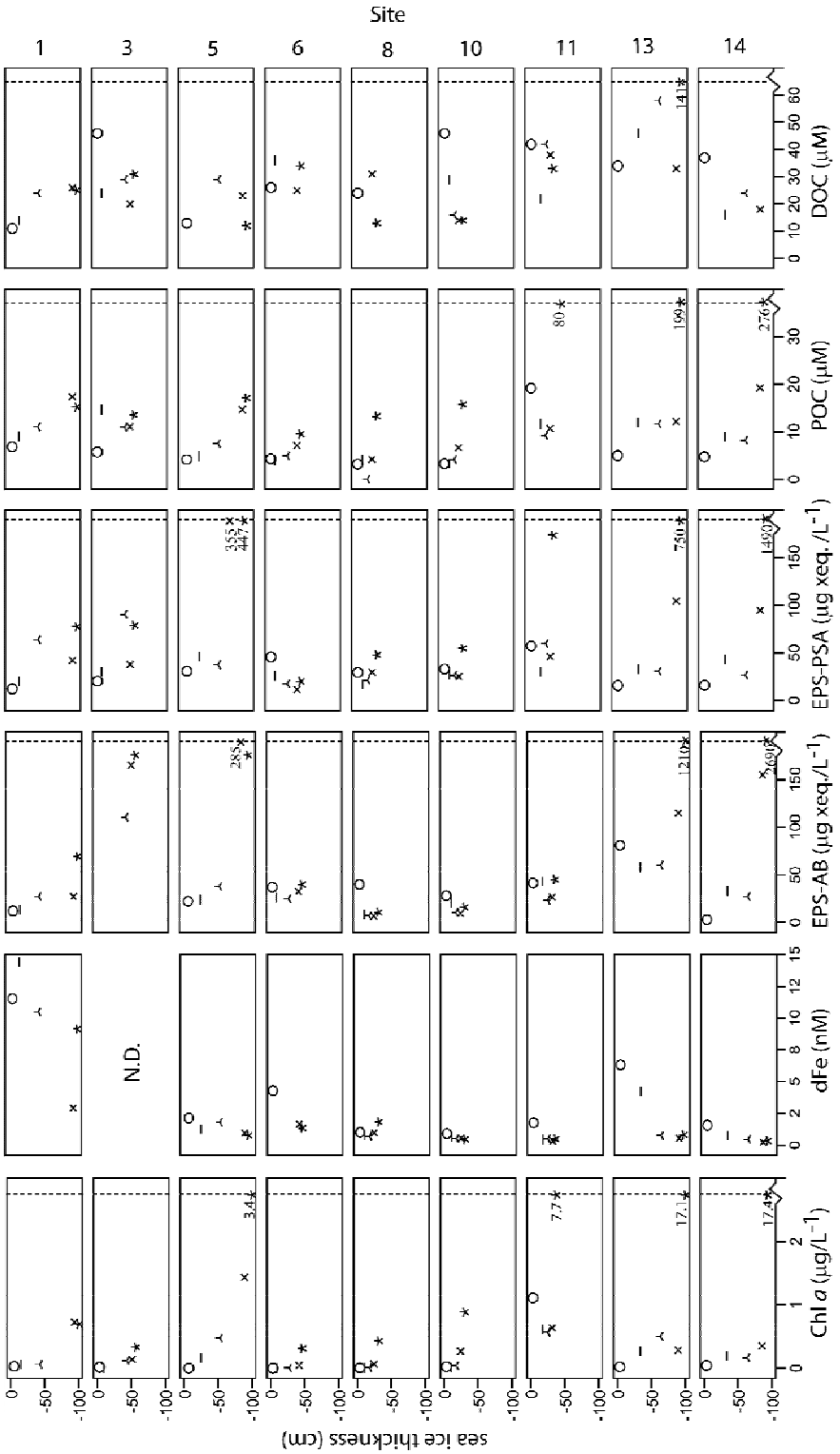

Figure 3.7: Sea ice profiles of Chl *a* (μg l^{-1}), dFe (nM), EPS (μg xeq.l^{-1}) (AB method), EPS (μg xeq.l^{-1}) (PSA method), POC (μM) and DOC (μM) at each site. ND: not determined.

The POC:PON ratio was elevated at the surface and some intermediate section of the cold and transition sites (1-10) (Fig. 3.6). Conversely, at the warm sites (11-14) all values were relatively lower and were in general very close to the Redfield C:N molar ratio of 6.6 typical of phytoplankton (Redfield, 1958). At all stations, the basal ice POC:PON ratio was approximately 6.6.

After inter-calibration, the PSA and AB methods produced values that correlated significantly at stations 1, 5, 13 and 14, but not significantly at stations 6, 8, 10 or 11 (Table 3.2). Similar EPS profiles and significant correlations were observed at the sites with higher overall concentrations while the correlation was weak at the lower concentrations. The exception to this is station 11 which was non-significant even though concentrations were higher at this site (Fig. 3.7). Log transformed values were linearly related (Model II regression) according to the equation:

$$\text{Log } \mu g \text{ xeq. } l^{-1} \text{ (PSA)} = 0.693 \times \text{Log } \mu g \text{ xeq. } l^{-1} \text{ (AB)} + 0.604, (R^2 = 0.746)$$

During the intercalibration, the mean filter capture efficiency for Xanthan Gum on 0.4 μm Nuclepore filters was 4.4 ± 0.7 %.

POC and EPS closely mirrored the concentrations of Chl *a* (Fig. 3.7). Low POC and EPS concentrations were found at most of the cold and transition sites, and higher values were observed at the warm sites particularly in the basal sea ice sections. POC concentrations varied greatly and ranged from 3.21 – 276 μM C with a basal ice mean of 70.9 μM C across all sites. EPS-AB concentrations varied by approximately 3 orders of magnitude from 2.84 to 2690 μg xeq. l^{-1} and the basal ice mean was 493 μg xeq. l^{-1}. C-shaped profiles were observed at three sites (6, 8, 10). In general, the highest POC and EPS concentrations were found within the basal ice particularly at the warm sites. The mean contribution of EPS-C to POC was 51 % (range 5 – 173 %) with variation between cores. Dissolved organic carbon was relatively constant both

vertically within ice core profiles and between sites. Mean DOC of all sea ice sections and stations was 30.5 ± 21 μM.

3.4.3. Property-property relationships

Correlations do not necessarily signify causality between variables and also do not rule out co-regulation by some common variable. However, in conjunction with graphing all data, these correlations do help identify trends. Significant correlations (non-parametric, Spearman's rho, $P < 0.01$) were observed between EPS - AB and POC ($R = 0.640$) and Chl *a* ($R = 0.509$) across all sites (Table 3.1). Chl *a* also correlated significantly with POC ($R = 0.824$) and EPS - PSA ($R = 0.684$). DOC did not correlate significantly with any measured variables. There was a relatively weak but significant inverse correlation between Chl *a* and apparent dFe ($R = -0.46$, $P < 0.01$) (Table 3.1). While a significant correlation was observed between apparent dFe and EPS-PSA, the very low R value (0.39) suggests a very weak relationship. No significant correlation was observed between EPS-AB and apparent dFe.

A significant inverse correlation (Spearmans rho $R = -0.619$, $P < 0.01$) was observed between EPS-AB per unit Chl *a*, and temperature. This result was driven primarily by strong logarithmic relationships at sites 6, 8 and 10 ($R^2 = 0.96$, 0.99 and 0.90 respectively, $P < 0.05$), while at the remaining sites the relationship was not significant.

			POC (µM)	DOC (µM)	Chl *a* (µg/L^{-1})	EPS-AB (µg xeq/L^{-1})	EPS-PSA (µg xeq/L^{-1})	apparent dFe (nM)
Spearman's rho	POC (µM)	Correlation Coefficient	1.000	-0.020	.824(**)	.640(**)	.706(**)	-.331(*)
		Sig. (2-tailed)	.	0.902	0.000	0.000	0.000	0.042
		N	45	40	45	43	45	38
	DOC (µM)	Correlation Coefficient	-0.020	1.000	0.071	0.234	0.040	-0.152
		Sig. (2-tailed)	0.902	.	0.663	0.157	0.807	0.392
		N	40	40	40	38	40	34
	Chl *a* (µg/L^{-1})	Correlation Coefficient	.824(**)	0.071	1.000	.509(**)	.684(**)	-.458(**)
		Sig. (2-tailed)	0.000	0.663	.	0.000	0.000	0.004
		N	45	40	45	43	45	38
	EPS-AB (µg xeq/L^{-1})	Correlation Coefficient	.640(**)	0.234	.509(**)	1.000	.625(**)	-0.158
		Sig. (2-tailed)	0.000	0.157	0.000	.	0.000	0.344
		N	43	38	43	43	43	38
	EPS-PSA (µg xeq/L^{-1})	Correlation Coefficient	.706(**)	0.040	.684(**)	.625(**)	1.000	-.389(*)
		Sig. (2-tailed)	0.000	0.807	0.000	0.000	.	0.016
		N	45	40	45	43	45	38
	apparent dFe (nM)	Correlation Coefficient	-.331(*)	-0.152	-.458(**)	-0.158	-.389(*)	1.000
		Sig. (2-tailed)	0.042	0.392	0.004	0.344	0.016	.
		N	38	34	38	38	38	38

Table 3.1: Spearman's rank correlation coefficients for POC, DOC, Chl *a*, apparent dFe, EPS-AB and EPS-PSA (sea ice only). The number of samples (n) is the sum of all sections and sites used in the correlation analysis. * = $P < 0.05$; ** = $P < 0.01$

Brines and sea water samples show relatively high concentrations of DOC and low concentrations of POC and EPS. Given that sack hole sampling potentially underestimates organic particulates due to their efficient attachment to brine channels (Krembs et al., 2001), we observed low concentrations of POC (mean 9.1 μM) and EPS (mean 50.9 μg xeq. l^{-1}) in the brines compared to the sea ice samples (basal ice mean 70.9 μM and 493 μg xeq. l^{-1} respectively).

3.5. Discussion

3.5.1. Physical variables

Based on ice temperature and Vb/V we can identify significantly different trends in the visited sites: sites 1 to 5 can be considered as cold winter, 6 to 10 as transition regime and 11 to 14 as warm, spring-type sites. An increase in air temperature at the transition and warm sites most likely influenced the observed increase in sea ice temperature. The ice textures at each site highlight the variable and dynamic conditions under which the sea ice grew. While sites 8 and 10 consisted of > 90% columnar ice, indicating calm conditions during ice formation, all remaining sites showed high proportions of granular ice and signs of deformation including rafting. As there is no trend in ice textures from sites 1 to 14, we infer that the physical conditions under which the ice formed had less influence on the enhanced biomass than changes in temperature and growth period would have had. However, it is evident from the good fit of the $Si(OH)_4$, $NO_2 + NO_3$ and PO_4^{3-} concentrations to the TDL, especially at the low Chl *a* sites, that physical processes were important in structuring at least these nutrient profiles.

The destructive nature of studying sea ice with traditional coring methods means that no single core can be resampled to follow a temporal evolution. Given the fact that significant sea ice

heterogeneity exists on the decimetre scale (Krembs et al., 2002b) a true temporal study should resample through time within a few meters of the original site. This was not possible in the present study and therefore all sites should be considered discrete. With this caution in mind, we believe we have observed a seasonal transition from cool winter conditions to early spring conditions.

The temperature profiles at each site show a significant warming from site 1 to 14. Due to the fact that sites 1 and 3, and sites 13 and 14 were at approximately the same latitude, we believe that this could be a winter to early spring transition. This warming trend is most poignantly highlighted in the increased brine volume fraction observed between the cold and warm sites which had mean values at 7.8 and 14.6 % Vb/V, respectively. This increased Vb/V has implications for the sea ice biota such as increased nutrient replenishment, increased habitable space and increased accessibility for larger heterotrophic predators (Becquevort et al., 2009; Krembs et al., 2000).

3.5.2. Exopolysaccharides

The two methods employed to measure EPS concentrations within the ice cores agreed well at sites 1, 5, 13 and 14 (Table 3.2). At the other stations (6, 8, 10, 11), the relationship was weak. This lack of correlation could stem from different size class or texture EPS particles at these sites, as the two methods used different pore size filters and vacuum. Also it could stem from actual differences between cores used for each analysis even though they were taken from within 10 cm of each other. However, it is most likely due to the low EPS concentration at these sites being close to the detection limit of the methods. The two methods measured EPS in different pore size fractions (0.2 vs 0.4 μm) and the PSA method also measured internal pools of polysaccharides. However, the agreement at sites 1, 5, 13 and 14, suggests that at these sites: (1) the internal pools are relatively insignificant compared to the external pools, and (2) the majority of the EPS is of the particulate form > 0.4 μm. This means that for future research,

either method could be employed with equal success to quantify EPS, particularly when concentrations are significantly higher than the detection limit. Although every effort was taken to minimise filter clogging, some of the higher values in the AB method may be affected by this methodological artefact. Furthermore, even though a smaller pore size was used for the PSA method, the higher vacuum used could have reduced some of these values due to smaller gel like particulates being drawn through the filters.

Table 3.2: Comparison of maximum and minimum concentrations as well as Pearsons correlation coefficients between AB and PSA EPS analyses. * = $P < 0.05$,; ** = $P < 0.01$

Station		EPS-PSA (μg xeq L^{-1})	EPS-AB (μg xeq L^{-1})	Pearson Correlation (Log transformed data)
1	max	77.5	69.3	0.91*
	min	12.2	12.1	
5	max	447.4	285	0.96**
	min	30.9	22.4	
6	max	45.7	39.6	0.23
	min	11.5	25.0	
8	max	47.9	40.0	0.22
	min	17.4	6.62	
10	max	54.7	28.0	0.32
	min	25.1	9.34	
11	max	174	45.0	0.24
	min	30.2	23.6	
13	max	750	1210	0.93*
	min	15.7	58.3	
14	max	1490	2690	0.97**
	min	16.0	2.8	

Sea ice EPS-AB concentrations varied by 3 orders of magnitude (2.8 to 2690 μg xeq. l^{-1} and averaged 141 μg xeq. l^{-1}). The mean concentration in basal ice was 490 μg xeq. l^{-1}. This is

relatively low in comparison to values observed during March (boreal spring) at a coastal fast-ice site near Barrow, Alaska by Krembs et al. (2002a) (790 – 7710 μg xeq. l^{-1}). However, our mean values are higher than the spring observations of Riedel et al. (2006) on the Mackenzie shelf (Canadian Arctic) during March (91-388 μg xeq. l^{-1}, mean 185 μg xeq. l^{-1}), but similar to values observed during November at the same site (mean 600 μg xeq. l^{-1}; Reidel et al. 2007). They also agree well with the range reported by Dumont et al. (2009) for early spring pack ice in the Australian Antarctic sector (20 - 2703 μg xeq. l^{-1}) and the Western Weddel Sea during spring-summer (3 – 3071 μg xeq. l^{-1}).

In the brines, the relatively low POC concentration (mean 9.1 μM) and EPS (mean 50.9 μg xeq. l^{-1}) compared to the sea ice samples (whole core mean 21.3 μM and 141 μg xeq. l^{-1}, respectively) indicate that these fractions may be attached to the walls of the brine channels, as suggested by Krembs (2001), and not easily dislodged into solution when collecting brines with the sack hole method. This could support the theory of biofilm development within the sea ice, as suggested by Becquevort et al. (2009), and therefore that the majority of EPS is of the surface-associated variety. The low particulate EPS and POC concentrations in seawater is likely due to these fractions remaining attached to the ice. In addition, those particles that eventuate in the underlying seawater would rapidly sink out of the water column leaving it deficient in POC and EPS, and relatively high in DOC.

3.5.3. Exopolysaccharide correlations

Sea ice Chl *a* concentrations correlated significantly with POC (R = 0.82) and EPS-AB (R = 0.64). Furthermore, the sea ice profiles were visually very similar, indicating that the majority of the POC and EPS were associated with approximately proportional concentrations of Chl *a*. Dissolved organic carbon did not correlate significantly with any measured variable (for all sites combined) and did not occur in "L-shaped" profiles. Instead, it remained relatively consistent

throughout each profile. Our data suggest that as Chl *a* increases with the spring-summer transition, EPS is actively produced by the sea ice microbial assemblage and this is superimposed over fossil organics incorporated into sea ice during formation. This observation is consistent with results of a study on exopolymeric particles in Antarctic pack ice sampled in the Bellingshausen Sea (Meiners et al. 2004), and also consistent with the results of Dumont (2009) in Antarctic pack ice.

Significant correlations were observed between both EPS methods, POC and Chl *a* across all sites (Table 3.1). The correlation between EPS and Chl *a* is in contrast to observations of Krembs et al (2002a) for coastal Arctic sea ice who noted that EPS did not correlate significantly with Chl *a*. Furthermore, Krembs et al. (2002a) noted a correlation between DOC and EPS which was not observed in the present study. Krembs et al. (2002a) noted that EPS concentration also correlated with bacterial abundance in their study. The observed differences between Krembs et al. (2002a) and the present study could reflect a greater autotroph:heterotroph ratio in the present study. This is evidenced by the coupling between Chl *a* and EPS and decoupling between EPS and DOC (i.e., there appears to be no relationship between the spatial and temporal distribution of EPS and DOC).

EPS-C averaged 51% of POC (range 5 – 173 %) and varied between cores. Although there was no apparent temporal trend, there was evidence of a higher contribution of EPS-C to POC in the interior and surface, compared with the basal sections. The range of EPS-C to POC was higher and varied more than those observed by Meiners et al. (2004; 2003) for the Antarctic (range 14 – 32 %) and Arctic (mean 24 %).

The highest outright values of EPS, POC and Chl *a* were always found within the basal layer, at the ice-water interface. Due to its proximity to seawater and its highly porous nature, the basal layer has several properties that make it favourable for algae growth including the warmest temperatures, lowest fluctuations in salinity and the highest rate of nutrient exchange with the underlying seawater (Thomas & Papadimitriou, 2003). This causes the data to be heavily

skewed towards this horizon. However, comparing the EPS per unit Chl *a* versus temperature, a significant and strong logarithmic relationship was observed at sites 6, 8 and 10, while at the remaining sites the relationship was not significant. This result could indicate that at these sites, as temperature decreases, EPS per unit Chl *a* increases exponentially.

This result should be interpreted with some caution as Chl *a* per cell is not a constant ratio and therefore, could have a confounding effect on this result. It is important to note that Chl *a* per cell can fluctuate based on photosynthetically active radiation (PAR) (Geider et al., 1996), and that snow cover and ice thickness could strongly influence PAR. However, snow cover was relatively consistent across all sites and no correlation between snow thickness and Chl *a* was observed. Furthermore, the mean sea ice thickness, and therefore light attenuation, was approximately the same at the first three sites (84 cm) compared to the last three sites (75 cm). Other possible explanations for this observation could be that EPS per unit Chl *a* can vary due to species specific rates of EPS production and/or that the ratio of algae to bacteria could vary throughout the profiles. Thus, bacteria are possibly producing the EPS enrichment at the mid to high ice core sections.

Our results may support the theory that one of the functions of EPS is cryoprotection for sea ice biota, as suggested by Krembs et al. (2002a) . By allowing supercooling, EPS can reduce the freezing point of the EPS/brine mix and therefore limit cell lysis due to freezing (Krembs & Deming, 2008). This could explain *in situ* production of EPS at the colder sections of the ice cores (i.e., closer to the surface). However, low concentration of Chl *a* in the colder sections and the presence of "fossil" organics incorporated during ice formation could also explain these results.

3.5.4. Biogeochemical variables

Dissolved Fe does not follow a conservative model of incorporation into sea ice. Rather, its concentration is most likely dependent on the biological activity (drawdown and bacterial

remineralisation) within the ice, the concentration within the water column during sea ice formation, and physical losses to the water column during brine drainage. In this study, the concentration of dFe did not follow the TDL and tended to be higher (Fig. 3.5d). When biological activity is at a minimum, $Si(OH)_4$ and NO_2+NO_3 that were incorporated into the ice during its formation, occur roughly in proportion to salinity. When Chl *a* is high, some of the nutrients are either drawn down by the sea ice biota or are lost via an increase in porosity/brine drainage, and thus the concentrations decrease relative to the TDL. Phosphate followed the TDL quite closely at all Chl *a* concentrations. The exceptions to this were 3 points that were considerably higher at the medium and low Chl *a* sites, all of which were the basal ice sections. Due to the very low sample number, interpretation is limited. However, cell lysis coupled with phosphorus remineralisation has been suggested as a probable explanation for PO_4 enrichment in sea ice (Thomas & Papadimitriou, 2003).

Dissolved Fe in the sea ice was found at low levels compared to the concentrations found in the Western Weddell Sea from November to January (sea ice range 0.70 - 36.8 nM, depth integrated sea ice mean 5.94 nM) (Lannuzel et al., 2008) or in east Antarctica during September to October (sea ice range 2.60 – 26.0 nM, depth integrated sea ice mean 10.7 nM) (Lannuzel et al., 2007). In the present study, the depth integrated, mean sea ice dFe concentration was approximately 2.5 times lower than Lannuzel et al. (2008) and 4.5 times lower than Lannuzel et al. (2007). Variability in the water column productivity and in the magnitude of the "new" iron supply (e.g., upwelling, lateral advection, delivery from shelf sediments) when sea ice formed could explain the differences in Fe concentrations measured in sea ice (Lannuzel et al., 2010).

In the basal sections only, at the high Chl *a* sites (13 and 14), bulk ice dFe was 0.55 nM compared to the basal ice mean at the low Chl *a* sites (1, 6, 8, 10; 3 N.D.) of 3.19 nM. This trend is reflected in the weak yet significant inverse correlation between Chl *a* and dFe. As the mean in the high and low Chl *a* seawater was 0.30 and 0.87 nM, respectively, we believe this deficit in dFe to be primarily the result of biological drawdown and conversion to the particulate

fraction, combined with a smaller fraction lost to the water column as brine drainage proceeds. We do not believe brine drainage to be the primary cause for the observed dFe profiles for the following reason: the brine salinities measured directly from sack holes below the -5˚ C isotherm (note this is not at the basal ice) at the high Chl *a* sites (13 and 14) were 80 and 69, respectively. These high values, relative to seawater, indicate that brine drainage (at least at the sampled ice section) was likely occurring during sampling as these high brine values would induce convective overturning until the salinity was closer to that of seawater. This brine drainage could lead to some losses of non-attached fractions of Fe. However, we know that in oceanic waters >99% of PFe is bound to organic matter (van den Berg, 1995) and that much of the dFe is associated with colloids (Gordon et al., 1997). This would most likely also be the case in sea ice as its composition reflects that of the sea water at the time of formation. As such, we could expect this complexed dFe, especially when associated with biologically released chelating ligands, to associate with attached particles or cells (Sunda, 2001) within sea ice and therefore reduce their loss to the water column when brine drainage occurs in the lower most sections. Thus, as observed in our study, dFe could occur in high concentration even while brine drainage is occurring.

Dissolved Fe was not associated with directly proportional concentrations of EPS or POC in our study. It was observed to decrease through the profile to the water column at 6 of the 8 stations measured. However, it was always elevated in the basal ice relative to seawater. Thus, if brine drainage was completely effective at removing the dFe from sea ice, then this horizon should be roughly equal to sea water. This was not the case and most likely reflects both the binding of dFe to organics such as EPS and bacterial remineralisation of the particulate Fe fraction to dFe within the basal layer.

The cores sampled during this study are indicative of newly formed sea ice, relatively unaltered by biotic activity except at the basal layers of the high Chl *a* sites. This is supported by the close fit of NO_2+NO_3 and PO_4 (and the reasonable fit of $Si(OH)_4$) to the TDL at the low Chl *a* cores,

indicating relatively unaltered conservative physical incorporation of these nutrients into the sea ice during its formation. Furthermore, the Chl *a* maxima observed at the ice water interface was always observed to be ~ 10 mm thick, and thus representative of a newly formed assemblage. Therefore, we can plausibly interpret the intermediate to high sea ice sections as being representative of initial stocks of dFe. Therefore, given the relatively unique characteristics of this sample set, we can make plausible assumptions that allow a calculation of a C:Fe ratio.

Assuming that surface dFe concentrations were representative of the initial stock of dFe incorporated into the sea ice during its growth, the difference between the dFe concentration at the surface and basal ice can be averaged to estimate algal uptake + losses to the particulate fraction and water column. This value, averaged for sites 11, 13 and 14, was 2.69 nM dFe and represents the observed uptake plus losses. Furthermore, we can estimate cellular carbon, without EPS contribution, by subtracting EPS-C from POC and then estimate the increase at the basal layer, by subtracting the mean sea ice surface value from the mean sea ice basal value. This mean value (sites 11, 13 and 14) was 95 μM C. Based on published C:Fe ratios for Fe replete large oceanic diatoms of 23,000 or 160,000 for Fe limited large oceanic diatoms (de Baar et al., 2008), we can estimate the expected Fe uptake given that we observed a mean of 95 μM of increased biomass. This equates to 4 nM of Fe uptake given a 23000 C:Fe ratio or 0.6 nM given a 160000 C:Fe ratio. Our observed uptake value was 2.69 nM, which includes some fraction lost and possibly non-bioavailable Fe species.

It is plausible from the decreasing trend in dFe coincident with increasing Chl *a*, that dFe should be further drawn down as Chl *a* increases throughout the growing season. The mean "apparent dFe" (Brine volume fraction × bulk ice dFe) in the basal ice of the high Chl *a* stations was 2.4 nM. This suggests no immediate iron limitation for the sea ice algae when we sampled, although the low iron concentrations in the under ice sea water may be limiting for phytoplankton growth. Here the low dFe values (mean 0.30 nM) could be approaching limiting concentrations for some species, since the large oceanic diatom *Chaetoceros dichaeta*,

for instance, has a half saturation constant (K_m) of 1.12 nM (Timmermans et al., 2001). However, the smaller diatom *Fragilariopsis kerguelens* has a K_m of 0.19 nM (Timmermans et al., 2004). These sea water dFe levels could co-limit algal development together with light and grazing at the time of sampling.

It is plausible to consider that one of the functions of EPS at the ice water interface is a means to bind dFe. Structural elucidation studies of Antarctic sea ice bacterial EPS produced in laboratory cultures have shown that uronic acids may be a significant component of EPS (Mancuso Nichols et al., 2005a). At ambient pH, the negatively charged carboxyl groups of uronic acid would make EPS efficient at binding positively charged cations such as Fe^{2+} and Fe^{3+} (Krembs & Deming, 2008). Therefore, if the cells were growing under low dFe conditions, as observed in the under ice sea water, it would be a competitive advantage to produce EPS and selectively bind trace nutrients that could be in low concentrations in the water column as the spring summer season progresses. In this way the biota can concentrate not only dFe, but other trace elements, and in doing so, enrich the microenvironment around each cell.

3.6. Conclusion

Although not specifically sampled to study a temporal evolution, we believe we observed the transition between cold, winter sea ice conditions and warmer, early spring conditions. Evidence for this is given in the increasing ice-temperature profiles together with the associated increasing brine volume fractions observed at each site. We observed the onset of high, spring Chl *a* concentrations coincident with increased EPS and POC concentrations, and decreased $NO_2 + NO_3$, $Si(OH)_4$ and dFe concentrations, consistent with biological drawdown and losses to the water column and particulate fractions. Estimates of cellular carbon to Fe ratios observed in the present study compared with published values suggest that the sea ice microbial biota was not limited by dFe concentrations but may have been by NO_2+NO_3 or $Si(OH)_4$. Conversely, under ice seawater algal communities may have been limited by dFe and/or light and grazing at

the time of sampling. EPS and POC correlate significantly with Chl *a* indicating the production of organic matter in the basal layers most likely by autotrophic sea ice biota. However physical incorporation of organics and nutrients into sea ice during its formation, primarily as a result of frazil ice scavenging and wave field pumping through columnar ice, likely structured the nutrient profiles. An inverse correlation between EPS per unit Chl *a* and temperature was observed, possibly supporting the theory of the role of EPS as a cryoprotectant. However, high concentrations of EPS within the basal ice coincident with elevated dFe relative to seawater, could plausibly be linked to the Fe binding properties of EPS.

3.7. Acknowledgments

We gratefully acknowledge the officers and crew of R.S.V. Aurora Australis, as well as colleagues and support personnel involved in the SIPEX expedition. This work was funded by the Australian Government's Cooperative Research Centres Programme through the Antarctic

Climate and Ecosystems Cooperative Research Centre (ACE CRC). This work was sponsored by an Australian Antarctic Science projects (#2767 and #3026). The participation of D.N.T. and L.N. was funded by the Natural Environment Research Council, U.K. We would like to thank Dr Tony Worby for his support and training during SIPEX. We are indebted to the Commonwealth Scientific and Industrial Research Organization, Marine Research division for providing a clean container for iron concentration enumeration during SIPEX. We are greatly indebted to Dr Christopher Krembs for providing valuable insight during the method development stage of this project. Many thanks to four anonymous reviewers, and internal ACE CRC reviewers Tom Trull and Benedict Pasquer for their valuable input, and to Dianna Davis for her training in processing the POC samples. The analysis for total nitrogen, carbon and hydrogen was determined by Dr Thomas Rodemann at the Central Science Laboratory, University of Tasmania.

3.8. Chapter 3 appendix

kilo	section	DATE (DD/MM/YYYY)	Long-S	Lat-E	Section depth (cm)	Depth adjusted Temp (°C)	Salinity	relative Vb/V %	ug glu eq. /L (PSA)	ug xeq. /L (PSA)	ug eq./L (AB)	ug POC/L	ug DOC/L	ug chl a/L	EPS-C (AB)	% EPS-C to POC	PO_4 (µM)	[Si] (µM)	$NO_2 + NO_3$ (µM)	dFe (nM)
1	SNOW				20		0.7		14.9	15.4	35.1	105		<DL	24.8	24	0.07	1.02	1.44	0.43
1	1	14/09/2007	64°13.773'	127°57.152'	5.0	-7.9	12.3	9.1	11.7	12.2	12.1	67.0	132	0.032	9.69	11	0.73	17.69	9.38	11.58
1	2				15.0	-8.8	9.7	9.5	16.2	19.6	13.8	109	166	0.089	16.2	9	0.57	14.33	3.76	14.41
1	3				43.0	-4.3	6.3	9.5	64.7	63.9	27.9	152	286	0.090	20.5	15	0.29	12.67	2.22	19.30
1	4				94.0	-2.0	4.6	11.6	42.4	42.2	27.3	256	312	0.729	22.0	12	0.07	3.06	1.51	3.62
1	5				100.0	-1.6	4.8	11.7	78.6	77.8	89.3	183	300	0.897	52.0	28	0.06	3.39	1.66	8.14
1	Deep Brine				60		106.0		88.6	97.0	64.3	178		0.519	48.2	28	4.58	141.8	72.10	3.53
1	Shallow Brine				30.9				47.4	47.1	51.8				89.9					2.85
1	Sea water 0m				0.0	-1.6	32.9		16.7	17.2	25.9	91.2	846	0.017	19.4	21	1.24	45.68	28.03	0.45
1	Sea water 1m				100.0	-1.6	31.9		19.4	20.4	47.9	64.8	492	0.018	35.8	55	1.05	49.95	28.52	0.41
2	SNOW				20.0		2.7				11.8	84.8		<DL	8.28	10	0.56	1.11	1.87	0.33
2	1	14/09/2007	64°24'	127°08'	3.0	-11.6	13.0	8.2	19.9	25.8		89.2	662	0.018			0.80	15.96	8.34	
2	2				9.0	-11.0	7.0	3.5	30.1	30.2		176	288	0.003			0.09	8.16	11.77	
2	3				43.0	-5.8	4.8	3.7	62.1	66.7	111	192	348	0.118	85.0	83	23.47	4.91	4.84	
2	4				91.0	-4.0	5.5	9.7	57.9	57.8	165	153	240	0.140	124	93	0.59	5.29	6.44	
2	5				97.0	-2.8	8.0	15.2	90.0	78.8	179	163	372	0.304	192	91	0.59	5.77	5.73	
2	Deep Brine				45	-5.0	141.2				34.0	86.5		0.322	25.9	39	10.09	41.18	33.00	1.24
2	Sea water 0m				0.0	-1.8	32.9				12.2	20.2	648	0.023	9.18	45	1.81	45.89	27.94	0.52
2	Sea water 1m				100.0	-1.6	31.9				4.89	25.0	612	0.029	3.64	15	1.56	49.12	27.66	0.36
5	SNOW				20.0		5.6					62.7	184	<DL			1.31	41.97	26.74	0.54
5	1	16/09/2007	65°31.897'	124°45.122'	7.0	-14.6	9.0	3.5	30.8	30.9	29.4	50.3	156	0.003	16.8	33	0.42	15.97	7.90	2.12
5	2				23.0	-15.3	7.2	3.5	40.7	46.4	23.8	59.6		0.159	17.9	30	0.58	9.46	4.50	1.27
5	3				53.0	-7.1	5.6	4.0	57.7	57.8	57.9	90.6	348	0.477	29.4	31	0.24	3.99	1.90	1.90
5	4				89.0	-5.3	6.2	9.2	364	356	285	178	276	1.43	215	121	0.11	6.05	1.56	0.94
5	5				95.0	-2.8	8.0	14.4	458	447	176	205	144	3.89	152	64	1.56	11.29	7.66	0.75
5	Deep Brine				99		43.0				31.4			0.240	58.6		4.68	134.5	73.76	2.38
5	Shallow Brine				60		105.2				59.0				44.3		1.60	152.9	76.54	3.26
5	Sea water 0m				0.0	-1.86	30.4				30.3	19.5	672	0.009	23.2	119	1.84	55.62	26.01	0.60
5	Sea water 1m				100.0	-1.89	31.6				18.4	15.9	629	0.010	11.3	71	2.43	64.34	28.75	0.34
8	SNOW				2.0		6.3				19.0	25.6	972	<DL	11.2	44	1.13	32.27	58.60	1.14
8	1	21/09/2007	65°35.304'	122°35.042'	3.0	+10.0	17.8	8.6	46.0	45.7	37.2	31.9	312	0.001	27.5	54	1.34	25.28	15.17	4.29
8	2				9.0	-9.2	13.4	7.6	23.8	26.0	26.0	46.6	432	0.002	19.5	42	0.91	16.89	8.73	
8	3								17.0	17.4	25.0	59.0		0.005	18.9	32				
8	4				41.5	-3.6	6.8	9.3	18.9	11.5	32.5	69.0	300	0.046	24.4	29	0.23	5.79	3.83	1.65
8	5				46.5	-2.6	8.6	16.4	19.5	19.9	39.6	114	408	0.314	29.1	26	0.42	13.62	8.16	1.35
8	Deep Brine				45	-2.4	45.7		6.80	7.30	40.9	39.4		0.044	30.7	84	3.82	75.48	44.02	0.79
8	Shallow Brine				30	-7.6	113.2		3.72	4.90	50.7	21.2		0.001	38.9	182	8.10	178.7	102.88	3.19
8	Sea water 0m				0.0	-1.86	33.9		5.06	5.81	31.1	59.7	840	0.011	23.3	139	1.91	58.18	27.69	0.60
8	Sea water 1m				100.0	-1.96	32.9		6.40	7.31	31.1	59.7	605	0.009	23.8	151	1.71	54.86	26.80	2.21
9	SNOW				3.0		13.1				<DL	46.6	324	<DL	0.16	0	1.11	19.45	13.62	0.48
9	1	25/09/2007	65°33.281'	119°52.480'	3.5	-4.5	9.4	10.7	29.4	29.5	40.8	24.8	288	0.006	20.0	76	1.56	14.23	10.49	1.01
9	2				10.5	-4.0	7.6	9.2	17.0	17.9	9.72	39.7		0.004	9.56	12	0.56	11.29	6.26	0.75
9	3				17.5	-3.5	6.3	6.7	21.0	21.4	7.06			0.010	8.30		0.42	8.19	6.42	0.68
9	4				24.5	-2.6	7.8	13.0	39.5	29.7	5.62	50.6	372	0.065	4.97	10	0.61	10.88	9.48	0.66
9	5				31.5	-2.3	9.4	16.2	46.3	47.9	10.7	99	156	0.437	9.02	8	0.48	13.09	8.36	1.62
9	Deep Brine				25	-2.6	42.4		23.6	24.1	16.1	51.3		0.184	12.6	23	3.42	75.19	37.20	0.49
9	Shallow Brine				15	-4.3	69.3				34.8	56.3		0.022	25.9	44	4.63	103.2	69.03	0.62
9	Sea water 0m				0.0	-1.85	31.4		<DL	<DL	27.9	23.7	684	0.039	20.7	87	1.63	59.16	27.63	1.00
9	Sea water 1m				100.0	-1.86	31.7		4.41	5.17	29.1	32.5	672	0.027	21.8	67	1.47	59.27	28.43	2.82
10	SNOW				15.0		5.6				9.91	54.5	228	<DL	6.16	10	1.53	30.54	10.66	0.53
10	1	30/09/2007	65°56.552'	119°07.065'	3.5	-8.5	8.7	10.8	33.1	33.1	28.0	39.4	552	0.024	21.0	117	0.27	13.60	8.39	0.89
10	2				10.5	-4.0	7.7	9.3	28.6	28.9	20.1	39.7	348	0.010	15.1	89	0.24	9.70	9.04	0.69
10	3				17.5	-3.5	7.3	10.7	28.2	29.4	10.5	50.0	192	0.042	7.89	72	0.27	10.16	8.16	0.51
10	4				24.5	-2.9	6.8	11.3	34.5	35.1	9.54	79.6	168	0.397	7.00	53	0.04	9.63	5.23	0.54
10	5				30.3	-2.4	7.8	16.0	58.2	54.7	16.0	589	168	0.686	12.0	35	0.36	12.05	9.43	0.45
10	Deep Brine				29	-2.2	33.1		12.8	13.1	20.9	43.4		0.218	15.0	34	4.76	59.86	32.49	0.57
10	Shallow Brine				15	-4.3	62.0				20.0			0.674	15.9		4.95	99.80	60.53	1.99
10	Sea water 0m				0.0	-1.94	33.1		6.19	3.94	10.0	39.8	540	0.040	7.49	45	1.47	50.96	26.34	0.32
10	Sea water 1m				100.0	-1.94	31.5		4.30	5.16	9.0	22.8	552	0.086	7.49	33	1.60	58.56	27.98	0.24
11	SNOW				20.0		0.5		<DL	<DL		54.5		<DL			0.56	5.42	0.89	0.31
11	1	3/10/2007	65°01.416'	117°41.570'	3.5	-2.8	14.2	29.7	57.9	57.2	41.4	230	504	1.11	31.0	30	0.64	15.16	1.94	1.76
11	2				10.5	-2.5	14.0	7.7	60.1	60.2	45.2	140	264	0.018	32.4	35	0.01	12.62	0.80	9.43
11	3				24.5	-2.4	5.4	10.8	60.2	59.8	29.6	110	324	0.060	17.7	46	0.05	4.22	2.77	0.93
11	4				31.5	-2.3	7.2	15.5	46.4	48.1	25.7	128	456	0.039	20.0	54	0.01	3.60	0.36	0.32
11	5				36.5	-2.2	9.5	22.6	177	173	45.0	364	396	7.47	33.7	26	2.86	5.73	4.60	0.47
11	Deep Brine				30		37.9		28.5	29.4	24.6	60.2		0.299	25.9	32	0.66	66.23	29.29	1.11
11	Shallow Brine				15		62.7		17.6	18.1	47.2	79.2		0.204	35.4	45	1.48	93.66	34.19	2.16
11	Sea water 0m				0.0	-1.88	31.7		<DL	<DL	12.7	14.4	564	0.012	9.50	66	1.83	55.73	27.99	0.53
11	Sea water 1m				100.0	-1.86	31.5		6.67	7.37	11.5	16.5	504	0.024	8.64	54	1.82	54.35	28.05	0.28
13	SNOW				12.5		10.1		<DL	<DL		31.5	408	<DL			0.12	6.86	0.91	0.33
13	1	6/10/2007	64°42.869'	118°48.926'	3.5	-9.4	10.6	13.0	15.2	15.7	31.1	66.0	408	0.023	69.8	172	1.16	27.00	1.11	6.55
13	2				33.5	-4.8	7.6	8.1	33.1	33.1	58.3	144	552	0.276	43.9	50	0.25	11.80	1.15	4.25
13	3				43.5	-3.3	6.4	8.1	39.8	35.9	60.3	140	696	0.552	45.2	68	0.25	4.87	1.21	6.74
13	4				49.5	-2.8	6.1	12.1	104	104	115	146	396	0.287	86.1	92	0.04	2.09	0.56	0.53
13	5				56.8	-2.2	10.0	23.1	768	780	1210	2580	1680	17.1	911	42	3.52	5.27	5.87	0.79
13	Deep Brine				80		79.1		31.7	31.8	51.8	200		0.629	38.9	19	3.77	104.2	47.76	14.78
13	Shallow Brine				30		62.0		53.6	51.6	39.6	403		1.42	29.7	7	4.48	156.1	84.50	0.68
13	Sea water 0m				0.0	-1.86	31.0		<DL	<DL	8.49	19.5	408	0.036	4.86	25	1.76	55.58	27.29	0.39
13	Sea water 1m				100.0	-1.85	31.1		<DL	<DL	<DL	19.2	504	0.018			1.85	54.06	28.03	0.45
14	SNOW				10.0				<DL	<DL		32.9		<DL						0.31
14	1	7/10/2007	64°16'	118°55'	3.5	-8.5	13.4	19.8	16.5	16.0	2.84	57.1	444	0.044	2.15	52	0.04	24.27	1.84	1.58
14	2				33.5	-4.3	9.2	9.2	42.9	42.7	33.2	107	192	0.199	24.7	56	0.22	11.50	1.06	0.74
14	3				53.5	-2.8	5.2	9.1	28.7	25.9	27.3	68.5	288	0.156	20.5	54	0.15	3.29	0.78	0.45
14	4				65.5	-2.0	6.3	15.3	96.4	94.8	155	291	216	0.555	116	76	0.05	1.41	0.67	0.23
14	5				93.5	-1.90	9.9	34.0	1530	1490	2660	3340		17.4	2020	98				0.32
14	Deep Brine				90	-4.6	68.7		139	150	90.0	266		1.48	71.2	29	1.21	89.47	17.52	0.92
14	Shallow Brine				25	-5.0	98.0		103	101	114	359		1.61	85.5	24	5.24	136.8	66.67	1.19
14	Sea water 0m				0.0	-1.84	31.1		<DL	<DL	7.26	20.0	708	0.021	5.40	27	1.75	58.30	27.61	<DL
14	Sea water 1m				100.0	-1.84	31.7		<DL	<DL	7.92	18.5	540	0.011	5.04	31	1.82	57.16	28.04	0.21
mean						-3.9	28.1	11.3	84.5	83.2	90.6	146.8	436.2	0.8	87.1	55.6	1.8	89.0	20.5	1.8
SD						2.8	29.6	5.8	214	208	329	444	246	3.66	241	56	5.95	42.86	22.28	2.32
sea ice only mean						-4.1	8.7	11.3	108.6	107.6	140.2	286.4	396.7	1.3	106.3	61.3	1.1	12.6	5.3	2.3
sea ice only SD						3.1	3.5	5.8	252	246	434	590	253	3.66	206	38	2.52	14.77	4.09	3.40
max						-1.8	141.2	26.7	1530	1490	2660	3340	1680	17.4	2020	182	10.47	178.7	102.6	14.78
min						-14.6	0.5	3.5	<DL	<DL	<DL	14.8	132	<DL	0.16	0	0.06	1.11	0.36	<DL

4. Iron fractionation in pack and fast ice in East Antarctica: temporal decoupling between the release of dissolved and particulate iron during spring melt.

This chapter is in press to be published:

van der Merwe, P., Lannuzel, D., Bowie, A., Mancuso Nichols, C., & Meiners, K. (In Press). Iron fractionation in pack and fast ice in East Antarctica: temporal decoupling between the release of dissolved and particulate iron during spring melt. Deep-Sea Research Part II Oceanographic Research Papers.

4.1. Abstract

Iron is a fundamental nutrient limiting phytoplankton growth in vast regions of the Southern Ocean. Sea ice, which covers ~80 % of the Southern Ocean (south of 60˚S) during maximum extent, can concentrate iron up to two orders of magnitude higher than in the underlying sea water. The fractionation of iron between the particulate and dissolved fractions depends on the location and type of sea ice formation and can impact on the bioavailability of this important trace element. This study is the first to document iron fractionation and concentration in both pack and fast ice during a single research study. Sampling was from within the 110-130˚ E sector of Antarctica. We observed markedly higher concentrations of particulate iron at our fast ice site (0.96 – 214 nM) relative to several pack ice sites (0.87 – 77.7 nM). Comparison of plFe and pFe revealed the highly refractory nature of the particulate enrichment at the basal layer of our fast ice site, thus indicating its sedimentary origin. A high particulate-to-dissolved iron ratio was observed at the fast ice site (285:1) relative to the highest observed in pack ice (23:1). This

suggests a decoupling between the sources and/or sinks of the dissolved and particulate fractions. Preferential release of dissolved iron (and not particulate iron) into brines at all sites sampled with the sack hole method (and therefore indicative of brine drainage), indicates the diffuse nature of the dissolved fraction. Furthermore, this indicates that there may be a temporal decoupling between the release of the dissolved and particulate fractions into the water column as sea ice becomes more permeable during the seasonal melt. Implications for phytoplankton production in Antarctic sea ice are discussed.

4.2. Introduction

The Southern Ocean is the largest High Nutrient Low Chlorophyll (HNLC) zone where phytoplankton production is limited by light, grazing and the micronutrient iron (Fe) (Bowie et al., 2001; Boyd et al., 2000; Martin et al., 1990a). Approximately 17×10^6 km^2 of the Southern Ocean is covered by seasonal sea ice and its formation and subsequent melt is one of the largest seasonal events on Earth (Lowe, 1997). While sea ice chemistry is commonly indicative of the seawater from which it formed (Eicken, 2003), its capacity to concentrate trace metals such as Fe up to two orders of magnitude higher than in the under lying sea water (Grotti et al., 2005; Lannuzel et al., 2008; Lannuzel et al., 2007), makes it a significant temporal storage of this important micronutrient element. The annual melt of sea ice releases this reservoir into the surrounding water column (Lannuzel et al., 2008; Sedwick & Ditullio, 1997). When the released Fe is coupled with the release of algae and stratification of the water column (Tagliabue & Arrigo, 2006), vast phytoplankton blooms are triggered (Fitzwater et al., 2000), which are observable by satellite. These large blooms substantially impact the local carbon cycle and the radiative properties of the atmosphere (Arrigo et al., 2008b; Boyd, 2007; Legendre et al., 1992) and therefore potentially play a significant role in global climate.

Fe bioavailability is difficult to predict and is a function of its chemical form, and the uptake strategies employed by the various biota (Hassler & Schoemann, 2009). However, the fractionation of Fe within sea ice between the dissolved and particulate phases should theoretically have a strong effect on the bioavailability of this reservoir. The dissolved fraction (dFe) consists of inorganic complexes, organically complexed Fe and small colloids (< 0.2 μm) which can be mobilised through photo-reduction or thermal dissolution (Rich & Morel, 1990). In oxic sea water dFe is present as FeII and FeIII, with the former being the most bioavailable but the latter the more thermodynamically favoured and therefore abundant (Croot et al., 2004; Rich & Morel, 1990). In sea water, the vast majority of Fe (>99 %) is bound to strong organic ligands (Macrellis et al., 2001; Rue & Bruland, 1995) and it appears that most phytoplankton and bacteria can access this pool via a reduction step to free the bound Fe at the cell surface (Hopkinson & Morel, 2009; Maldonado & Price, 1999). Organic complexation of dFe also generally increases its solubility by slowing the formation of Fe oxyhydroxides (Boye et al., 2001; de Baar & de Jong, 2001). Particulate Fe (pFe) is the result of coalescence of colloidal oxyhydroxides which will generally become more insoluble with time through the formation of more stable Fe oxides (Sunda, 2001) and thus, theoretically less bioavailable. Therefore, on this basis and in a general sense, dFe should be more bioavailable than pFe.

The location of sea ice formation, specifically its proximity to the continental shelf, may significantly affect the fractionation of the Fe reservoir due to advection of sedimentary pFe (de Baar & de Jong, 2001; Lannuzel et al., 2010; Sedwick et al., 2000). Furthermore, the release of Fe stored within sea ice upon melting may be non-linear and fraction-specific with temporal decoupling of the release of the particulate and dissolved fractions. These factors would have implications for the subsequent Fe dependent ice-edge phytoplankton blooms. Furthermore, no global ocean biogeochemical models currently include sea ice Fe. While sea ice is not a new

source of Fe, it can act as a significant temporal storage of this fundamental trace nutrient, only releasing it when conditions are coincidentally ideal for phytoplankton blooms. With large scale changes in sea ice thickness and extent forecast with climate change we may also expect changes in the distribution of this fundamental trace element within this HNLC zone.

The aim of this study was to investigate the fractionation of Fe observed in several sea ice locations both above and removed from the continental shelf within the 110˚ – 130˚ E region of East Antarctica during the onset of sea ice melting from September – October 2007. The data set collected is the first to quantify both the particulate and dissolved Fe fractions within land fast and pack ice and thus allows a direct comparison. Snow, brines and under ice seawater were also sampled to investigate if there is a preferential release of specific Fe fractions during melting/brine drainage. Our results are compared to the available data in the literature for Fe in Antarctic pack and fast ice. The possible effect of this release on the subsequent phytoplankton blooms is discussed.

4.3. Method

4.3.1. Sampling and sample processing

Sampling was carried out between 64˚ and 66˚ S in the 110˚ – 130˚ E region of East Antarctica during the transition from maximum sea ice extent (September) to the onset of melting (October) in 2007 (Fig. 4.1). This research was undertaken as part of the Sea Ice Physics and Ecosystem eXperiment (SIPEX) (Worby et al., this volume) onboard RV *Aurora Australis*.

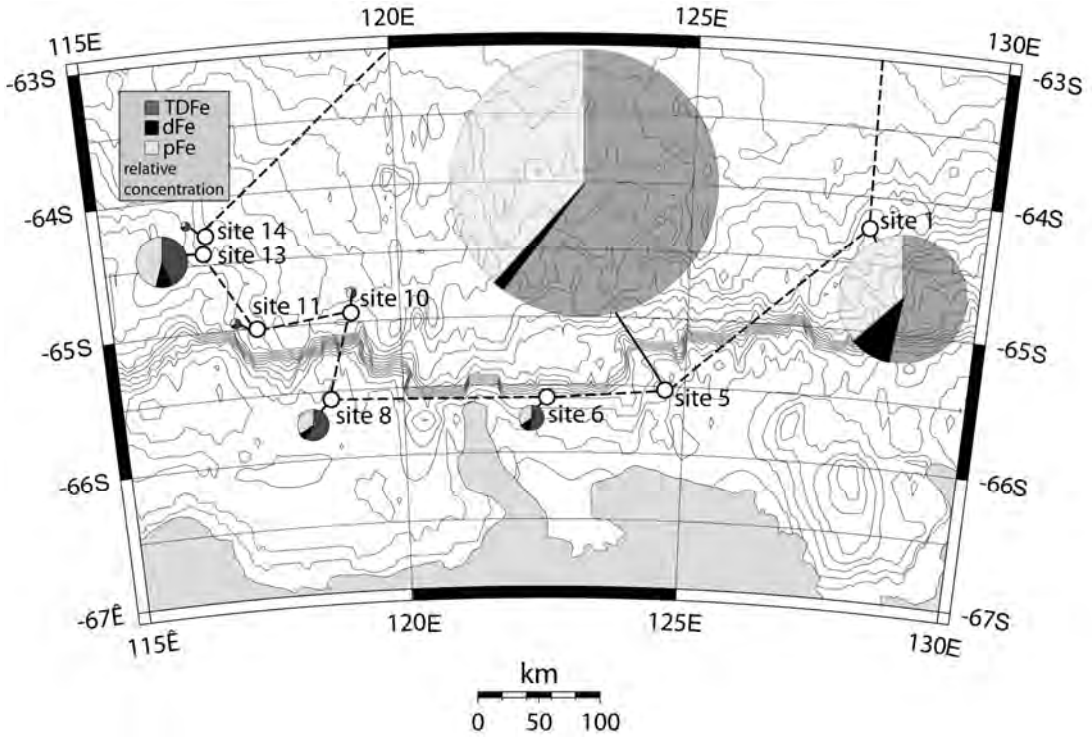

Figure 4.1: Fractionation of Fe into total dissolvable (TDFe), particulate (pFe) and dissolved (dFe) at each of the SIPEX sampling sites. Pie graphs are scaled to show relative concentration at each site investigated. Bathymetry contours represent 200 m increments. Image created using Online Map Creation (OMC) (Weinelt, 1996).

All samples were collected and analysed using trace metal clean protocols as described by Lannuzel et al. (2006) and van der Merwe et al. (2009). Briefly, all cores were collected up wind and at the greatest feasible distance from the ship. An electropolished, stainless steel corer (140 mm internal diameter) (Lichtert Industrie Belgium) was used to collect cores that were sectioned immediately on the ice using a stainless steel saw. The sections were placed in individual, acid cleaned, sealable polycarbonate containers and transported to a trace metal clean container on the ship. Core sections were melted in the dark at ambient laboratory temperature (18˚ C) for 12-18 hours or until melted. The corer and saw were cleaned immediately after each station by rinsing with copious amounts of deionised water (DIW) (>18.2 megohm) within the class 100

clean room, and allowed to dry at room temperature in front of a laminar flow hood before triple bagging for use in the field.

The corer used during SIPEX was the same design and manufacturer as in Lannuzel et al., (2006) which was proven to be non contaminating. Our electropolished stainless steel corer has titanium cutting chisels and the barrel and saw are made of high grade stainless steel which has a high percentage of chromium and nickel. As a precaution, we checked for stainless steel contamination by monitoring particulate chromium and nickel in all samples. By comparing the concentration of these metals in sea ice and in the sea water and snow, which had no metal sampling equipment used in their collection, any significant difference could imply either concentration within sea ice or contamination by the corer or saw. Results showed that for all of these elements, sea ice data were comparable with the concentration in snow and sea water. Although considerable variation in concentration can occur between these ice and water types, the comparable concentrations observed confirmed that there was negligible contamination from either the corer or the stainless steel saw. Furthermore, DIW used to rinse the corer and saw was collected, acidified and analysed on the FIA system to ascertain an Fe blank for this equipment. In all cases they were found to be negligible (i.e., below the detection limit (0.19 ± 0.06 nM) with one minute preconcentration (data not shown)).

Acid cleaned filtration devices fitted with acid cleaned 0.2 μm poresize, 47 mm diameter polycarbonate (PC) filters (Osmonics Inc) (stored in DIW) were used in a laminar flow hood, housed within a class 100 clean laboratory container. The melted samples were homogenised by stirring and then fractionated into total dissolvable (unfiltered, acidified to pH 1.8; TDFe), dissolved (0.2 μm filtrate, acidified to pH 1.8; dFe) and particulate (collected onto a 0.2 μm filter; pFe) samples. Seastar Baseline HCl was used for the acidification of these samples. TDFe and dFe samples were stored in low-density polyethylene (LDPE) bottles (Nalgene) in the dark

at ambient laboratory temperature until analysis in the home laboratory (3 months dFe, > 6 months TDFe) as per the recommendations of Bowie and Lohan (2009). pFe filters were stored in individual polystyrene petri dishes at – 20 ˚C before analysis at the Central Science Laboratory at the University of Tasmania (~ 12 months). Small particles within the samples can have high concentrations of Fe (Raiswell et al., 2008b; Raiswell et al., 2006), and therefore thorough mixing of the sample prior to filtration/sub-sampling (without rupturing cells) is important to minimise the effect of inhomogeneous particle distribution between subsamples/fractions. This methodological artefact may have influenced some of the results presented here and will be discussed later in the manuscript.

4.3.2. Particulate Fe

All digestion and evaporations were carried out under a laminar flow hood coupled to a suitable fume hood extraction. Acid and filter blanks, sample filters and Certified Reference Materials (CRM) were digested in 15 ml acid cleaned, Teflon PFA (perfluoroalkoxy) screw cap vials (Savillex) using a mixture of ultra pure, strong acids (500 µl 11 M HCl, 250 µl 16 M HNO_3, 250 µl 29 M HF) (Seastar Baseline) heated to 120 ˚C for 12 hours on a Teflon coated hotplate. Acid cleaned new filters were used for filter blanks and treated as per samples from the beginning of the digestion stage. This protocol, particularly the addition of HF, was used to ensure complete digestion of the most refractory particles. For a full analysis of digestion protocols and Certified Reference Material (CRM) recoveries see Lannuzel et al. (accepted) and Bowie et al. (2010). The samples were evaporated to dryness at 120 ˚C under a class 100 laminar flow hood. The dry residue was then resuspended in 10 % HNO_3 (Seastar Baseline) (10 ml final volume) and 10 ppb indium added as an internal standard. Samples were analysed by Sector Field Inductively Coupled Plasma Mass Spectrometry (SF-ICP-MS) (Finnigan Element I,

Thermo Scientific) (Cullen & Sherrell, 1999; Townsend, 2000) at a mass resolution of >3000 amu (10 % valley definition).

The SF-ICP-MS instrument was prepared for trace level analysis by installing a complete trace metal clean front end (i.e. new/cleaned cones, torch, spray chamber, pump tubes and nebuliser) and the instrument was purged for two days with alternating solutions of 5% HCl and 5% HNO_3 (1 hour each) and finally conditioned with the 10% HNO_3 sample matrix solution. A portable laminar flow hood was installed alongside the SF-ICP-MS to allow trace metal clean sample handling/loading. Samples were introduced to the SF-ICP-MS via a standard quartz concentric nebuliser (Glass Expansion, Melbourne, Australia) at a typical flow rate ~0.5 ml/min. A linear calibration was achieved by daily analysis of 0 (calibration blank), 1, 5 and 10 ppb standard solutions in 10% HNO_3. Duplicate measurements were performed on all samples to check for analytical reproducibility. The instrument sample introduction front-end was rinsed regularly during analysis with 10 % HNO_3, while a 5 ppb calibration standard was run periodically to check for analytical drift.

The digest acid blank average for Fe was 0.15 ± 0.05 nmol L^{-1} (n = 3), while the digested/evaporated filter blank average was 1.75 ± 0.29 nmol L^{-1} (n = 11). Therefore, the mean detection limit for pFe (3 × standard deviation of digested/evaporated filter blank) was 0.86 nmol L^{-1}. Analysis of CRM MESS-3 (Marine Sediments for Trace Metals, NRC Canada) for Fe, gave a mean value of 3.91 ± 0.15 mg L^{-1} (n = 8) which is a 90 % recovery of the certified value of 4.34 ± 0.11 mg L^{-1}. Analysis of CRM BCR-414 (Trace elements in Plankton, Commission of the European Community, Community Bureau of Reference) for Fe, gave a mean value of 1.87 ± 0.01 mg L^{-1} (n = 5) which is a 101 % recovery of the indicative value of 1.85 ± 0.19 mg L^{-1}.

4.3.3. Dissolved and total dissolvable Fe

For complete dFe analysis protocol, see van der Merwe et al. (2009). Briefly, all sample manipulation and filtering was performed within a class 100 laminar flow hood and standard trace metal protocols were employed. Analysis of dFe and TDFe samples were performed by flow injection analysis with luminol chemiluminescence detection (FIA-CL) with in-line preconcentration and matrix exclusion onto a 8-hydroxiquinoline (8-HQ) resin (FeIII method), adapted from de Jong et al. (1998) and Obata et al. (1993). This method has been recommended by the international program GEOTRACES (Bowie & Lohan, 2009). Reagent blanks were below the detection limit. The mean detection limit (3 × standard deviation of acidified DIW) of the FIA-CL method with 1 minute preconcentration was 0.19 ± 0.06 nM (n = 7). Analysis of SAFe (Sampling and Analysis of Fe) deep reference sea water D2 was 0.88 ± 0.05 nM (n = 9), which was not significantly different from the D2 consensus value of 0.91 ± 0.17 nM (one-sample t-test).

4.3.4. Chlorophyll *a*

Homogenised liquid samples for analysis were filtered onto 25 mm Whatman GF/F filters (volume range 310-2300 mL) immediately after collection and extracted in 10 ml of 100 % methanol for 12 h in the dark at 4 ˚C. Chlorophyll *a* concentration was determined on board according to the method of Holm-Hansen et al. (1965) using a Turner 10AU fluorometer (*in vitro* detection limit of 0.02 μg L^{-1}). .

4.3.5. Particulate Organic Carbon

Liquid samples (volume range 100 – 1000 ml) for analysis were filtered onto pre-combusted (550 ˚C for 12 h) 25 mm Whatman GF/F filters, stored at -20 ˚C and analysed within

3 months of sample collection. Particulate organic carbon was analysed using a Thermo Finnigan EA 1112 Series Flash Elemental Analyser (estimated precision ~1%) at the Central Science Laboratory, University of Tasmania.

4.4. Results and Discussion

4.4.1. Sampling sites

For an analysis of physical and biogeochemical parameters at the "trace metal site" during SIPEX, refer to van der Merwe et al. (2009) and for the "biological sites" refer to Meiners et al. (this volume). Briefly, there was a significant (1-way ANOVA, $P < 0.05$) warming of air and sea-ice between the first three sampling sites (1, 3 and 5) and the last three sampling sites (11, 13 and 14). This resulted in a significant (1-way ANOVA, $P < 0.05$) increase in mean brine volume fraction and mean Chl *a* concentration at the warmer sites. The fast ice site (# 5) was visually identified as such by being completely hemmed in by large icebergs to the west and north, its stationary character and the relatively shallow bathymetry (380 m) over which it was located (Fig. 4.1). Satellite imagery before, during and after the site occupation confirmed these field observations (P Heil, pers. comm.). Pack ice was found about 1 km to the north, separated from the fast ice by a narrow belt of fast moving sea ice (P. Heil, pers. comm.).

To avoid high standard deviations on arithmetic means, in most cases we have given total ranges of parameters or compared specific sections separately. Separate sections include basal ice only (lowermost 4-7 cm depending on total core length), the remainder of the core excluding basal ice, brines, seawater or snow.

4.4.2. Particulate Fe

Pack ice pFe ranged from 0.87 to 77.7 nM (Fig. 4.2). In the basal ice only, the mean was 6.9 ± 2.9 nM (n = 7), while the seawater below the ice (mean of 0 and 1 m depth) was 0.89 ± 0.76 nM (n = 11). Conversely, the fast ice site (5) ranged from 7.54 to 215 nM (mean 81.4 nM (n = 5)) and exhibited a strong L shaped pFe profile unlike any of the pack ice profiles (Fig. 4.2). The seawater below the ice at site 5 was also relatively high in pFe with a mean value of 1.7 nM (n = 2) (0 and 1 m depths). Interestingly however, the mean sea water dFe concentration at the same site was only 0.37 nM (n = 2) giving a mean pFe:dFe ratio of 4.5 (n = 2) (Table 4.1). The markedly higher mean pFe concentration in the fast ice were ~ 2.2 × higher than the next highest mean pack ice concentration (site 1). More strikingly however, the basal ice at the fast ice site was ~31 × higher than the basal ice mean in pack ice. This pFe enrichment, primarily to the basal ice, seems to be characteristic of fast ice and highlights the effect of sedimentary advection from the continental shelf which contains Fe almost entirely in the particulate fraction (Grotti et al., 2005). The pFe concentration in pack ice brines ranged from 0.11-3.74 nM, while at the fast ice site the pFe concentration in the deep brine was 0.96 nM and in the shallow brine was 2.12 nM. Thus, the pFe concentration in the brines from pack and fast ice sites were very similar even though the bulk ice pFe concentrations were often more than 10 × higher in the fast ice. This result suggests that the pFe, unlike the dFe, may be retained in the ice by attachment to or incorporation with attached organic matter within brine channels (Schoemann et al., 2008) or frozen into the ice itself.

Table 4.1: Comparison of all Fe fractions and ratios in a) pack and b) fast ice stations. Ranges, means and standard deviations are given for comparison. Note the number of samples used for each statistic varies particularly at the fast ice station.

A)

PACK ICE		TDFe	dFe	PLFe	pFe	pFe:dFe	pFe:PLFe
all data	mean	10.6	1.99	8.55	7.89	5.34	1.13
	SD	16.3	3.16	14.2	14.7	5.74	1.82
	max	104	14.8	93.8	77.7	27.3	10.5
	min	0.41	0.14	0.00	0.06	0.00	0.00
	N =	71	69	68	63	61	61
all sea ice	mean	15.4	2.62	13.0	13.0	7.52	1.73
	SD	21.1	3.65	18.9	18.1	5.40	2.30
	max	104	14.4	93.8	77.7	22.5	10.5
	min	1.17	0.23	0.71	0.87	0.84	0.23
	N =	36	34	34	35	33	33
basal ice only	mean	10.4	2.05	8.39	6.88	8.49	2.25
	SD	8.77	3.17	8.53	2.86	5.92	3.33
	max	1.36	0.32	0.89	3.00	0.84	0.43
	min	28.0	9.14	26.1	11.13	18.3	9.64
	N =	7	7	7	7	7	7
sea ice without basal ice	mean	16.6	2.77	14.2	14.6	7.26	1.59
	SD	23.1	3.80	20.7	20.0	5.34	2.00
	max	104	14.4	93.8	77.7	22.5	10.5
	min	1.17	0.23	0.71	0.87	0.97	0.23
	N =	29	27	27	28	26	26
snow	mean	2.90	0.48	2.42	3.37	8.80	1.39
	SD	2.09	0.32	2.00	4.11	9.19	0.54
	max	6.85	1.14	6.42	11.63	27.3	2.26
	min	0.70	0.21	0.49	1.10	2.40	0.90
	N =	7	7	7	6	6	6
sea water	mean	2.97	0.70	2.27	0.89	1.90	0.30
	SD	2.55	0.76	2.01	0.76	1.83	0.23
	max	7.44	2.60	6.44	2.02	5.76	0.70
	min	0.41	0.14	0.00	0.06	0.04	0.00
	N =	14	14	14	11	11	12
brine	mean	9.62	2.49	7.12	1.03	0.75	0.11
	SD	8.43	3.67	5.47	1.11	1.00	0.08
	max	34.3	14.8	19.5	3.74	2.86	0.26
	min	1.54	0.49	0.88	0.11	0.00	0.02
	N =	14	14	14	11	12	11

B)

FAST ICE

Site 5		TDFe	dFe	PLFe	PFe	pFe:dFe	Pfe:PLFe
all data	mean	65.45	1.38	64.07	41.58	46.10	0.69
	SD	116.42	0.98	116.54	70.51	90.92	0.95
	max	378.13	3.28	377.19	214.98	285.19	3.28
	min	2.97	0.34	2.43	0.56	0.40	0.09
	N =	10	10	10	10	10	10
all sea ice	mean	122.20	1.38	120.82	81.38	89.34	1.04
	SD	149.75	0.58	149.98	85.00	117.98	1.26
	max	378.13	2.12	377.19	214.98	285.19	3.28
	min	16.56	0.75	15.29	7.54	5.91	0.28
	N =	5	5	5	5	5	5
basal ice only		66.35	0.75	65.59	214.98	285.19	3.28
	N =	1	1	1	1	1	1
sea ice without basal ice	mean	136.16	1.54	134.63	47.98	40.38	0.48
	SD	169.12	0.53	169.48	46.87	50.76	0.14
	max	378.13	2.12	377.19	106.53	113.47	0.62
	min	16.56	0.94	15.29	7.54	5.91	0.28
	N =	4	4	4	4	4	4
snow		2.97	0.54	2.43	2.36	4.35	0.97
	N =	1	1	1	1	1	1
sea water	0 m	7.79	0.40	7.40	2.90	7.31	0.39
	1 m	6.88	0.34	6.53	0.56	1.63	0.09
brine	shallow	15.21	3.28	11.94	2.12	0.65	0.18
	deep	10.68	2.38	8.30	0.96	0.40	0.12

Table 4.2: Comparison of pFe concentrations in fast and pack ice. Ranges and mean values are also given for a fast ice study in Terra Nova Bay, Ross Sea by Grotti et al. (2005) and also the

first measurements (closest date to SIPEX and therefore most similar degree of melting) from a time series in Weddell Sea pack ice by Lannuzel et al. (2008).

		FAST ICE (pFe nM)					PACK ICE (pFe nM)						
		SIPEX	(n)	Grotti et al. (2005)	(n)	median	SIPEX	(n)	Lannuzel et al. (2008) Nov 29 ONLY	(n)	median	difference between fast and pack ice pFe (nM)	% increase in fast ice relative to pack ice
sea ice core (excluding basal ice)	range	7.5 - 107	(4)	26 - 627	(30)	163	0.87 - 77.7	(28)	10.1 - 38.9	(3)	22	141	87
	mean	**47.9**		**279**			**14.6**		**29.2**				
basal ice	range	n.a	(1)	869-1162	(5)	615	3.0 - 11.1	(7)	n.a.	(1)	74	541	88
	mean	**215**		**1015**			**6.9**		**141.2**				
underlying sea water	range	0.56 - 2.9	(2)	28.1-44.9	(5)	19	0.06 - 2.02	(11)	0.1 - 1.0	(2)	1	18	96
	mean	**1.73**		**36.5**			**0.89**		**0.55**				

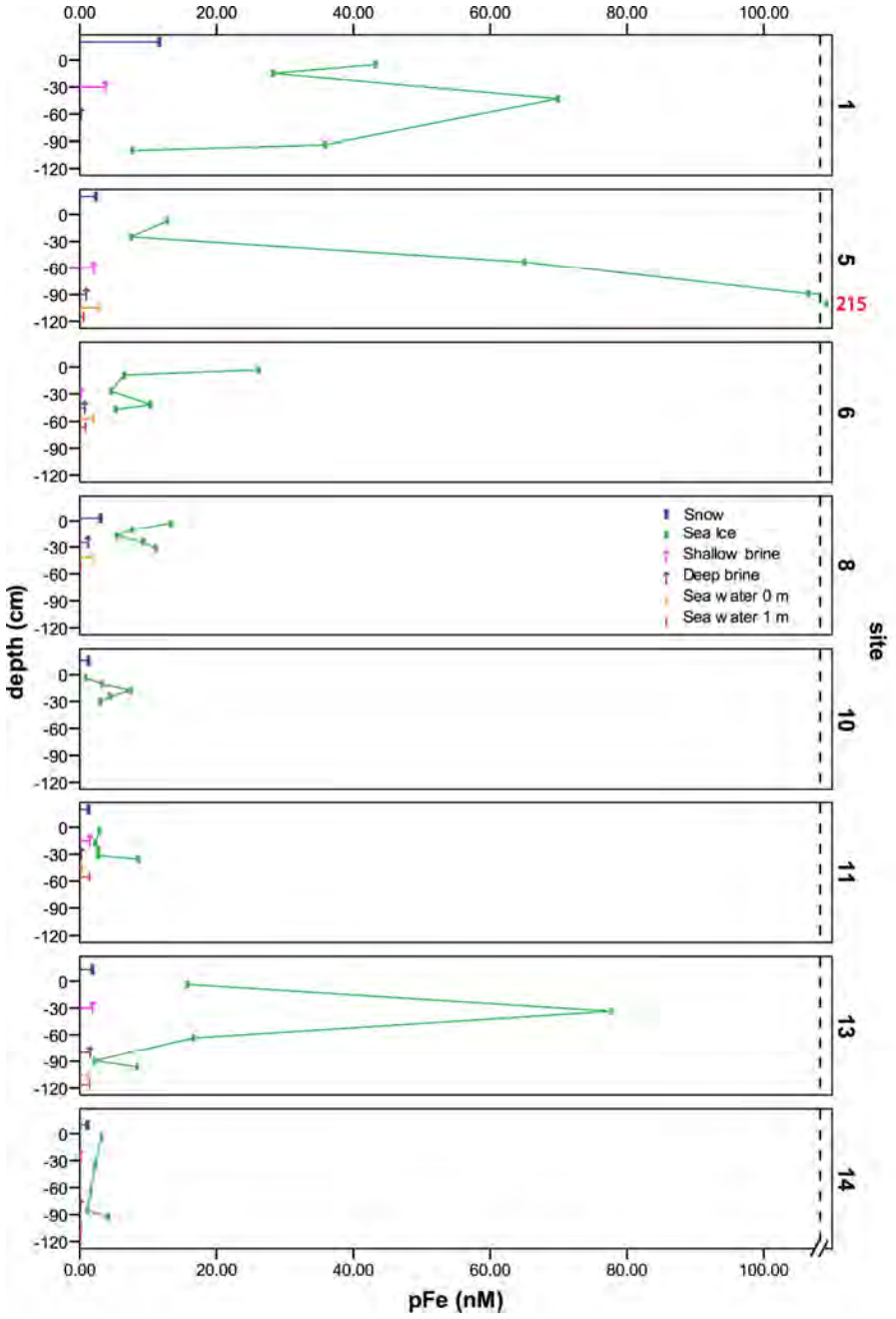

Figure 4.2: Particulate Fe (pFe) concentrations in fast ice (site 5) and pack ice (all other sites). Snow, sea ice and sea water (0 and 1 m) concentrations are displayed. Shallow brines (< 5˚ C) and deep brines (> 5˚ C) are displayed with upward facing arrows to indicate that they were collected by brine drainage from above into sack holes.

Grotti et al. (2005) sampled fast ice near the coast in Terra Nova Bay, Ross Sea Antarctica and recorded higher pFe values than during SIPEX (Table 4.2). The higher pFe values determined by the study can probably be explained by the 2 km distance to the coast of their sample site compared with ~ 75 km for site 5 during SIPEX. Furthermore, the Ross Sea shelf is one of the largest surrounding Antarctica and substantially wider than around East Antarctica. Therefore, there is more area over which sediment re-suspension and mixing could occur. The sea water depth that Grotti et al (2005) sampled above was 430 m compared with 380 m for site 5. Therefore, the proximity to the seafloor seems to have less of an impact on the differences in pFe concentrations between the two studies, compared to proximity to the coast and variability in regional advection processes. In particular, the Grotti et al. (2005) study site was adjacent to a seasonally persistent polynya that normally opens in January each year. Sedwick et al. (2000) attributed changes in dFe and dMn in the Ross sea polynya to changes in upwelling of metal rich bottom water and input from melting sea ice. Therefore, the sea ice formed when the mixed layer was deep in this coastal, latent-heat polynya is likely to contain more trace metals due upwelling of nutrient rich deep water and entrainment during sea ice formation.

4.4.3. Dissolved Fe

Dissolved Fe profiles including seawater, brines and snow are presented in Figure 4.3. Briefly, we observed a general transition from high to low dFe concentrations down the sea ice profiles at sites 5, 6, 10, 11, 13 and 14 (Fig. 4.3). This decreasing trend is most likely due to both uptake by sea ice algae, conversion to the biogenic particulate fraction and losses to the water column through brine drainage (van der Merwe et al., 2009). Brine dFe concentrations at sites 5, 6, 10, 11, 13 and 14 were elevated compared with the associated sea ice mean indicating that dFe was either concentrated into the brines during sea ice formation or remineralised from pFe *in situ*.

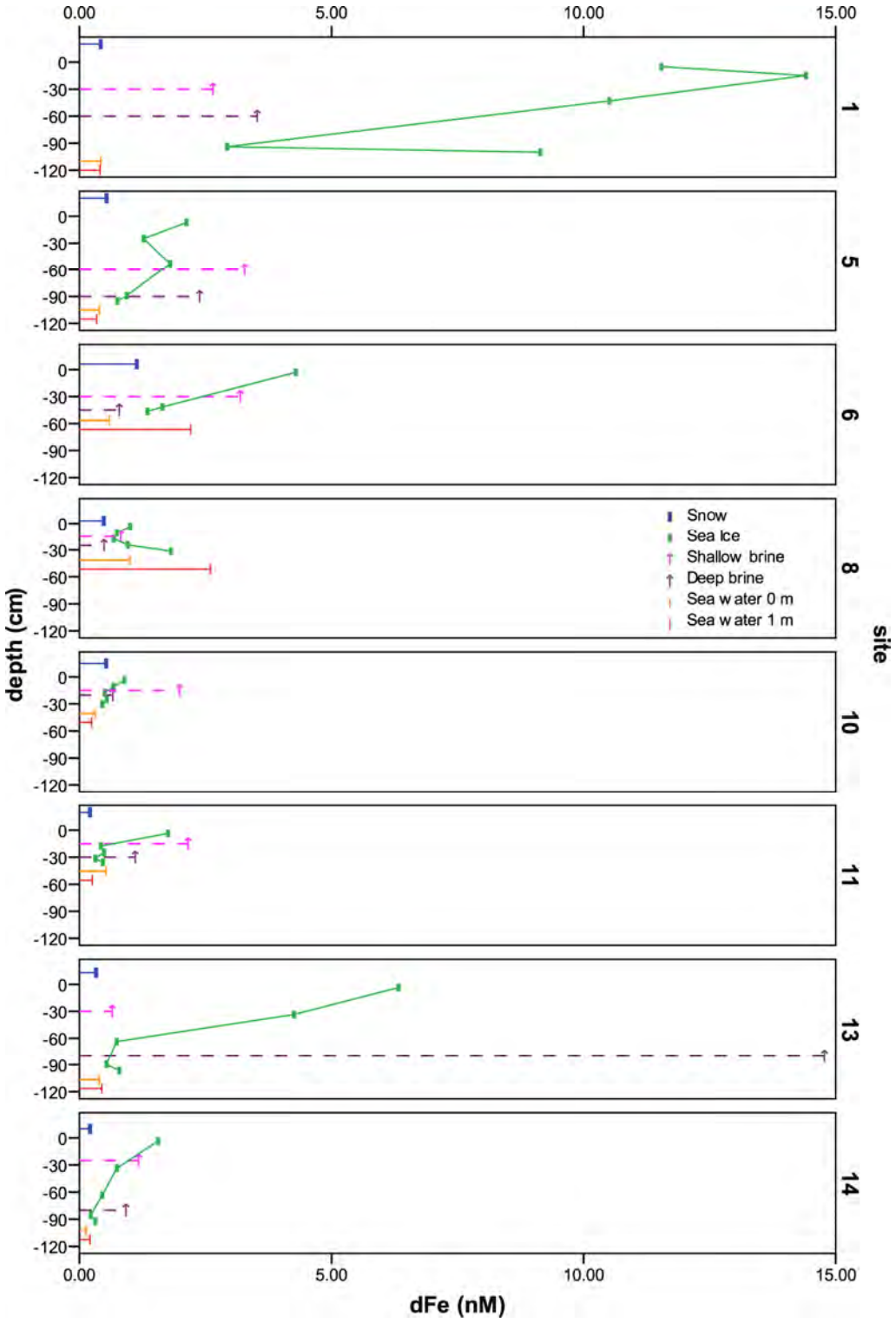

Figure 4.3: Dissolved Fe (dFe) concentrations in fast ice (5) and pack ice (all other sites). Snow, sea ice and sea water (0 and 1 m) concentrations are displayed. Shallow brines (< 5˚ C) and

deep brines (> 5° C) are displayed with upward facing arrows to indicate that they were collected by brine drainage from above into sack holes.

At site 1, where the ice was particularly cold and impermeable, the Chl *a* concentrations were low and the mean sea ice dFe concentrations were significantly higher (1-way ANOVA, $P < 0.01$). Interestingly, dFe concentrations within the fast ice at site 5 were not significantly different from pack ice sites 6-14 (1-way ANOVA, $P < 0.05$). Thus, the high pFe concentrations observed at the fast ice site occurred independently of the dFe, possibly implying independent sources and/or sinks for each fraction.

4.4.4. Particulate to dissolved Fe ratio

The pFe:dFe ratio plotted for all sites highlights the high particulate content at the fast ice site (5) relative to the dissolved fraction (Fig. 4.4). Mean pFe:dFe in the pack ice was 7.5 ± 5.4 (n = 33) while at the fast ice site it ranged from 5.9 to 285, with a median ratio of 140 (n = 5). At this site the basal ice pFe:dFe ratio is more than 10 times that of the nearest pack ice section. Furthermore, the sea water immediately below site 5 had the highest pFe:dFe ratio for sea water observed during the study period. The pFe:dFe ratios calculated from Grotti et al. (2005) also show a strong bias towards the particulate fraction in fast ice, although being an austral summer study (5th November-11th January) some brine drainage, and possibly loss of dFe, may have already occurred. Their mean values for the pFe:dFe ratio were 131 within sea ice, excluding the basal ice, 175 within the basal ice only and 33 in the seawater below the ice. Due to the large difference between the dFe and pFe at site 5 of SIPEX, the Fe source must have been primarily particulate at that site. The alternative explanation that dFe was supplied in proportion to pFe at site 5 and subsequently lost due to brine drainage or biological uptake would be unlikely due to the time of year of sampling (18th September, early austral spring) and resultant

unequalised brine salinities indicating a lack of thorough brine drainage (van der Merwe et al., 2009). Also, we observed a relatively low Chl *a* concentration (max 3.39 μg L^{-1}) indicating an algal community with a low standing stock and therefore less likely to alter the dFe concentration. The physical conversion of dFe to pFe cannot be ruled out; however, the magnitude of the differential between dFe and pFe was not observed at any of the pack ice stations with similar physical conditions.

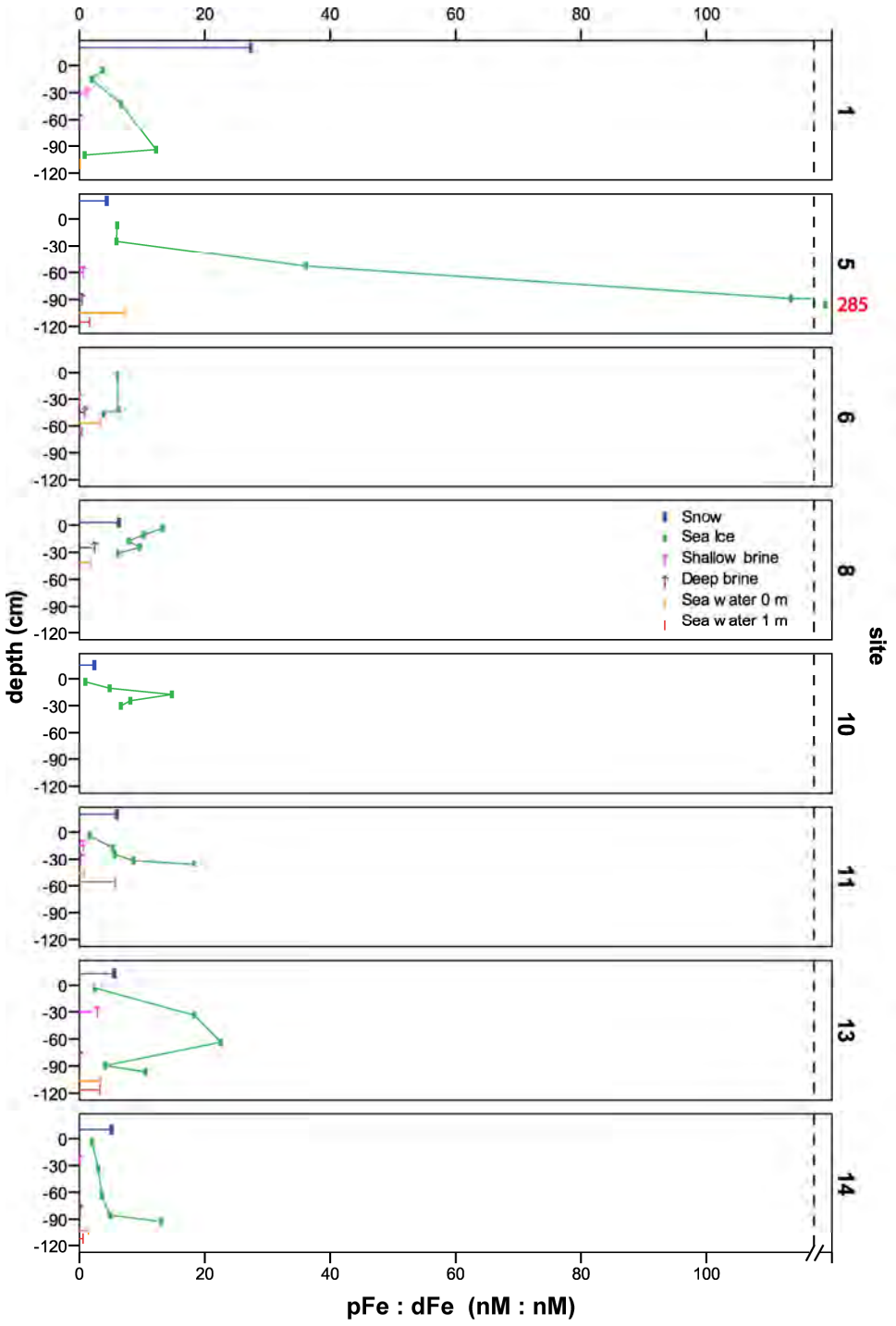

Figure 4.4: Particulate : dissolved Fe ratio (nM:nM) in fast ice (5) and pack ice (all other sites). Snow, sea ice and sea water (0 and 1 m) are displayed. Shallow brines (< 5˚ C) and deep brines

(> 5˚ C) are displayed with upward facing arrows to indicate that they were collected by brine drainage from above into sack holes.

Due to the Fe scavenging processes occurring during frazil ice formation, sea ice unaltered by biological activity, should represent the Fe concentration (albeit generally elevated) in the seawater from which it formed (Lannuzel et al., 2010). The pFe:dFe ratio at site 5, 11, 14 and generally for site 13, increases down the sea ice profiles. Unlike site 5, sites 14, 13 and 11 had the highest outright Chl *a* concentrations (basal ice max, 17.4, 17.1 and 7.7 μg Chl *a* L^{-1} respectively) (Appendix 1). For these pack ice sites, this trend could be interpreted as a conversion of dFe to pFe in these lower sections through biological processes. That is, Fe uptake by ice algae and conversion to biogenic particulate Fe coupled with some fraction of dFe lost to the water column through brine drainage. In contrast, site 5 had 2–5 times less Chl *a* and 3–25 times more pFe, indicating that biological activity had less to do with the observed profile at site 5 than input from sedimentary sources.

Snow represents an individual niche in Antarctic sea ice as its Fe content is almost exclusively derived from atmospheric and extraterrestrial input (Johnson, 2001). During SIPEX, the pFe:dFe ratio was generally consistent within the snow (mean 4.97 ± 1.4, n = 7, except for site 1). This suggests that snow Fe fractionation within the study region is somewhat homogeneous, similar to that found by Edwards and Sedwick (2001) at 3 sites in East Antarctica, and could be due to homogeneity in the composition of the major sources to snow; dust and extraterrestrial Fe (Edwards & Sedwick, 2001; Johnson, 2001).

4.4.5. Total dissolvable Fe (TDFe)

TDFe is measured on an unfiltered subsample and is operationally defined as all Fe that can be released into solution after > 6 months at pH 1.8 (Bowie et al., 2004). Therefore, TDFe is a measure of the "easily exchangeable" or "labile Fe", but does not include the most refractory and hence least bioavailable fraction of the pFe pool. TDFe was also elevated at the land fast ice site with values reaching 378 nM at section 4 within the profile, ~3.5 times higher than the next highest pack ice section (Fig. 4.5). These high values at the fast ice site imply that the Fe particles, which were 91 – 99.8 % of the TDFe (calculated by subtracting dFe from TDFe), were released into solution with a relatively mild acid treatment (pH 1.8 for > 6 months). Therefore, these particles at sections 1-4 were not highly refractory in nature. This cannot also be said of the basal ice (section 5) at site 5, as the high concentration of PFe was only observed after a strong acid treatment (see next section) Site 1 had the next highest TDFe concentrations, due to the high dFe contribution while the remaining sites were relatively low in comparison.

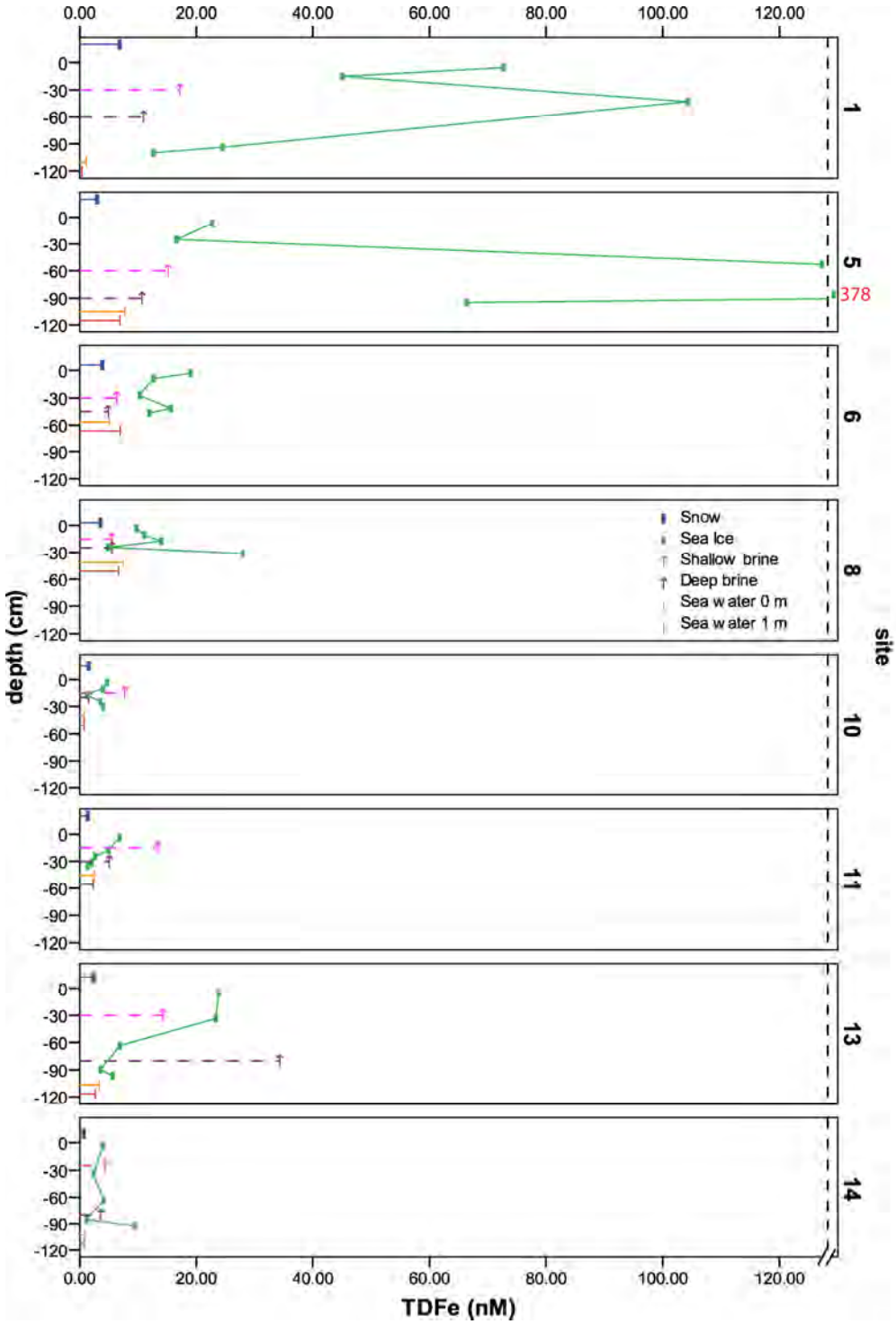

Figure 4.5: Total dissolvable Fe (TDFe) concentrations in fast ice (5) and pack ice (all other sites). Snow, sea ice and sea water (0 and 1 m) concentrations are displayed. Shallow brines (< 5˚ C) and deep brines (> 5˚ C) are displayed with upward facing arrows to indicate that they were collected by brine drainage from above into sack holes.

4.4.6. Particulate leachable Fe (plFe)

The difference between TDFe and dFe, plFe may have limited bioavailability to phytoplankton as it includes Fe fractions leached into solution over a period of > 6 months at pH 1.8. plFe and pFe should be similar with the exception that pFe, unlike plFe, quantifies most of the refractory particles (Bowie et al., 2010). Indeed, during SIPEX the two variables correlate significantly (log transformed data, Pearsons Corr., $R = 0.679$, $P < 0.001$), although some of the plFe values are higher than the pFe (Fig. 4.6). This methodological artefact is most obvious in the seawater and brine samples due to the low concentrations generally observed in these fractions. One possible explanation is that small particles or EPS bound aggregates of algae may have been present in one sub-sample and not in the other leading to sample heterogeneity (Lannuzel et al., 2008). This highlights the difficulties of completely homogenising samples without rupturing fragile algae cells and we recommend special attention to be paid to this step in future studies. With this caveat in mind, at the fast ice site (5), the maximum plFe concentration was observed at sea ice section 4, which was >6 cm away from the ice-water interface. Conversely, at sea ice section 5 (basal ice), the plFe concentration was approximately 150 nM lower than the pFe concentration. Due to the strong acid treatment required to leach the pFe fraction, this indicates the highly refractory nature of the Fe at this horizon and is thus most likely sedimentary in origin. In contrast, this was not clearly observed at any of the pack ice stations (Fig. 4.2 & 4.6).

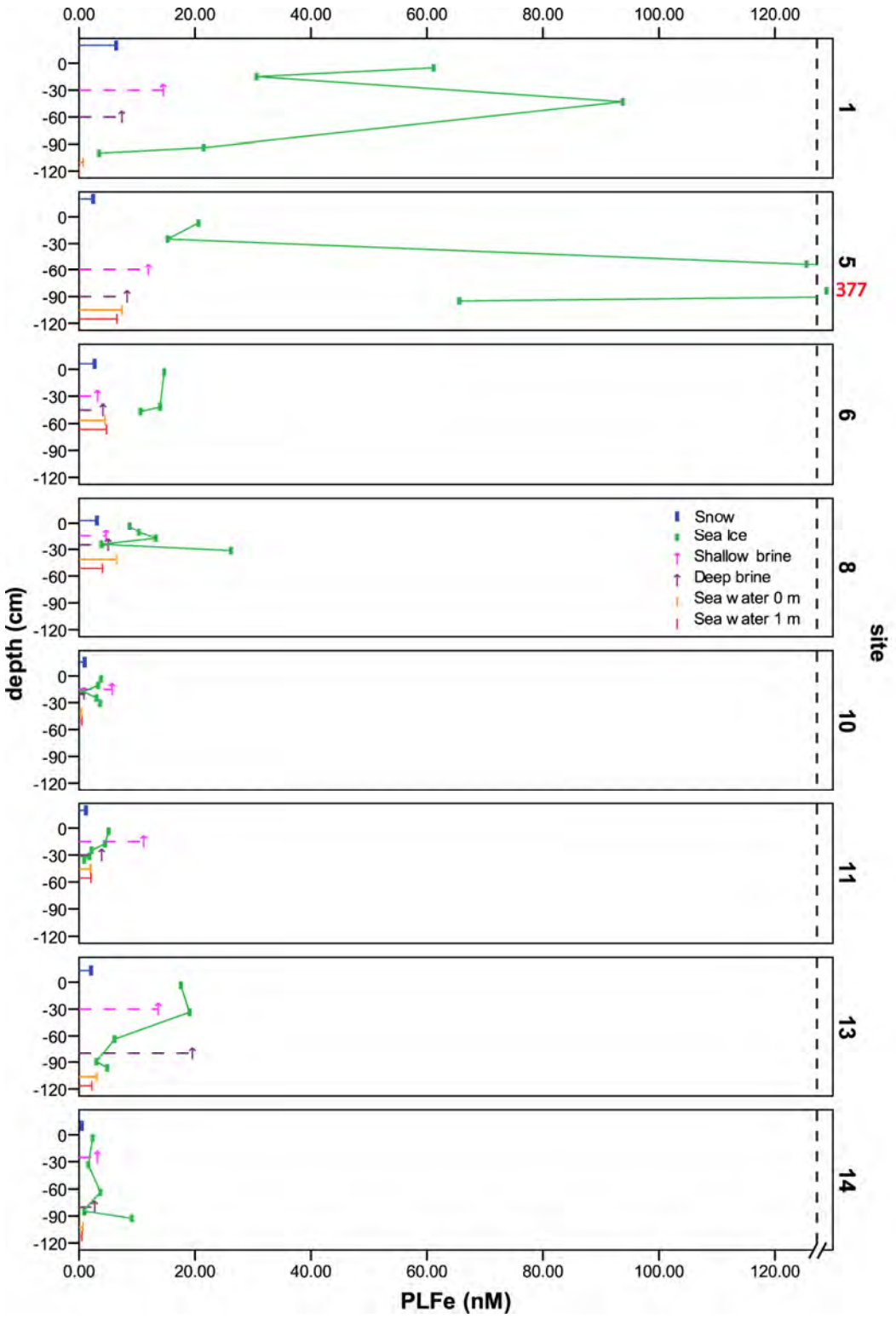

Figure 4.6: Particulate leachable Fe (plFe) concentrations in fast ice (5) and pack ice (all other sites). Snow, sea ice and sea water (0 and 1 m) concentrations are displayed. Shallow brines (<

5˚ C) and deep brines (> 5˚ C) are displayed with upward facing arrows to indicate that they were collected by brine drainage from above into sack holes.

4.4.7. Temporal decoupling in the release of Fe fractions

The collection of brines by the sack hole method is a good proxy for brine drainage into the water column. Thus, when looking at the pFe:dFe ratio for brine and the corresponding sea ice (Fig. 4.4), we observe that the sea ice is generally highly enriched relative to the brines for pFe, while for dFe the brines are generally more enriched. This suggests that pFe, unlike dFe, is not easily released into the water column via brine drainage. Lannuzel et al. (2008) showed that 70% of stored dFe was released from melting pack ice over a period of approximately 10 days (November 29 – December 9). However, an increase in brine volume fraction and porosity due to melting most likely occurred from before the study period commenced, as historically melting occurs from late October onwards (Worby et al., 1998). The release of dFe through brine drainage would likely be controlled by the density differential between seawater and brines, until an equilibrium is formed with seawater, at which point, only limited exchanges would occur through diffusion (Tison et al., 2008). This would allow a somewhat gradual release of dFe into the underlying seawater, the duration of which would depend on ice thickness, salinity and local temperature regimes. Furthermore, this suggests that pFe together with organic matter is released into the water column later in the season due to physical release after melting rather than brine drainage. Therefore, there may be a temporal decoupling of the release of the particulate and dissolved fractions into the water column.

As this process leads to a sustained release of both dFe and then pFe over the melting season it would be more effective at triggering ice edge blooms by pelagic phytoplankton than a large rapid pulse. This is due to the fact that dFe, which has a very short residence time (Hunter & Boyd, 2007), may be fully utilised before being oxidised into Fe hydroxides and lost to depth as

would be more likely if a rapid pulse occurred (Blain et al., 2007). Phytoplankton species composition may be affected as well. Mesoscale Fe enrichment experiments have shown that diatoms generally out compete and dominate during rapid pulse enrichments (Boyd et al., 2007). Conversely, a sustained release of dFe first and then subsequently pFe, could result in enriched water column concentrations over a longer period as observed by Grotti et al. (2005) and Lannuzel et al (2008; 2007). The subsequent release of pFe would be generally less bioavailable, however photo-reduction, thermal dissolution and mobilisation by strong organic ligands (Rich & Morel, 1990) particularly of Fe colloids (>0.2 μm) would aid the transformation of pFe to dFe. Photo-reduction would be particularly enhanced at this time of the season with increased light attenuation due to less snow and ice cover. This leads to retention/transformation of Fe into forms generally accessible for phytoplankton coincident with the lowering of planktonic Fe demands (Tagliabue et al., 2009b). This would likely occur concurrently with water column stratification driven by freshening of surface waters with melt water, thus producing favourable phytoplankton growth conditions (Tagliabue & Arrigo, 2006).

4.4.8. Input of continental shelf derived pFe to fast ice

The vast majority of the Fe at the fast ice site was in the particulate fraction. The dFe was not significantly different at the fast ice site compared to the pack ice, except site 1. Therefore, it is possible to estimate the amount of pFe incorporated into fast ice as a result of sedimentary advection from the continent. This estimate of the excess pFe in fast ice compared to pack ice is based on our measurements of pFe in fast and pack ice, those of Lannuzel et al (2008) for pack ice, and those of Grotti et al (2005) for fast ice (Table 4.2). This incorporates all the published sea ice pFe measurements to date. The ranges and mean values used in this calculation are summarised in Table 2. Due to the lack of data we assumed that the

concentration of pFe decreases linearly from the coast to out over the shelf break. The median value between our value from the outer edge of the fast ice and the Grotti et al. (2005) value from the inner coastal ice can be used as a general estimate.

In all sections including sea ice core without basal ice, basal ice only and underlying seawater, we see between 87 and 96 % more pFe at the fast ice sites relative to the pack ice (Table 4.2). Although considerable variability between measurements exists, this translates to 541 nM supplied to the basal ice, 142 nM supplied to the rest of the sea ice core and 18 nM supplied to the underlying water column. We attribute this large increase in pFe to be due primarily to sediment advection from the shelf (Bowie et al., 2009; de Baar et al., 1995; Sedwick et al., 1997) and to a lesser extent, sediment input from ice bergs (Loscher et al., 1997; Raiswell et al., 2008a; Smith et al., 2007) that surrounded site 5. This fraction (particularly in the basal ice) was refractory in nature, and thus would be generally less bioavailable in its immediate form.

4.5. Conclusions

Markedly higher concentrations of pFe were observed in fast ice compared to pack ice. This result is supported by the independent studies of both Grotti et al. (2005) for fast ice and Lannuzel et al. (2008) for pack ice. This data, particularly the pFe sea ice concentrations, significantly adds to the literature database on different chemical forms of Fe in Antarctic sea ice and is of vital importance for coupled biogeochemical models. The high pFe : dFe ratio observed at the fast ice site relative to the pack ice indicates a decoupling between the sources and sinks of the dissolved and particulate fractions. It also implies that the non-refractory particulate fraction may not be readily converted to the dissolved fraction at a rate capable of offsetting the losses/conversions. Preferential release of dFe, and not pFe, into brines sampled with the sack hole method indicates the diffuse nature of the dissolved fraction. Furthermore,

the preferential release demonstrates that there should be a decoupling between the release of the dissolved and particulate fractions into the water column as sea ice becomes more permeable and melts during spring. The release of bioavailable dFe through brine drainage and then subsequently, potentially bioavailable pFe (after transformation), may result in enriched water column Fe concentrations over a sustained period. A sustained release of Fe is similar to natural Fe fertilisation, as seen for instance over the Kerguelen plateau (Blain et al., 2007), rather than an artificial pulse enrichment. Therefore the higher efficiency of the biological pump and thus carbon sequestration characteristic of natural Fe fertilisations (Blain et al., 2007) should be expected of these ice edge blooms, further adding weight to their role in carbon cycling in seasonally ice-covered waters of the Southern Ocean surrounding Antarctica.

4.6. Acknowledgments

We gratefully acknowledge the officers and crew of R.S.V. *Aurora Australis*, as well as colleagues and support personnel involved in the SIPEX expedition. This work was funded by the Australian Government's Cooperative Research Centres Programme through the Antarctic Climate and Ecosystems Cooperative Research Centre (ACE CRC). This work was sponsored by Australian Antarctic Science projects (#2767 and #3026). We would like to thank Dr Tony Worby for his support and training during SIPEX. We are indebted to the Commonwealth Scientific and Industrial Research Organisation (CSIRO) Marine and Atmospheric Research for providing a trace metal clean container laboratory during SIPEX. This manuscript was improved by the input of two anonymous reviewers so we thank them for their time and effort. We would like to thank Dr Ashley Townsend for his invaluable mentoring and support with the SF-ICP-MS analyses. The analysis for total nitrogen, carbon and hydrogen was determined by Dr Thomas Rodemann at the Central Science Laboratory, University of Tasmania.

4.7. Chapter 4 appendix

Appendix 1: Values for depth adjusted temp (˚C), relative brine volume fraction (Vb/V %), POC (μg l^{-1}), Chl *a* (μg l^{-1}), TDFe (nM), dFe (nM), plFe (nM), pFe (nM), pFe:dFe (nM:nM), POC:pFe (μg l^{-1} :nM) (site 5 is fast ice, all remaining are pack ice). Data is summarised (mean, SD, maximum and minimum) for each section in the lower table.

Station	Section	DATE (DD/MM/YYYY)	Long-S	Lat-E	Section depth (cm)	Depth adjusted temp (°C)	relative Vb/V %	ug POC/L	ug chl a/L	TDFe (nM)	DFe (nM)	PLFe (nM)	PFe (nM)	PFe:DFe	POC:Pfe
1	Snow	11/09/2007	64°13.773'	127°57.132'	20			105	<DL	6.9	0.4	6.4	11.6	27.3	9.0
1	Shallow brine				30					17.2	2.7	14.5	9.7	1.4	
1	Deep brine				60			175	0.519	10.9	3.5	7.4	0.2	0.1	949
1	Sea ice section 1				5	-7.9	8.1	82.0	0.032	72.7	11.5	61.2	43.2	3.7	1.9
1	Sea ice section 2				15	-6.8	6.5	109	0.069	45.0	14.4	30.6	28.3	2.0	3.8
1	Sea ice section 3				40	-4.3	9.5	132	0.060	104	10.5	93.6	69.9	6.7	1.9
1	Sea ice section 4				84	-2.0	11.8	208	0.728	24.5	2.9	21.5	35.9	12.2	5.8
1	Sea ice section 5				100	-1.9	11.7	185	0.697	12.6	9.1	3.5	7.7	0.8	23.7
1	Sea water (0 m)				100	-1.8		91.2	0.017	1.2	0.4	0.7	0.1	0.1	1640
1	Sea water (1 m)				200	-1.8		64.6	0.018	0.4	0.4	0.0		0.0	
5	Snow	18/09/2007	65°31.465'	124°45.122'	20			47.7	<DL	3.0	0.5	2.4	2.4	4.4	20.2
5	Shallow brine				60					15.2	3.3	11.9	2.1	0.6	
5	Deep brine				90				0.240	10.7	2.4	8.3	1.0	0.4	
5	Sea ice section 1				7	-14.6	3.5	50.3	0.002	22.7	2.1	20.6	12.8	6.0	3.9
5	Sea ice section 2				25	-11.3	3.5	58.8	0.158	16.8	1.3	15.3	7.5	5.9	7.8
5	Sea ice section 3				53	-7.1	4.0	90.6	0.477	127	1.6	125	65.0	39.1	1.4
5	Sea ice section 4				89	-3.3	9.2	178	1.43	278	0.9	277	107	112	1.7
5	Sea ice section 5				95	-2.8	14.4	205	3.39	66.3	0.8	65.6	215	285	1.0
5	Sea water (0 m)				95	-1.66		19.5	0.009	7.8	0.4	7.4	2.9	7.3	6.7
5	Sea water (1 m)				195	-1.86		15.9	0.010	6.9	0.3	6.5	0.6	1.6	28.5
6	Snow	21/09/2007	65°35.304'	122°35.043'	2			23.6	<DL	3.9	1.1	2.7		0.0	
6	Shallow brine				30	-7.6		21.2	0.001	6.4	3.2	3.2	0.2	0.1	126
6	Deep brine				45	-2.4		35.4	0.044	4.9	0.8	4.1	0.7	0.9	49.4
6	Sea ice section 1				3	-10.0	9.6	51.9	0.001	19.0	4.3	14.7	26.2	6.1	2.0
6	Sea ice section 2				9	-9.2	7.8	46.8	0.002	12.6			6.5		7.2
6	Sea ice section 3							59.0	0.005	10.3			4.6		12.8
6	Sea ice section 4				42	-3.6	6.3	85.0	0.046	15.6	1.6	14.0	10.3	6.3	8.2
6	Sea ice section 5				47	-2.6	16.4	114	0.314	12.0	1.3	10.6	5.2	3.9	21.8
6	Sea water (0 m)				47	-1.86		18.7	0.011	5.1	0.6	4.5	2.0	3.4	9.2
6	Sea water (1 m)				147	-1.85		15.7	0.009	7.0	2.2	4.8	0.8	0.4	18.8
8	Snow	25/09/2007	66°33.281'	118°52.480'	3			40.6	<DL	3.8	0.5	3.1	3.1	6.3	13.3
8	Shallow brine				15	-4.3		58.3	0.022	5.5	0.8	4.6		0.0	
8	Deep brine				25	-2.8		51.3	0.194	5.5	0.5	5.0	1.2	2.5	42.5
8	Sea ice section 1				4	-4.5	10.7	38.6	0.005	9.7	1.0	8.7	13.4	13.3	2.9
8	Sea ice section 2				11	-4.0	9.2	50.7	0.004	11.1	0.7	10.3	7.7	10.2	6.6
8	Sea ice section 3				18	-3.5	8.7		0.010	14.0	0.7	13.3	5.4	7.9	
8	Sea ice section 4				25	-2.9	13.0	50.6	0.065	4.9	1.0	3.9	9.3	9.6	5.5
8	Sea ice section 5				32	-2.3	16.2	159	0.432	28.0	1.8	26.1	11.1	6.1	14.3
8	Sea water (0 m)				32	-1.86		23.7	0.009	7.4	1.0	6.4	1.9	1.9	12.8
8	Sea water (1 m)				132	-1.86		32.6	0.007	6.7	2.6	4.1	0.1	0.0	326
10	Snow	30/09/2007	64°56.553'	119°07.985'	15			54.5	<DL	1.5	0.5	1.0	1.3	2.4	42.8
10	Shallow brine				15	-4.3			0.074	7.7	2.0	5.7		0.0	
10	Deep brine				20	-2.2		43.4	0.216	1.5	0.7	0.9		0.0	
10	Sea ice section 1				3.5	-4.5	10.6	39.4	0.024	4.7	0.9	3.8	0.9	1.0	45.4
10	Sea ice section 2				10.5	-4.0	6.3	39.7	0.010	4.0	0.7	3.3	3.3	4.8	12.1
10	Sea ice section 3				17.5	-3.5	10.1	50.0	0.042	1.2	0.5	0.7	7.5	14.8	8.7
10	Sea ice section 4				24.5	-2.9	11.3	79.8	0.257	3.6	0.5	3.0	4.4	8.2	17.9
10	Sea ice section 5				30.3	-2.4	19.0	189	0.888	4.1	0.5	3.6	3.0	6.6	62.9
10	Sea water (0 m)				31	-1.84		16.8	0.040	0.7	0.3	0.4		0.0	
10	Sea water (1 m)				131	-1.84		22.8	0.060	0.7	0.2	0.5		0.0	
11	Snow	3/10/2007	65°01.419'	117°41.870'	20			34.3	<DL	1.4	0.2	1.2	1.3	6.0	26.8
11	Shallow brine				30			79.2	0.204	13.3	2.2	11.2	1.5	0.7	53.9
11	Deep brine				15			80.2	0.299	5.0	1.1	3.9	0.2	0.2	376
11	Sea ice section 1				3.5	-2.5	28.7	230	1.11	6.8	1.8	5.1	2.8	1.6	79.7
11	Sea ice section 2				17.5	-2.5	7.7	140	0.616	4.9	0.4	4.5	2.3	5.3	61.5
11	Sea ice section 3				24.5	-2.4	10.6	110	0.569	2.7	0.5	2.2	2.7	5.6	40.1
11	Sea ice section 4				31.5	-2.3	15.5	128	0.639	2.1	0.3	1.8	2.7	8.6	47.1
11	Sea ice section 5				35.5	-2.2	22.5	954	7.67	1.4	0.5	0.9	8.6	18.3	111
11	Sea water (0 m)				36	-1.86		14.4	0.012	2.5	0.5	2.0	0.4	0.7	40.8
11	Sea water (1 m)				136	-1.86		16.0	0.024	2.3	0.3	2.1	1.5	5.8	10.9
13	Snow	6/10/2007	64°42.888'	116°48.106'	12.5			31.9	<DL	2.4	0.3	2.1	1.9	5.6	17.2
13	Shallow brine				30			402	1.42	14.3	0.6	13.7	1.9	2.9	216
13	Deep brine				60			200	0.629	34.3	14.8	19.5	1.5	0.1	132
13	Sea ice section 1				3.5	-6.4	13.3	60.0	0.023	23.9	6.3	17.6	15.7	2.5	3.8
13	Sea ice section 2				33.5	-4.6	8.1	144	0.278	23.3	4.3	19.1	77.7	18.3	1.9
13	Sea ice section 3				63.5	-3.3	8.1	140	0.502	6.9	0.7	6.1	16.7	22.5	8.4
13	Sea ice section 4				89.5	-2.4	12.7	146	0.287	3.5	0.5	3.0	2.2	4.1	66.3
13	Sea ice section 5				96.5	-2.2	23.1	2386	17.1	5.7	0.8	4.9	8.4	10.6	284
13	Sea water (0 m)				97	-1.86		19.5	0.036	3.4	0.4	3.0	1.3	3.4	14.6
13	Sea water (1 m)				197	-1.86		19.2	0.016	2.7	0.4	2.2	1.5	3.5	13.2
14	Snow	7/10/2007	64°18	116°50	10			32.9	<DL	0.7	0.2	0.5	1.1	5.2	29.9
14	Shallow brine				25	-5.9		359	1.67	4.3	1.2	3.2	0.1	0.1	2680
14	Deep brine				80	-4.6		286	1.48	3.6	0.9	2.7	0.1	0.1	2500
14	Sea ice section 1				3.5	-8.3	10.8	57.1	0.044	3.9	1.8	2.4	3.2	2.0	18.0
14	Sea ice section 2				33.5	-4.3	9.2	107	0.198	2.4	0.7	1.6	2.2	3.0	47.6
14	Sea ice section 3				63.5	-2.8	9.1	98.6	0.166	4.1	0.5	3.7	1.6	3.6	60.8
14	Sea ice section 4				85.5	-2.0	15.3	231	0.355	1.2	0.2	0.9	1.1	4.9	208
14	Sea ice section 5				92.5	-1.90	24.0	3310	17.4	9.4	0.3	9.1	4.1	13.1	800
14	Sea water (0 m)				93	-1.84		20.0	0.021	0.8	0.1	0.7	0.2	1.4	98.9
14	Sea water (1 m)				193	-1.84		19.3	0.011	0.7	0.2	0.5	0.1	0.6	152
				all data	mean	-4	12	176	0.91	17.1	1.9	15.4	12.5	10.2	171
					SD	3	6	469	3.01	45.9	3.0	46.0	30.7	34.5	498
					max	-2	29	3310	17.4	378	14.6	377	215	285	2680
					min	-14.6	3.5	14.4	<DL	0.4	0.1	0.0	0.1	0.0	1.0
					N =	63	39	75	70	80	78	78	73	78	69
				sea ice only	mean	-4.4	11.6	271	1.40	28.2	2.4	26.7	21.6	18.3	54.3
					SD	2.9	5.5	639	3.91	63.1	3.4	64.2	39.4	48.1	105
					max	-2	29	3310	17.4	378	14.4	377	215	285	800
					min	-14.6	3.5	38.6	0.00	1.2	0.2	0.7	0.9	0.8	1.0
					N =	39	39	39	40	40	38	38	40	38	38
				basal ice only	mean	-2	18	937	5.99	17.4	1.9	15.5	32.9	43.1	165
					SD	0	4	1239	7.38	21.4	3.9	21.7	73.6	98.0	273
					max	-2	24	3310	17.4	68.3	9.1	65.6	215	285	800
					min	-2.8	11.7	114	0.31	1.4	0.2	0.9	3.0	0.8	1.0
					N =	8	8	8	8	8	8	8	8	8	8
				brine	mean	-4		149	0.53	10.0	2.5	7.5	1.1	0.6	712
					SD	2		134	0.62	8.0	3.4	5.2	1.1	0.9	1030
					max	-2		402	1.67	34.3	14.8	19.5	3.7	2.9	2680
					min	-7.6		21.2	0.00	1.5	0.5	0.9	0.1	0.0	42.5
					N =	8		12	14	16	16	16	13	16	16
				snow	mean			46.3	<DL	2.9	0.5	2.4	3.2	7.1	22.7
					SD			25.7	0.0	1.9	0.3	1.9	3.8	8.4	11.4
					max			105	<DL	6.9	1.1	6.4	11.6	27.3	42.8
					min			23.6	<DL	0.7	0.2	0.5	1.1	0.0	9.0
					N =			6	0	6	6	6	7	6	7
				sea water	mean	-1.8		26.9	0.02	3.5	0.7	2.9	1.0	1.9	183
					SD	0.0		21.0	0.02	2.8	0.7	2.5	0.9	2.2	447
					max	-1.8		91.2	0.09	7.8	2.6	7.4	2.9	7.3	1640
					min	-1.9		14.4	0.01	0.4	0.1	0.0	0.1	0.0	6.7
					N =	16		16	16	16	16	16	13	16	13

5. High temporal resolution observations of spring fast-ice melt and seawater iron enrichment in East Antarctica.

This chapter is submitted for publication:

van der Merwe, P., Lannuzel, D., Bowie, A., & Meiners, K. (Submitted). High temporal resolution observations of spring fast-ice melt and seawater iron enrichment in East Antarctica. JGR-Biogeoscience

5.1. Abstract

A time series experiment was conducted in late austral spring (November – December 2009) in coastal fast ice, East Antarctica (66˚ 13’ 07’’ S, 110˚ 39’ 02’’ E). Iron (Fe) measurements were made in sea-ice, snow, brines, and underlying seawater together with meteorological, physical and biogeochemical measurements to investigate the processes controlling the release of Fe into the underlying water column. Warming air temperatures were clearly associated with decreasing brine volume fractions. Macronutrient profiles revealed very low (<1 uM) nitrate + nitrite concentrations in the interior of the sea ice, and the brines suggest nitrate + nitrite drawdown exceeded Redfield ratios in comparison to phosphate and silicate. In the basal ice, nitrate + nitrite and silicate were drawn down through time but did not lead to a limiting condition. We found that the dissolved Fe tracked brine volume fraction and was readily transferred from the surface/interior to the underlying water column over time. In contrast, particulate Fe did not show this clear decreasing trend and correlated with Particulate Organic Carbon (POC) and Chlorophyll *a* distributions. Factor analysis revealed two components representing 53 and 28% of the total variance of all the variables. These were most closely

correlated with POC and macronutrient distribution respectively. Over the 28 days of sampling, two distinct mean air temperature warming events were observed (-12.1 to -1.3 ˚C and -6.4 to 0.8 ˚C). This resulted in the release of 419 μmol TDFe per m^2 of sea ice from our coastal fast-ice station into the underlying water column during the study period. Assuming an increase of 1 nM Fe is sufficient for Antarctic diatoms to bloom, this represents a fertilisation potential for 419 m^3 of Fe limited Southern Ocean surface seawater, per m^2 of coastal fast ice.

5.2. Introduction

The majority of the vast Southern Ocean is a high nutrient, low chlorophyll region where marine production is primarily limited by the micro nutrient trace element iron (Fe) (Bowie et al., 2001; Boyd et al., 2000; Martin et al., 1990a). The seasonal formation and subsequent melt of Antarctic sea ice covers approximately 17 million km^2 of sea water, an area greater than the size of the whole Antarctic continent. Sea ice has the ability to store two orders of magnitude higher concentrations of Fe than the underlying water column (Lannuzel et al., 2007). Sea-ice formation can reduce the concentration of dissolved Fe in surface waters surrounding the continent by entrainment within the sea ice itself (Lancelot et al., 2009). However, during periods of melt, sea ice releases this stored reserve of Fe into the underlying water column at a time that is coincidentally ideal for algal growth (Lannuzel et al., 2007, 2008). During the winter, light limited conditions prevail. During spring and into summer however, stratification of the water column (due to increased meltwater and shallowing of the mixed layer), combines with increased solar radiation, seeding of the water column with sea ice algae, and the release of Fe. The result is large algae blooms that may significantly affect the regional carbon cycle with possible flow on effects to global climate (Arrigo et al., 2008a; Lancelot et al., 2009). However, considerable variability in the estimates of the size and relative contribution of these ice edge blooms exists and such variability has been attributed to various factors including atmospheric and oceanic forcings (Constable et al., 2003; Fitch & Moore, 2007). Most estimates of marginal ice zone (MIZ) blooms are based on satellite-derived distributions of chlorophyll which inherently only measure the top 12 – 25 m of the water column depending on the particulate content. Thus, to realistically constrain these complex and difficult to observe processes throughout the water column, we need to better understand the processes driving the production, namely, the release of Fe from melting sea ice.

Fe can be sourced to Southern Ocean surface waters from sediment resuspension (Sedwick et al., 1997), aeolian dust deposition (Wagener et al., 2008), hydrothermal plumes (Tagliabue et al., 2010) or from extraterrestrial dust (Johnson, 2001). Unlike these sources, sea ice entrained Fe is not a new source, although it does act as a medium for significant temporal storage. Importantly, there is growing evidence that sea ice entrained Fe may be one of the most bioavailable forms due to abundant organic complexation coupled with photo-oxidation either in situ or upon release into strongly stratified melt waters (Kim et al., 2010; Rijkenberg et al., 2008; Steigenberger et al., 2009; Tagliabue et al., 2009b).

Prior to this work, very few research studies have sampled Antarctic sea ice with sufficient replication and with the required complimentary data to make reliable comment. In an area of 17 million km^2 with characteristically high heterogeneity (Lannuzel et al., 2010; van der Merwe et al., in Press; van der Merwe et al., 2009), more validation is thus required. This work significantly adds to the known concentrations of Fe in Antarctic sea ice, and we present our data alongside measurements of physical and biogeochemical variables. Our results are based on a temporal study in fast ice off the coast of East Antarctica during the spring melt (November 4 – December 3, 2009) over a period of approximately one month. The aim of this research is to document, in high temporal resolution, the release of size fractionated Fe (<0.2 μm dissolved and >0.2 μm particulate), macronutrients, Chorophyll *a* (Chl *a*) and particulate organic carbon and nitrogen (POC, PON) from coastal fast ice, into the underlying water column during the spring melt. This information, coupled with high quality meteorological data, should increase our understanding of the processes that lead to the annual cycle of ecologically significant and climatically important marginal ice edge phytoplankton blooms.

5.3. Methods

5.3.1. Study site

The study site was located in seasonal fast ice, adjacent to "Jacks Donga" field hut approximately 12 km northeast of Casey Station (Australian Antarctic Territory) (66˚ 13' 07'' S, 110˚ 39' 02'' E, see Fig 5.1). The fast ice study site was located in between the coast and Berkley Island to the north, Hailstorm Island to the west and Honkala Islands to the southwest. These islands are several of the islands that make up the Swain Group and are home to Adelie penguin (*Pygoscelis adeliae*) colonies and many Weddell seals (*Leptonychotes weddellii*) haul-out on the ice in the vicinity (Fig 5.1). On the ridge line parallel to the coast runs an exposed rock moraine and within the layers of glacial ice below this feature are seams of gravel, mud and fine silt. The study site chosen was 500 m off the coast, at a water depth of 15-17 m. The fast ice here was undeformed and level (i.e. thermodynamically formed fast ice).

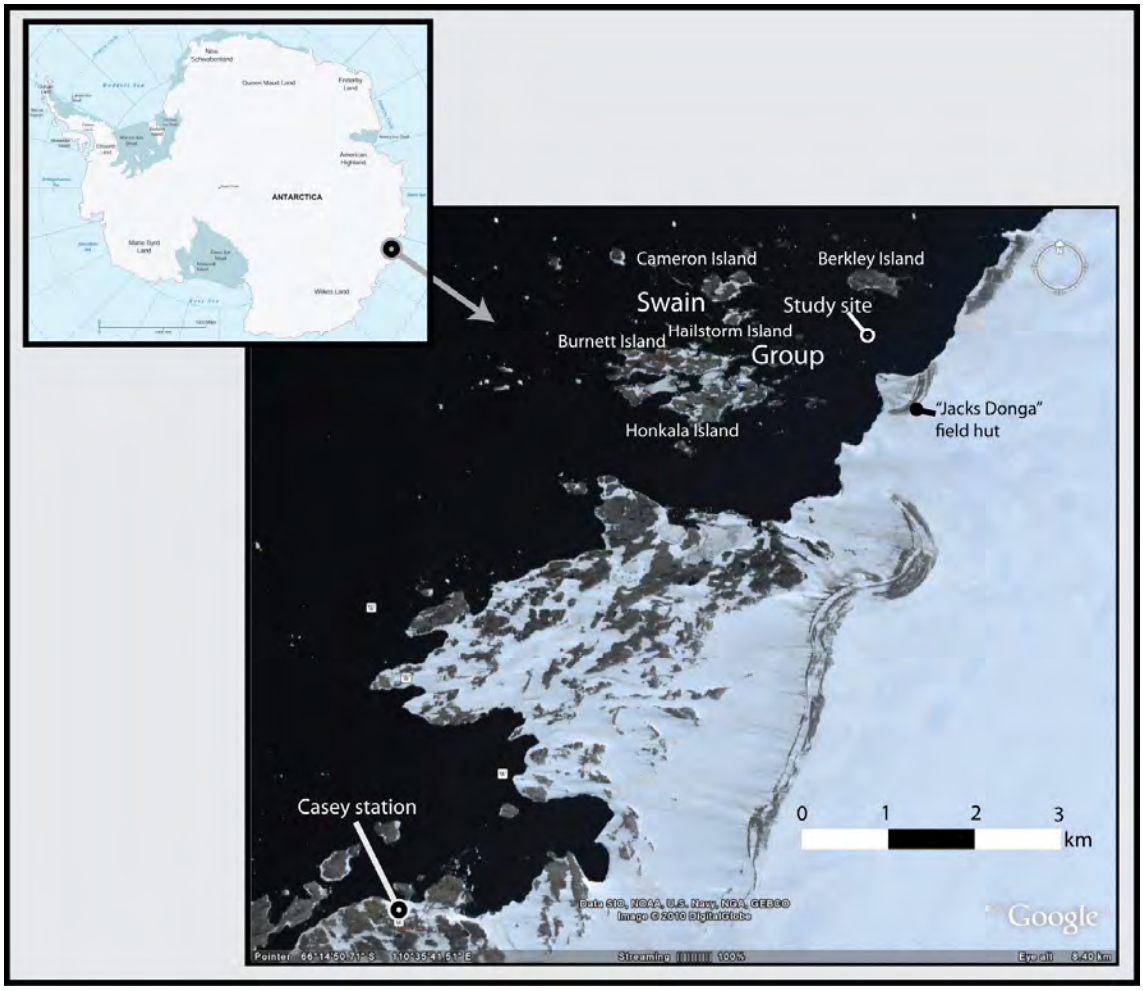

Figure 5.1: Map indicating the location of the study site. Note the presence of cliffs and rock moraines in the vicinity of the study site. Base map is produced using Google Earth (http://www.google.com/earth/index.html) and modified to suit the purpose.

5.3.2. Sample collection

All plastic-ware was acid cleaned in accordance with methods reported in Lannuzel et al. (2006). The method employed to collect snow and brines, and to remove and section cores is identical to that reported in van der Merwe et al (2009). Briefly, snow was collected from a designated site approximately 10 m from the coring site and re-sampled each visit. An acid cleaned polyethylene (PE) hand shovel was used to collect loose snow from the surface of the sea ice, which was then transferred to acid cleaned 1 L wide-mouth Nalgene polyethylene (PE)

bottles. To collect sea ice, an electropolished stainless steel corer of 140 mm internal diameter (Lichtert Industrie, Belgium) driven by a high-torque, low-rpm electric drill was used. This equipment has been proven to be non-contaminating (Lannuzel et al., 2006; van der Merwe et al., 2009). Once cored from the ice, a high quality stainless steel bone saw was used to section the ice cores downwind of the sampling site out on the ice, starting with the highly permeable basal ice section, after performing multiple cleaning cuts in waste cores. The core was sectioned so that one top (0-6 cm = SI1), two intermediate (30-36 cm = SI2 and 70-76 cm = SI3) and two continuous sections in the lowermost basal ice (SI4 and SI5) were collected. SI5 was from the ice-water interface to 6 cm above and SI4 was from 6 cm above the ice-water interface to 12 cm above the ice-water interface. The sections were then placed into individual acid-cleaned polycarbonate (PC) containers and transported to the laboratory at Casey Station, where they were melted in the dark at ambient temperature and then immediately processed. Brines were collected from sack holes drilled at 50 and 100 cm deep, named B- and B+, respectively. The liquid brine was removed from the sack holes by means of a peristaltic pump (Masterflex, Cole Parmer) with acid cleaned tubing.

Seawater was collected using a custom made 7 L Helmond-Byrne (H-B) sampler suspended from a Kevlar line and triggered at the nominated depth using an all-Teflon® messenger (Sedwick et al., 1997). The H-B sampler and associated bracket (which attaches to the Kevlar line) is completely PC in construction, except for several titanium fulcrum pins. The sampler was lowered through 3 linked core holes in the ice, triggered at the desired depth (0, 5, 10 or 15 m deep; hereafter referred to as SW0, SW5, SW10 and SW15), retrieved, and the seawater sample decanted into several acid washed 1L Low Density Polyethylene (LDPE) Nalgene bottles for each of the required analyses (see below).

5.3.3. Physical variables

Temperature was measured along a dedicated core every 5 cm using a Testotherm 720 temperature probe (± 0.1 ºC accuracy) by insertion into drilled holes, starting from the basal ice. Salinity was measured on melted core sections, melted snow, brines and sea water using a TPS AQUA-C conductivity meter. Where temperature and salinity were measured at different depths within a core, temperature was linearly interpolated to match salinity depth. Brine volume fraction (V_b/V) was calculated from temperature and salinity data according to Cox and Weeks (1988). Meteorological observations were made by a trained observer at nearby Casey Station.

5.3.4. Fe measurements

Melted sea ice and snow samples, together with brine and seawater samples were filtered through acid washed, 0.2 µm PC membrane filters (47 mm diameter, Sterlitech) using a Perfluoroalkoxy (PFA) filtration rig (Savillex) and vacuum pump. Standard trace metal techniques were followed, with all processing occurring under a ISO5 (Class 100) laminar flow hood (Air Clean Systems) at the Casey Station laboratory immediately after sampling (or after melting). Filtered volumes depended on the organic content but ranged from 40 – 1000 ml. Filtrate was collected and acidified to pH 1.8 using hydrochloric acid (Seastar Baseline HCl, Choice Analytical) and stored at ambient temperature until analysis at the home laboratory in Hobart, Australia; hereafter referred to as the dissolved Fe (dFe) fraction. The filters were placed into acid cleaned PC petri dishes and frozen at -18 ºC until analysis at the home laboratory; hereafter referred to as the particulate fraction (pFe). Unfiltered samples were also collected after careful homogenisation and acidification to pH 1.8 using HCl (Seastar Baseline); hereafter referred to as total dissolvable Fe (TDFe). Particulate leachable Fe (plFe) was calculated from the difference between TDFe and dFe.

5.3.4.1. TDFe and dFe

dFe and TDFe samples (sea ice, brine, snow and seawater) were analysed using flow injection analysis with luminol chemiluminescence detection (FIA-CL) coupled with in-line preconcentration onto an 8-hydroxyquinoline (8-HQ) resin (FeIII method), adapted from de Jong et al. (1998) and Obata et al. (1993). This method has been recommended for the International Polar Year projects by the new program GEOTRACES (Bowie & Lohan, 2009). The mean detection limit (3× analytical blank standard deviation) of the FIA-CL method with 1 minute pre-concentration was 0.05 ± 0.03 nM (n = 21). For samples with high dFe and TDFe concentrations (> approximately 20 nM), the method was detuned to a 10 second load and/or the samples diluted. Similar sample types were always run together with a calibration based on an identical matrix to minimise matrix effects (e.g., due to salinity variations). The mean detection limit (3× analytical blank standard deviation) of the FIA-CL method with 10 second pre-concentration was 0.27 ± 0.2 nM (n = 6). Analysis of SAFe (Sampling and Analysis of Fe) deep water reference seawater samples D2 (#467) using the 1 minute pre-concentration was 0.91 ± 0.13 nM (n = 11), which was in excellent agreement with the D2 consensus value of 0.91 ± 0.17 nM.

5.3.4.2. pFe

All digestions and evaporations were carried out within a digestion hood (SCP Science), the air in which was filtered through HEPA filters during intake and subsequently extracted into a fume hood. Acid and filter blanks as well as sample filters were digested in 15 ml acid cleaned, Teflon PFA screw cap vials (Savillex) using a mixture of ultra pure, strong acids (500 µl 11 M HCl, 250 µl 16 M HNO_3, 250 µl 29 M HF) (Seastar Baseline) heated to 95 ˚C for 12 hours on a Teflon coated hotplate (SCP Science DigiPREP) following the method outlined in Bowie et al. (2010). The samples were evaporated to dryness at 95 ˚C within the above mentioned clean air

digestion hood, and the dry residue was then resuspended in 10 % HNO_3 (Seastar Baseline) (10 ml final volume) and 10 ppb indium added as an internal standard. Samples were analysed by Sector Field Inductively Coupled Plasma Mass Spectrometry (SF-ICP-MS) (Finnigan Element II, Thermo Scientific) (Cullen and Sherrell, 1999; Townsend, 2000).

The digest acid blank average for pFe was 0.15 ± 0.05 nmol L^{-1} (n = 3), while the digested/evaporated filter blank average was 1.93 ± 1.37 nmol L^{-1} (n = 3). Therefore, the mean detection limit for pFe (3 × standard deviation of digested/evaporated filter blank) was 4.12 nmol L^{-1}.

5.3.5. Macro-nutrients, POC/PON and Chl *a*

Macro-nutrient ($Si(OH)_4^-$, PO_4^{3-} and NO_3+NO_2) samples were filtered through 0.2 µm Sterlitech PC membrane filters immediately after collection or melting, and the filtrate was immediately frozen upright in 10 ml PE nutrient tubes. Macronutrient analysis was performed at CSIRO Marine and Atmospheric Research laboratory (Hobart), within 6 months of collection. Dissolved inorganic nutrients were determined using standard colorimetric methodology (Grasshoff et al., 1983) as adapted for flow injection analysis on a 5 channel LACHAT Quik-Chem 8000 autoanalyser (Hales et al., 2004).

All glassware in contact with POC samples was pre-combusted prior to the field work (550 °C for 12 h). Melted sea ice, seawater and brines were filtered (40–1000 ml depending on organic matter content) onto pre-combusted 47 mm diameter, Whatman GF/F filters. Filters were then cut in half; one half was used for POC analysis and the other half for Chl *a* analysis. The halved filters were placed into individual, sterile cryotubes and stored at -18 °C in the dark until analysis (within 6 months of collection for POC/PON and within 1 month for Chl *a*). The analysis for total nitrogen, carbon and hydrogen was determined at the Central Science

Laboratory, University of Tasmania, using a Thermo Finnigan EA 1112 Series Flash Elemental Analyser (estimated precision ~1%).

Filters for Chl *a* concentration were extracted in 10 ml of 100% methanol for 12 h in the dark at 4 °C. The Chl *a* concentration was then determined following the method of Holm-Hansen et al. (1965) using a Turner Designs, 10AU fluorometer (in vitro detection limit 0.02 μg L^{-1}).

5.3.6. Microscopic examinations

Observations were made immediately after collection of brine and melted basal ice samples to qualitatively identify the most dominant species. Samples were imaged using a Zeiss AxioScope coupled with an Olympus digital camera. Species identification was based on Scott and Marchant (2005).

5.4. Results and Discussion

5.4.1. Physical variables

5.4.1.1. Air temperature

In this region of East Antarctica, cyclic katabatic wind patterns are common, and due to the atmospheric temperature inversion that drives such winds, their presence is characterised by relatively warm air temperatures and their absence by colder air temperatures. Therefore, mean daily air temperatures (measured at the Casey weather station) are related to wind run (defined here as wind above 3 m for 24 h before 9 am local time) such that periods of high wind run are associated with relatively warm mean daily temperatures (Fig 5.2). Conversely, quiescent periods are characterised by colder mean daily air temperatures. For the month of October (i.e. one month prior to this study period) the local air temperature was characterised by a closely

correlated (R = 0.66) cyclic fluctuation between the mean daily air temperature and wind run, reoccurring with an approximately 6 day period. It should be noted that this 6 day period could also imply some influence by synoptic-scale systems between katabatic episodes.

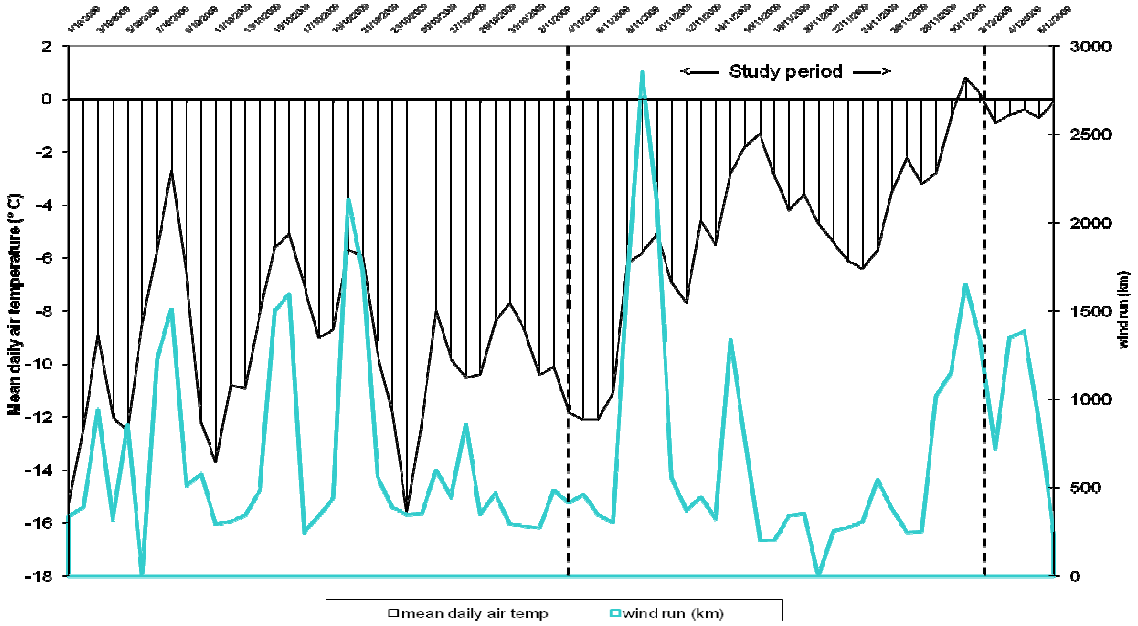

Figure 5.2: Chart of wind run (defined as wind measured in km above 3 m for 24 h before 9 am local time) plotted with mean daily air temperature. Note that periods of high wind run are associated with warmer mean daily air temperatures.

Sea ice temperature profiles commonly start at a temperature set by the underlying sea water in the skeletal layer of the basal ice and decrease linearly to a surface temperature set by the overlying atmosphere (van der Merwe et al., 2009). The lower temperature at the surface ice can often be less than -10 °C (van der Merwe et al., 2009). Given that sea water never gets colder than -1.84 °C without freezing, and given that the surface ice often gets much colder, the role of the atmosphere in maintaining the temperature profile is clear. Thus, when comparing ambient air temperatures to sea ice physical properties, we are observing this balance between relatively warm underlying sea water and a frigid atmosphere. If the atmosphere warms, it is no

longer providing the necessary "refrigeration" for the underlying sea ice and thus the relatively warm sea water drives melting from below.

The study period (4 November – 3 December, 2009), hereafter referred to as study days (SD) 4 through 32, was characterised by a cold start (SD 4-7) in ambient air temperatures, followed by two distinct warming periods separated by a cool period (SD 17-24), and finally positive air temperatures by the end (Fig 5.2). The initial cold start (mean -11.8 ˚C) resulted from a relatively long quiescent period of 17 days from October 22 until November 7 (most of which was prior to the study period) during which mean daily wind run was 426 ± 147 km. On SD 7, 8 and 9, a strong blizzard persisted (wind run mean 2213 ± 600 km) and caused the mean daily air temperature to increase from -11.1 to -5.1 ˚C. Four quiescent days followed, causing the temperature to fall slightly, only to be raised again by two high wind days on SD 15 and 16 (mean 1054 km) which saw temperatures rise to -1.3 ˚C on SD 17. A quiescent period followed, resulting in the air temperature falling to a low of -6.4 ˚C on SD 24. However, after this low, temperatures rose relatively consistently until positive temperatures were observed on SD 31. Relatively high mean daily air temperatures persisted after the study period and until the end of our observations on December 6.

5.4.1.2. The influence of air temperature on sea ice physical properties

The sea ice thickness was relatively consistent throughout the study period, with a mean thickness of 118.4 ± 2.4 cm. The basal ice on SD10 had a very high brine volume fraction which melted off after this station presumably in response to the higher air and sea water temperatures that led up to this station. This is evidenced by the thinning of the overall sea ice by the amount associated with the highest brine volume fraction (Fig 5.3) and the observation of

a visibly thinner skeletal layer from SD14 onwards (data not shown). The ice thickness at the first and last station was 120 cm but on SD 23 and 26 it was only 115 cm. The fact that a low salinity, seawater layer has been observed to develop at the ice water interface during ice melt (Archer et al., 1996), it is plausible that ice growth resulting from the increased melting point of this fresher layer could explain this anomalous increase in ice thickness at the final station and/or simple heterogeneity in the sampled ice floe itself.

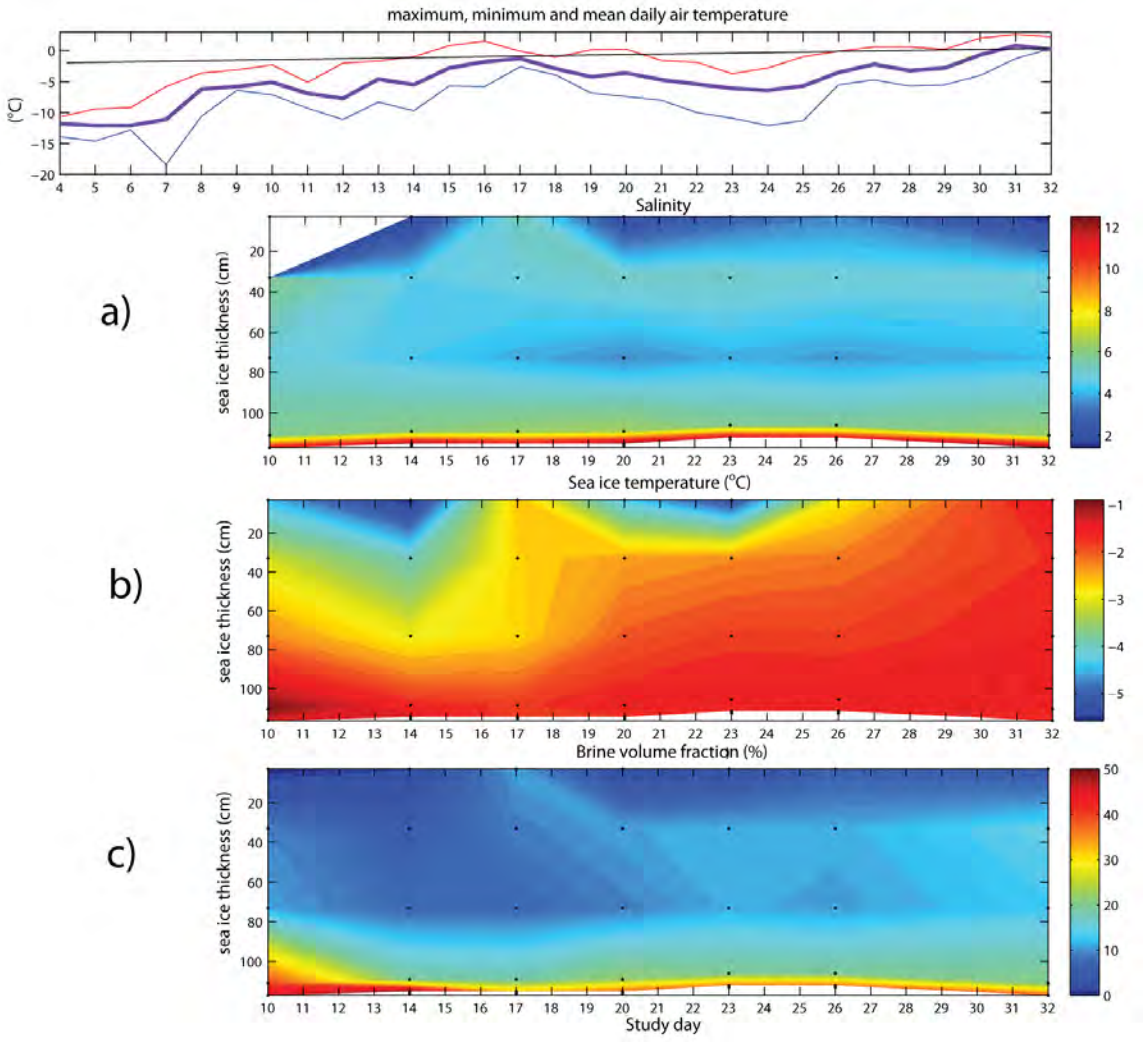

Figure 5.3: Sea ice physical properties (a) salinity, b) temperature and c) brine volume fraction) through time within the study period. Sampling days within the study period are days 10, 14, 17, 20, 23, 26 and 32.

The progression of the brine volume fraction and sea ice temperature through time indicates that there is a close relationship with the ambient air temperature (Fig 5.3). The initial rapid warming in mean daily air temperature from -11.1 to -5.1 ˚C on SD 10 resulted in a high brine volume fraction (9.3%) within the interior ice (SI2) and some brine drainage, which led to a lowering of the shallow brine salinity between SD 10 and 14 by 14 units (appendix table) and in the ice salinity itself by 2.3 units (Fig 5.3). Immediately after the station on SD 10, there was a colder period for 3 days, and combined with the lower salinity of the ice and brine, resulted in a lowering of the brine volume fraction on SD 14. After this, a relatively consistent decrease in shallow brine salinity was observed (appendix table), and combined with increasing ice temperatures, this resulted in increasing brine volume fraction to a maximum for the interior ice (SI2) on the last day of sampling of >14 %. The basal ice was buffered for both salinity and temperature by the underlying seawater, with temperatures fluctuating by only half a degree and salinity by 1.5 units over the duration of sampling.

5.4.2. POC and Chl *a*

Vertical profiles of POC concentration show variability between study days (Fig 5.4). This could be due to inter-core heterogeneity, issues with homogenising the subsample thoroughly before filtering or real fluctuations in the POC content. Firstly, the intermediate sea ice section (SI3) shows, with some variability, a relatively consistent increase through time from 225 – 299 μg L^{-1}, possibly due to new sea ice algae growth as the spring season progresses (Fig 5.4). In contrast, SI4 shows an increase between SD 10 and 17 and then a gradual decrease after this for the remainder of the stations (Fig 5.4). In the basal ice (SI5), the large variability from one station to the next could reflect the growth and then melting of the skeletal layer with aggregates being released into the water column below (Fig 5.4). Indeed, as previously mentioned, the

skeletal layer was observed to decrease in its thickness by approximately 5 cm on SD 23 and 26, possibly reflecting the melting of large portions of this layer during warm periods. However in this layer, the extremely sticky nature of the Exopolysaccharide (EPS)-algae aggregates made thorough homogenisation of the filtered subsample very difficult and thus may have led to increased variability.

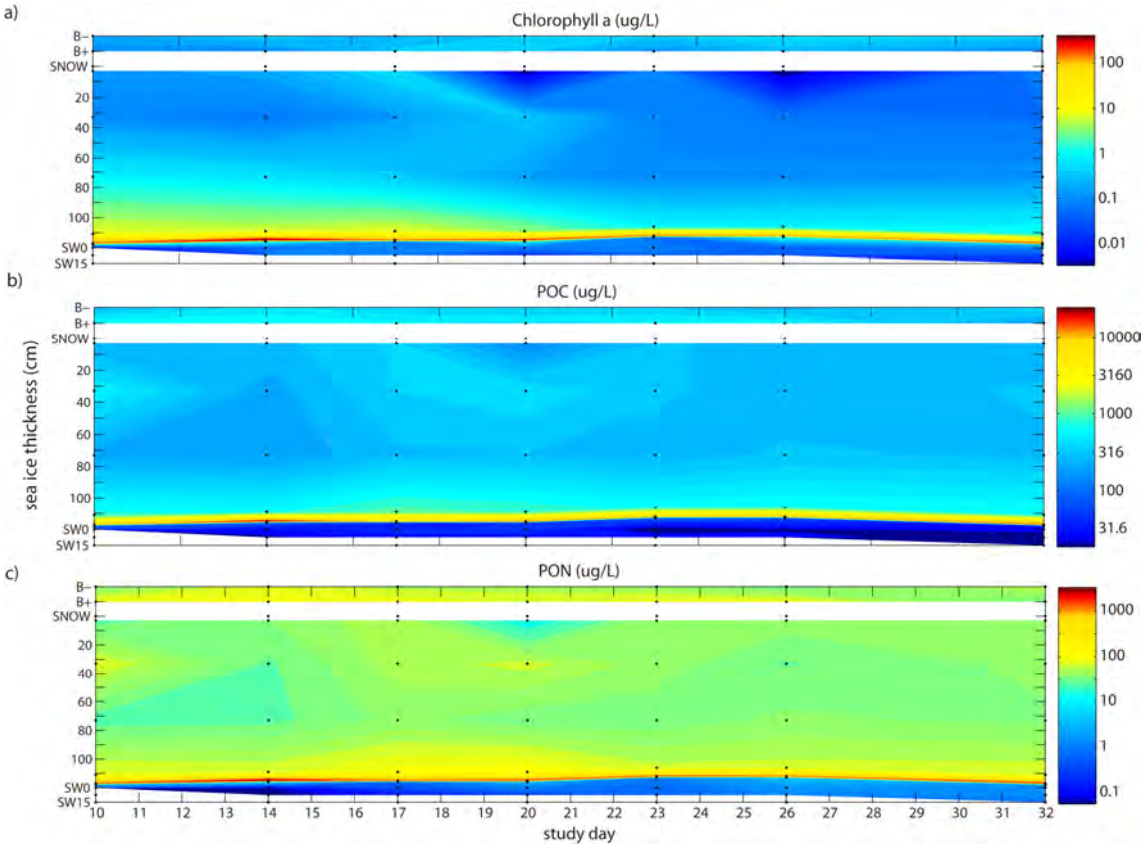

Figure 5.4: a) Chlorophyll *a*, b) Particulate organic carbon (POC) and c) particulate organic nitrogen (PON) throughout the sampling period, plotted against mean daily air temperature. Note the log colour scale on the contour plots. Shallow and deep brines (B- and B+ respectively) are plotted above the sea ice profile for ease of viewing. Snow is plotted immediately below the brines. Similarly, seawaters (SW0, SW5, SW10 and SW15) are plotted below the sea ice to allow direct comparison. White areas indicate a lack of data. Sampling days within the study period are days 10, 14, 17, 20, 23, 26 and 32.

The POC:PON ratio was very consistent at all sea ice sections with the exception of SI4. SI1, SI2, SI3 and SI5 ranged from 7.5-7.9 (mean 7.7 ± 0.9). In contrast, SI4 had a mean POC:PON ratio of 10.1 ± 1.1. According to Redfield's ratio, nitrate sufficiency would be at a ratio of 6.6 (Redfield, 1958). Thus, where a high standing stock of sea ice algae coincide with minimal nutrient resupply from below (namely at SI4), nitrate limitation may be a controlling factor.

The profiles of Chl *a* demonstrated the high concentration of sea ice algae in SI5 and to a lesser extent SI4, with mean concentrations in these layers of 235 and 4.6 μg L^{-1} respectively (appendix table). This SI5 concentration is an order of magnitude higher than the 34.2 μg L^{-1} recorded on December 7, 2000, in fast ice in Terra Nova Bay, Western Ross Sea (Grotti et al., 2005). In all three of the upper sections of the sea ice in the present study, the mean Chl *a* concentration was an order of magnitude lower again than in SI4. As noted before, particulates including algal cells are under-sampled in the brines when using the sack-hole method of collection due to the fact that the cells remain attached to the brine channel walls (Papadimitriou et al. 2007, van der Merwe et al. 2009). Thus, the mean Chl *a* concentration in both the shallow and deep brines were very low in (0.23 and 0.41 μg L^{-1} respectively). Chl *a* was significantly correlated (Spearman's rho, $p < 0.001$) with all Fe fractions, with the highest correlation observed for the dissolved Fe fraction ($R = 0.625$) (Table 5.1). POC and PON were also strongly correlated with Chl *a* ($R = 0.698$ and 0.674, respectively), as previously observed in East Antarctic sea ice (van der Merwe et al., 2009). Thus, although large variability exists in the sea ice Chl *a*, it is associated with proportional quantities of Fe and organics. The fact that dFe is not inversely correlated with Chl *a* (i.e., due to algal draw-down as noted in van der Merwe et al (2009)) is an indication of the excessive concentrations of dFe in this coastal fast ice station (i.e., there is no Fe limitation). Rapid decreases in basal ice Chl *a* concentration were also observed in fast ice off the coast of Davis station during November – December (Archer et al., 1996 and references therein). Archer et al (1996) noted that in their study and others conducted

in East Antarctica, that the peak standing crop in coastal, basal fast ice occurred in November. After November it declined as water and ice temperatures increased. Although the exact reason for the observed decrease was unclear, they suggested that it may have resulted from the persistence of a fresh sea water layer at the ice water interface due to melt water accumulation.

Table 5.1: Spearmans rank correlation table for each of the sea ice variables measured.

Correlations

			dFe	TDFe	pFe	PLFe	PON	POC	CHLa	SAL	phosphate	silicate	nitrate
Spearman's rho	dFe	Correlation Coefficient	1.000	.767**	.674**	.739**	.757**	.792**	.625**	-.190	-.060	-.312**	-.368**
		Sig. (2-tailed)	.	.000	.000	.000	.000	.000	.000	.107	.592	.005	.001
		N	81	81	81	81	69	69	69	73	81	81	81
	TDFe	Correlation Coefficient	.767**	1.000	.943**	.997**	.748**	.766**	.558**	-.511**	-.116	-.472**	-.387**
		Sig. (2-tailed)	.000	.	.000	.000	.000	.000	.000	.000	.303	.000	.000
		N	81	81	81	81	69	69	69	73	81	81	81
	pFe	Correlation Coefficient	.674**	.943**	1.000	.944**	.710**	.719**	.521**	-.579**	-.185	-.533**	-.380**
		Sig. (2-tailed)	.000	.000	.	.000	.000	.000	.000	.000	.098	.000	.000
		N	81	81	81	81	69	69	69	73	81	81	81
	PLFe	Correlation Coefficient	.739**	.997**	.944**	1.000	.729**	.748**	.548**	-.530**	-.110	-.477**	-.366**
		Sig. (2-tailed)	.000	.000	.000	.	.000	.000	.000	.000	.327	.000	.001
		N	81	81	81	81	69	69	69	73	81	81	81
	PON	Correlation Coefficient	.757**	.748**	.710**	.729**	1.000	.968**	.674**	-.093	-.130	-.361**	-.308**
		Sig. (2-tailed)	.000	.000	.000	.000	.	.000	.000	.451	.287	.002	.010
		N	69	69	69	69	70	70	70	68	69	69	69
	POC	Correlation Coefficient	.792**	.766**	.719**	.748**	.968**	1.000	.698**	-.119	-.155	-.412**	-.312**
		Sig. (2-tailed)	.000	.000	.000	.000	.000	.	.000	.333	.202	.000	.009
		N	69	69	69	69	70	70	70	68	69	69	69
	CHLa	Correlation Coefficient	.625**	.558**	.521**	.548**	.674**	.698**	1.000	-.015	.044	-.281*	-.044
		Sig. (2-tailed)	.000	.000	.000	.000	.000	.000	.	.901	.717	.020	.722
		N	69	69	69	69	70	70	70	68	69	69	69
	SAL	Correlation Coefficient	-.190	-.511**	-.579**	-.530**	-.093	-.119	-.015	1.000	.516**	.750**	.327**
		Sig. (2-tailed)	.107	.000	.000	.000	.451	.333	.901	.	.000	.000	.005
		N	73	73	73	73	68	68	68	73	73	73	73
	phosphate	Correlation Coefficient	-.060	-.116	-.185	-.110	-.130	-.155	.044	.516**	1.000	.798**	.757**
		Sig. (2-tailed)	.592	.303	.098	.327	.287	.202	.717	.000	.	.000	.000
		N	81	81	81	81	69	69	69	73	81	81	81
	silicate	Correlation Coefficient	-.312**	-.472**	-.533**	-.477**	-.361**	-.412**	-.281*	.750**	.798**	1.000	.615**
		Sig. (2-tailed)	.005	.000	.000	.000	.002	.000	.020	.000	.000	.	.000
		N	81	81	81	81	69	69	69	73	81	81	81
	nitrate	Correlation Coefficient	-.368**	-.387**	-.380**	-.366**	-.308**	-.312**	-.044	.327**	.757**	.615**	1.000
		Sig. (2-tailed)	.001	.000	.000	.001	.010	.009	.722	.005	.000	.000	.
		N	81	81	81	81	69	69	69	73	81	81	81

**. Correlation is significant at the 0.01 level (2-tailed).

*. Correlation is significant at the 0.05 level (2-tailed).

In the underlying seawater, mean Chl *a* concentrations were an order of magnitude higher at the shallowest depth (0.66 µg L^{-1}; 0 m) than in any of the other depths measured (0.07, 0.05 and 0.01 µg L^{-1} at 5, 10 and 15 m respectively) . Due to the lowest solar attenuation at 0 m, we can plausibly attribute this finding to be due to the highest PAR coupled with seeding of the water column with sea ice algae.

5.4.3. Dissolved macronutrients

Seawater dissolved macronutrient concentrations showed very low variability throughout time and water column depth (silicate 55.2 ± 0.78 μM, nitrate 30.5 ± 0.48 μM and phosphate 2.1 ± 0.06 μM, see Fig 5.5). Redfield (1958) revealed the incredible consistency in the ratio of phytoplankton nutrient requirements and Brzezinski (1985) adapted this ratio to include silica for marine diatoms. Based on a C:Si:N:P ratio of 106:15:16:1 (Brzezinski, 1985), our observations reveal that in sea water, nitrate is depleted relative to silicate and phosphate. Snow is consistently low in all macronutrients but interestingly, shows an excess of nitrate relative to silicate. Using the above ratio as a guide, the brines show a dramatic excess of silicate (mean 61.8 and 47.8 μM in the B- and B+, respectively) while phosphate is low (mean 0.3 and 0.5 μM in the B- and B+, respectively). However, given that dFe is in excess (see section below), nitrate is most likely limiting with the mean below the detection limit in the B- and only 0.5 μM in the B+ (Fig 5.5).

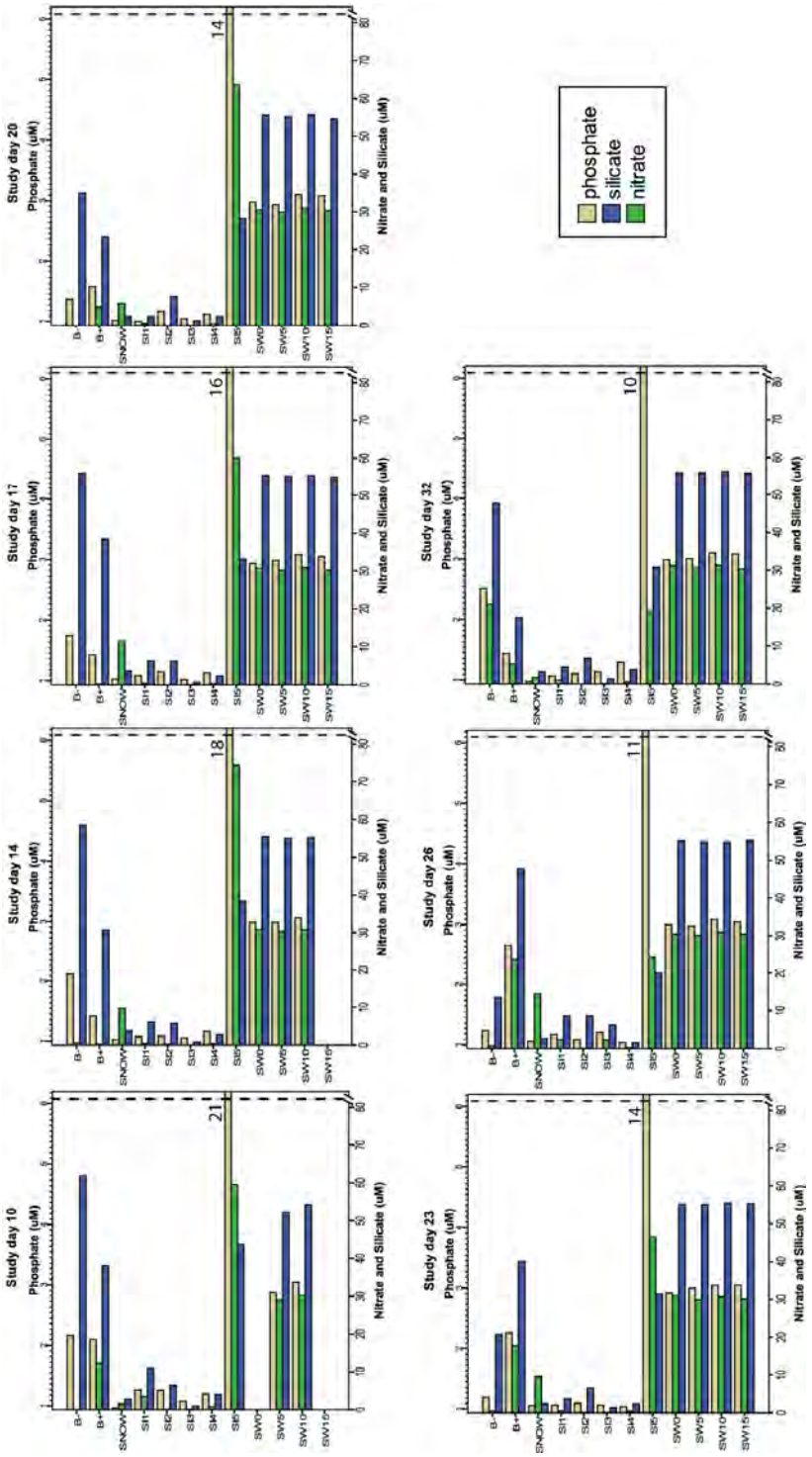

Figure 5.5: Phosphate, silicate and nitrate concentrations at each section and for all study days throughout the time series. Phosphate is plotted on a separate axis, scaled 16:1(Brzezinski, 1985) to allow direct comparison between macronutrients for relative sufficiency. B- and B+

are shallow and deep brines respectively, SI1-5 are sea ice sections from the upper most to the lower most sea ice respectively and SW0-15 is sea water sampled at 0-15 m depth respectively.

Interestingly, when normalised using the brine volume fraction, the sea ice sections SI1-SI4 show extremely low levels of nitrate relative to silicate or phosphate. When using phosphate as a reference, we see a P:N ratio of 7.4, 0.4, 2.7 and 2.0 in SI 1-4, respectively. Assuming a sufficiency of nitrate is close to 1:16 (Brzezinski, 1985), these results again suggest limitation of the entrained algal assemblage due to a lack of adequate resupply of nitrate from the seawater below. In contrast, the basal ice has a P:N ratio of 27.6. In the basal ice, we see an interesting progression in nitrate where on SD 10, it is in excess relative to the underlying seawater, but during the successive study days it becomes depleted relative to seawater. Phosphate is relatively high in basal ice compared to seawater and silicate is consistently low relative to seawater. Thus in the basal ice, there is evidence of nitrate and silicate drawdown through time, but due to resupply from below, these concentrations would most likely not be limiting.

5.4.4. Biological observations

Microscopy of the algal assemblage from the basal ice sections qualitatively identified the dominant species to be the tube dwelling diatom, *Berkeleya sp.*. *Berkeleya rutilans* has been identified in the region previously (McConville & Wetherbee, 1983). *Berkeleya sp.* was observed to form a thick fibrillose biofilm within the skeletal layer. Microscopic observations revealed that it outnumbered all other species by at least an order of magnitude in the basal ice. Within its tubes were copious amounts of EPS as identified with the acid polysaccharide stain, Alcian Blue. This species was highly dominant from the start until the end of our study period.

5.4.5. Iron

5.4.5.1. Snow

The pFe, TDFe and particulate leachable Fe (plFe) concentrations in snow were all high with values in the range of 2.3-100, 9.6-47 and 8.7-40 nM, respectively, and all fractions varied greatly between stations (Fig 5.6). Dissolved Fe concentrations in the snow showed a general decreasing trend from approximately 4 to <1 nM through time (mean 3.1 nM), with one exception on SD 23 when >7 nM was measured. Due to the fact that the study site was surrounded by exposed moraines as well as penguin and seal colonies, and that the study site was frequently visited by penguins, such heterogeneity in snow Fe concentration should be expected. Thus this anomalous day could be explained by patchy aerosol dust deposition from the ice free moraines or from Fe-rich mammal faeces (Nicol et al., 2010). On four of the seven stations, pFe was observed to be much higher than the plFe, while on the remaining three days it was similar. Given the strong acid treatment used to leach the pFe fraction and the relatively weak acid treatment used for the plFe fraction, this result indicates that on the anomalously high pFe days, the particles were refractory and therefore most likely of lithogenic origin. Thus, heterogeneous dust deposition over the snow is the most likely explanation for the observations.

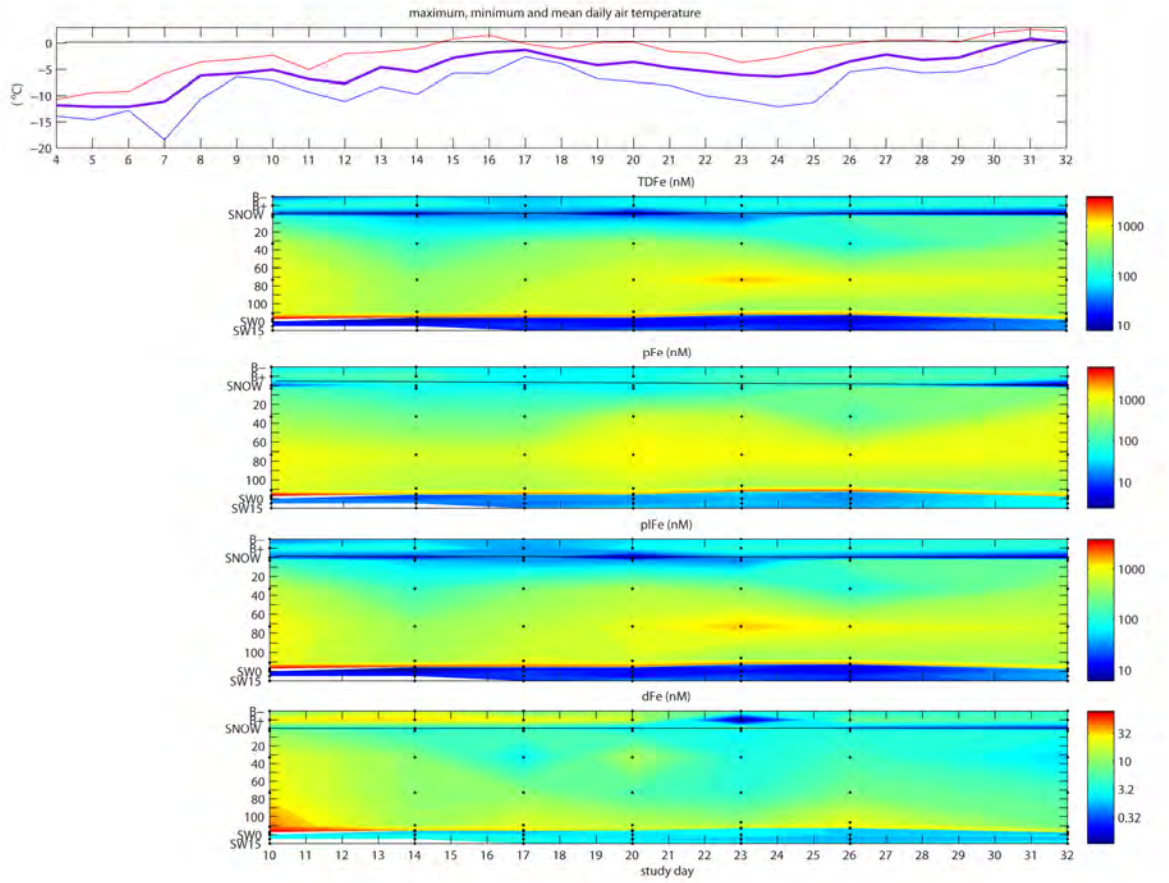

Figure 5.6: All Fe fractions throughout the study period plotted with mean, max and min daily air temperature. Note the log colour scale on the contour plots. Shallow and deep brines (B- and B+ respectively) are plotted above the sea ice profile for ease of viewing. Snow is plotted immediately below the brines. Similarly, seawaters (SW0, SW5, SW10 and SW15) are plotted below the sea ice to allow direct comparison. White areas indicate a lack of data. Sampling days within the study period are days 10, 14, 17, 20, 23, 26 and 32.

On the last station, when the ice was the warmest and with the greatest permeability, all Fe fractions were the lowest recorded for snow which could be due to dilution resulting from snow melt. Interestingly, we observed a strong inverse correlation (Spearman's rho) between maximum air temperature and snow plFe ($R = -0.79$, $p<0.05$), TDFe ($R = -0.79$, $p<0.05$) and dFe ($R = -0.94$, $p<0.01$). Conversely, there was no significant correlation observed with snow pFe

and air temperature. This suggests that on days of high temperature, snow melt may lead to transfer of these fractions, particularly the dissolved and non-refractory particulate fractions, into the underlying sea ice layers.

5.4.5.2. Sea ice and brines

The surface sea ice layer (SI1) was somewhat enriched in pFe, plFe and TDFe (~125 nM) on SD 10 and then approximately half that for all fractions on the subsequent four stations (SD 14, 17, 20 and 23) (~50 nM) (Fig 5.6). However on the last two stations (SD 26 and 32), all the particulate fractions were much higher (~200 nM). This particulate enrichment occurred independently of the dissolved fraction as dFe in SI1 actually decreased through time, with one of the lowest values recorded on the last day of sampling. Thus, the particulate enrichment most likely occurred from primarily dissolvable particles of biogenic or lithogenic origin from the overlying snow being concentrated in this low permeability layer after melt.

The sea ice brines were divided into those which accumulate into a sack hole of 50 cm deep and those which accumulate into a sack hole of 100 cm deep. Ideally, this would represent brines <-5º C (B-) and >-5º C (B+) respectively. However due to the warm conditions at our sampling site, all the ice was warmer than -5º C and essentially always permeable with brine volume fractions generally above the 5% threshold (Golden et al., 1998). Regardless, sampling both shallow and deep brines gives insight into brine movement through time. Mean brine volume fraction was 4.7, 10.3, 9.9, 22.8 and 39.4 % at SI1-5 respectively (Appendix table). Due to the fact that the ice was already quite warm at the beginning of our sampling, we did not see an obvious increase in brine volume fraction through time in the lowermost sections of the ice. However, as already mentioned at SI2 (30-36 cm), we observed a clear increase in brine volume fraction with time that was consistent with the average air temperature, with an approximately 3 day delay.

The depth of the shallow brine (50 cm) means that SI1 and SI2 would drain directly into it upon collection. We observed dFe in the B- to decrease with time, consistent with an increasing brine volume fraction, starting at more than 30 nM and decreasing to approximately 5 nM on the last day (Fig 5.6). Given the extremely low Chl *a* concentration in these layers, this decrease in dFe concentration of more than a factor of 6 cannot be explained by the observed brine dilution (less than a factor of 3) and therefore must indicate significant drainage of this brine into the underlying brine channels. Indeed, the deep brine (B+) shows evidence of enrichment from above on SD 14 and 20 but also shows the subsequent loss of dFe (presumably to the underlying water column but also possibly due to biological uptake) on SD 17 and 23 (Fig 5.6). After this, on SD 26 and 32, low concentrations in the B- do not allow considerable enrichment into the B+ and therefore, it remains low presumably until some form of remineralisation of pFe can occur.

In the particulate Fe fractions, SI3 shows a similar trend to SI2 over the first 4 stations (Fig 5.6). That is, there is an initial high stock of TDFe and pFe on SD 10 that decreases on SD 14 following the rapid initial air and ice warming. After this, TDFe and pFe increases on SD 17 and again on SD 20. However on SD 23, SI2 decreases but SI3 continues to increase. This is intuitive if the particulate enrichment was from above as the higher section of ice becomes somewhat depleted and the lower section concentrates the Fe. Thus, the pFe and TDFe remain in this section with concentrations reaching 1290 and 1600 nM, respectively, on SD 23. After this, consistently high brine volume fractions lead to a lowering of the pFe and TDFe on the last day of sampling.

The last two sections, SI4 and SI5 comprise the basal ~12 cm and therefore are closely influenced by the underlying water column. However, somewhat similarly to SI3, in SI4 we see a large decrease from SD 10 to 14 in TDFe and pFe resulting from the rapid initial warming and

basal ablation (Fig 5.6). On the next two stations (SD 17 and 20), the level of TDFe was higher, similarly to SI3, most likely due to enrichment from the ice above. In the following 3 stations (SD 23, 26 and 32) the level was consistently lower. For SI5, the warming of air and ice (and presumably water), results in sea ice basal ablation and a reduction in ice mass and entrained particulate material, including Fe. Indeed, on SD 23 and 26, the sea ice was ~5 cm thinner than the previous stations.

In the dFe distribution within the sea ice there is a somewhat consistent trend of decreasing dFe with time (Fig 5.6). The highest values were observed for all sea ice sections on the first day of sampling, decreasing rapidly after the initial warming, and then were relatively consistently approaching minimum concentrations on the last day of sampling.

5.4.6. Factor analysis

Due to the high degree of correlation between variables (Table 5.1), a factor analysis data reduction technique was employed to determine the driving factors in the variables measured. The variables used for this analysis were the macronutrients, POC, PON and POH, all Fe variables and the 3 day mean maximum air temperature. The data were log transformed to satisfy the assumptions of a parametric correlation. The factor analysis revealed that 53% of the total variance of all the variables could be accounted for by one component and this component is most closely correlated with POC (log transformed). Thus, when high concentrations of POC are observed in a sea ice section, we generally find high concentrations of Chl *a*, dFe, PON, plFe, TDFe and pFe. The second component explained a further 27.6% of the total variance and this component was most closely correlated with phosphate concentration (log transformed), although nitrate was also closely correlated to this factor and thus the second most important component of the total variance was most likely related to macronutrient control. Together these two components account for 80.6% of the total variability in the original variables.

5.4.7. Comparison with published data

There have been few previously published biogeochemical studies of fast ice. The ranges observed for Chl *a* during our spring time series at Casey Station are one order of magnitude higher than that for fast ice samples collected during austral summer 2000/01 at Terra Nova Bay in the Ross Sea (Grotti et al., 2005). This large difference is mainly due to the high basal ice Chl *a* values at Casey compared to other sea ice studies (Table 5.2). However, under-ice seawater shows similar ranges for all studies, with only marginally higher values observed during the Casey time series (Table 5.2).

Table 5.2: Comparison of snow, sea ice and under-ice seawater Chl *a*, POC, pFe, dFe, TDFe and plFe for all known studies to date (see references within).

	location	season	reference	Chl *a* µg/L	TDFe nmol/L	dFe nmol/L	plFe nmol/L	pFe nmol/L	POC µg C/L
snow									
	East Antarctic fast ice	spring	this study	n/a	9.59-46.74	0.89-7.10	8.70-39.7	2.30-101	na
	East Antarctic pack ice	winter/spring	van der Merwe et al.(2009,in Press)	n/a	0.70-6.85	0.21-1.14	0.49-6.42	1.09-11.6	23.59-105
	Weddel pack ice	spring/summer	Lannuzel et al., 2008	n/a	7.80-22.30	0.70-3.20	5.30-19.1	7.80-13.8	na
	East Antarctic pack ice	winter/spring	Lannuzel et al., 2007	n/a	1.83-23.66	0.97-6.47	0.12-18.3	2.13-14.8	73.00-155
	East Antarctic land/sea ice	summer	Edwards and Sedwick, 2001	n/a	1.2-31.7	n/a	n/a	n/a	n/a
sea ice									
	East Antarctic fast ice	spring	this study	<dl-248	33.8-4240	2.11-81.0	30.87-4160	40.39-6830	153-25200
	East Antarctic pack ice	winter/spring	van der Merwe et al.(2009,in Press)	0.00-17.4	1.17-378	0.23-14.4	0.71-377	0.86-213	38.6-3310
	Weddel pack ice	spring/summer	Lannuzel et al., 2008	0.08-26.5	2.30-97.8	0.70-36.8	1.50-61.0	2.30-141	139-5640
	East Antarctic pack ice	winter/spring	Lannuzel et al., 2007	0.04-34.3	3.27-112	2.64-26.0	<dl-85.5	<dl-96.6	352-4780
	Ross Sea land-fast ice	summer	Grotti et al., 2005	0.3-34.2	n/a	1.07-5.98	n/a	26-1160	n/a
under-ice seawater									
	East Antarctic fast ice	spring	this study	<dl-0.60	11.9-47.8	1.47-3.69	9.08-46.3	11.45-59.5	18.2-93.3
	East Antarctic pack ice	winter/spring	van der Merwe et al.(2009,in Press)	0.01-0.09	0.41-7.79	0.14-2.60	<dl-7.40	0.05-2.88	14.4-91.2
	Weddel pack ice	spring/summer	Lannuzel et al., 2008	0.03-0.21	0.50-4.10	0.70-1.70	<dl-2.90	0.40-4.00	<dl-162
	East Antarctic pack ice	winter/spring	Lannuzel et al., 2007	0.02-0.10	1.24-3.82	1.07-4.50	<dl-1.67	<dl-4.36	27.7-116
	Ross Sea land-fast ice	summer	Grotti et al., 2001	n/a	n/a	0.7-4.1	n/a	28.1-36.5	n/a

The ranges observed for POC in fast ice are one order of magnitude higher than in pack ice samples collected in the East Antarctic (van der Merwe et al., in Press) and Western Weddell Sea sector (Lannuzel et al., 2008), especially at the ice-water interface (Table 5.2). This large

difference is due mainly to the abundant algal community thriving in the lowermost 10 cm of the ice cover. However, under-ice seawater shows similar POC ranges for both fast and pack ice studies.

Similar to Chl *a* and POC, the concentration ranges observed for TDFe, PFe and PLFe in sea ice and seawater from the Casey study are one to two orders of magnitude higher than for pack ice samples in the East Antarctic and Western Weddell Sea sector, especially at the ice-water interface. However, unlike Chl *a* ,POC, TDFe, PFe and PLFe, the concentration ranges observed for dFe in coastal sea ice and seawater from the Casey study are similar to other sea ice studies (Table 5.2). This demonstrates that most the Fe found in coastal sea ice is associated with biogenic or lithogenic particles.

5.4.8. Seawater Fe concentrations and fluxes

Seawater Fe measurements were made at four depths: 0, 5, 10 and 15 m. Although not significantly different, the mean dFe concentrations were slightly lower at the surface than at depth with concentrations starting at 2.0 ± 0.44 nM at 0 m and increasing consistently to 2.9 ± 0.54 nM at 15 m depth, approximately an order of magnitude lower than the brine-volume-normalised SI5 dFe concentration. Interestingly, these values are within the same order of magnitude as some of the surface values observed during a pack ice study tens -hundreds of kilometres from the coast (van der Merwe et al., in Press). The consistency of the observed concentrations in dFe, regardless of the proximity to Fe sources such as the continental shelf and coast around Antarctica, may indicate a dFe limit for seawater, possibly imposed by the kinetics of Fe in seawater (i.e. the rapid utilisation and conversion to the biogenic particulate fraction including Exopolysaccharide particle scavenging coupled with the short residence time of the dFe fraction in oxygen rich sea water), although further investigation is required to confirm this.

For the TDFe fraction, we observed a continual increase in concentration in the surface seawater over the first 4 stations (SD 14, 17, 20 and 23). On SD 26, we see a decrease to 14 nM of TDFe, likely resulting from reduced input from the melting sea ice above due to steady (rather than increasing) brine volume fractions in the sea ice. This is most evident in SI2 and is likely driven by the cooling of air temperature between SD 18 and 24. During the final station we observed a rapid increase to 48 nM TDFe in seawater as a result of the highest air temperatures recorded and associated brine volume fraction (appendix table). Thus, it is apparent that the air temperature is controlling the ice melt and associated TDFe flux into the underlying sea water, which in this case is primarily in the particulate form. Similarly, the mean TDFe concentration over the whole water column shows an overall increase between the first and last stations of 26 nM (appendix table).

To determine if the sea ice alone contains enough TDFe to account for the 26 nM flux into seawater, we estimated the absolute TDFe in sea ice by taking the difference between the initial and final amount of TDFe in each sea ice section. Linear interpolation with ice depth then enabled an estimate of the TDFe flux from the sea ice into the seawater during the time series which equalled 419 μmol/m^2. This flux estimate averaged over the water column below (melted volume:volume) equalled 28 nM. Thus, the TDFe flux from the overlying sea ice can entirely explain the observed enrichment in the underlying 16 m of sea water. The same calculation for the dFe fraction resulted in a flux estimate of 25 μmol/m^2 released into the water column during the study period. This dFe flux averaged over the 16 m water column results in an enrichment of 1.6 nmol/L and thus does not completely explain the observed enrichment.

The TDFe flux estimate equates to 419 μmol /m^2 of similar coastal fast ice during the study period (i.e. 28 days). Thus, the TDFe flux observed was an order of magnitude higher than

during a 31 day study period in pack ice in the Western Weddel Sea (Lannuzel et al., 2008). Conversely, the dFe fraction was only twice that observed during Lannuzel et al (2008). Although Lannuzel et al (2008) sampled later in the season (November 29 – December 30) and therefore may have missed some of the initial Fe stock, our result indicates the potential of coastal fast ice as a significant TDFe reservoir. The similar dFe flux and vastly different TDFe flux observed between these two studies indicates, either, some controlling factor on the concentration of dFe and not TDFe, and/or that the sources of these two fractions are independent which has been suggested by prior research (Grotti et al., 2005; Lannuzel et al., 2008; Lannuzel et al., 2010; van der Merwe et al., in Press). A likely explanation is that the source is primarily in the particulate fraction (from sediment derived deep water) and this is only converted to the dissolved fraction upon *in situ* biogenic and photooxidative transformations and remineralisation.

Although there is growing evidence that sea ice entrained Fe may be one of the most bioavailable forms due to abundant organic complexation coupled with photo-oxidation either in situ or upon release into strongly stratified melt waters (Kim et al., 2010; Rijkenberg et al., 2008; Steigenberger et al., 2009; Tagliabue et al., 2009b), much of this Fe will be supplied in the particulate form when released from melting sea ice, and therefore, not readily available for phytoplankton uptake. Thus, the majority of this Fe will not be delivered to the Fe limited waters further off shore without significant heterotrophic remineralisation and photooxidation to keep it in solution. However, it is possible that regional circulation patterns within the water column could allow the northward movement of this Fe enriched fast ice and associated sea water, past the Antarctic Divergence via diversions in the East Wind Drift that carry ice northward (Worby et al., 1998). These divergences have been observed within the vicinity of the study site at 95 and 130˚ E and may supply large quantities of Fe enriched seawater northwards.

Thus, and with the above caveat in mind, if this amount of Fe was delivered into typical Fe limited Southern Ocean surface waters (which often have ~0.1 nmol L^{-1} ambient dFe concentration in summer, (Bowie et al., 2001)) it is sufficient to raise 419 m^3 of sea water by 1 nmol L^{-1} per m^2 of similar coastal sea ice thereby typically alleviating limitation.

5.5. Conclusion

We conducted a series of physical and biogeochemical observations at a coastal fast ice station in a period of rapid warming and associated ice melt during late austral spring. The air temperature was clearly associated with changes in brine volume fraction. This was particularly evident within the upper interior ice, which was insulated from rapid changes from above and below. Macronutrient profiles revealed the nitrate deficient state of the interior ice; this is most obvious in the brine concentrations which show a large excess of silicate and a deficit of nitrate. In the basal ice, relative to sea water, nitrate and silicate were drawn down through time, but due to resupply from below, most likely did not lead to a limiting condition. POC and Chl *a* showed a degree of variability through the time series, reflecting inter-core heterogeneity, difficulties of complete sample homogenisation and rapid melting and ice mass loss in the skeletal layer at the ice water interface. Dissolved Fe is highly diffuse and readily transferred from the surface/interior to the basal sea ice layers as the ice melting progressed. In contrast, pFe did not show this clear decreasing trend and correlated with POC and Chl *a* distributions. Indeed, the factor analysis revealed that 53% of the total variance of all the variables could be accounted for by one factor most closely correlated with POC. Thus, POC and all fractions of Fe measured were closely correlated. Furthermore, the macronutrients (particularly phosphate and nitrate) were distinct (factor 2, 27.6 %), most likely due to active drawdown by the sea ice algal assemblage. The non-refractory plFe fraction did decrease through time in most sea ice sections and was deposited into the underlying seawater. Using TDFe concentration, we calculated the

decrease in sea ice entrained Fe through time as the melting progressed. This deficit in Fe was released into the underlying water column and can completely explain the seawater enrichment observed. Over the 28 days of sampling, two distinct mean-air-temperature warming events were observed of -12.1 to -1.3 ˚C and then -6.4 to 0.8 ˚C. This resulted in the release of 419 µmol TDFe and 29 µmol dFe per m^2 of sea ice from this coastal fast ice station into the underlying water column. This TDFe enrichment is an order of magnitude higher and the dFe is double prior observations in pack ice in the Western Weddell Sea and indicates the potential of coastal fast ice as a significant Fe reservoir. Given the trace quantities of Fe required by typical Antarctic diatoms to bloom, this represents a fertilisation potential for 419 m^3 of Fe limited surface Southern Ocean seawater with TDFe and 29 m^3 with dFe, per m^2 of similar coastal fast ice.

5.6. Acknowledgments

We gratefully acknowledge the management, laboratory manager and support staff at Casey Station (Australia). We would like to thank Andy Cianchi, Simon Cross and Mick Stapleton for field support to gain access to the sampling site. This work was partially funded by the Australian Government's Cooperative Research Centres Program through the Antarctic Climate and Ecosystems Cooperative Research Centre (ACE CRC). This project was sponsored by an Australian Antarctic Science grant (#3026). We would like to thank Dr Ashley Townsend and the Central Science Laboratory (CSL) at the University of Tasmania for invaluable mentoring and support with the ICP-MS analyses. Total nitrogen, carbon and hydrogen was determined by Dr Thomas Rodemann at the Central Science Laboratory, University of Tasmania. The analysis for macronutrients was made by the CSIRO Hydrochemistry team, Hobart.

5.7. Appendix table

		pFe (nM)	TDFe (nM)	dFe (nM)	pIFe (nM)	PON (ug/L)	POC (ug/L)	POH (ug/L)	Chl a	sal	ice temp	vb/v (%)	mean daily air temp	Max daily air temp
STN1	SNOW	12	29	4	25								-5.1	-2.3
	B-	119	126	33	93	95.9	760.6	887.2	0.15	68.4			-5.1	-2.3
	B+	51	30	8	23	37.8	297.0	211.6	0.17	41.9			-5.1	-2.3
	SI1	126	134	10	124	28.6	252.0	62.7	0.13		-4.4		-5.1	-2.3
	SI2	378	882	24	656	79.3	813.6	122.3	0.12	5.9	-3.1	9.3	-5.1	-2.3
	SI3	1250	1153	27	1126	27.8	225.5	59.2	1.03	4.9	-2.22	10.8	-5.1	-2.3
	SI4	949	1001	50	950	85.1	860.3	200.4	8.95	5.9	-0.86	39.9	-5.1	-2.3
	SI5	8828	4240	81	4159	1857.6	11195.8	2828.4	182.61	11.2	-1.3	46.1	-5.1	-2.3
	SW0					1.9	71.9	223.8	0.55				-5.1	-2.3
	SW5	19	18	2	16	1.0	69.8	467.5	0.01	33.9			-5.1	-2.3
	SW10	15	18	4	14					33			-5.1	-2.3
	SW15												-5.1	-2.3
STN2	SNOW	64	19	3	16								-5.5	-1.0
	B-	130	132	35	97	104.3	748.4	482.7	0.10	54.5			-5.5	-1.0
	B+	57	67	18	48	78.5	543.4	243.3	0.48	65.3			-5.5	-1.0
	SI1	57	53	4	49	39.5	287.9	70.1	0.19	1.7	-5.6	1.5	-5.5	-1.0
	SI2	188	139	10	129	30.3	226.3	45.7	0.07	4.5	-3.92	5.7	-5.5	-1.0
	SI3	813	392	10	382	29.3	204.9	72.1	0.72	4.4	-2.9	7.4	-5.5	-1.0
	SI4	551	463	12	451	75.4	750.3	177.1	5.87	6.1	-1.6	19.3	-5.5	-1.0
	SI5	2165	2857	38	2818	3533.1	25175.6	7126.4	495.24	12.1	-1.3	50	-5.5	-1.0
	SW0	10	8	2	6	8.3	94.5	158.5	1.36	33.7			-5.5	-1.0
	SW5	11	12	3	9	0.1	31.8	166.1	0.06	34.3			-5.5	-1.0
	SW10	23	20	4	16	8.1	23.1	126.2	0.11	33.8			-5.5	-1.0
	SW15												-5.5	-1.0
STN3	SNOW	33	41	3	38								-1.3	-0.1
	B-	43	87	29	37	94.5	873.2	325.0	0.44	57.1			-1.3	-0.1
	B+	34	47	7	40	56.8	403.4	172.8	0.29	52.4			-1.3	-0.1
	SI1	63	40	5	35	60.3	414.2	56.8	0.65	5.5	-2.5	10.7	-1.3	-0.1
	SI2	175	304	3	301	56.8	398.7	73.8	0.15	4.8	-2.62	8.9	-1.3	-0.1
	SI3	836	590	10	580	42.3	303.6	104.2	0.44	4	-2.66	7.3	-1.3	-0.1
	SI4	489	860	21	839	109.8	1129.2	543.9	8.41	6.4	-1.74	18.5	-1.3	-0.1
	SI5	3520	2458	32	2426	1448.2	10786.6	5853.4	162.40	11.2	-1.8	31.6	-1.3	-0.1
	SW0	16	11	2	10	0.7	39.2	161.5	0.09	33.9			-1.3	-0.1
	SW5	19	21	2	18	0.4	44.9	201.3	0.10	35.4			-1.3	-0.1
	SW10	14	24	4	20	0.2	36.3	185.8	0.07	33.7			-1.3	-0.1
	SW15	24	19	3	16					33			-1.3	-0.1
STN4	SNOW	52	11	2	9								-3.6	0.2
	B-	58	94	20	74	78.0	588.4	317.4	0.43	46.9			-3.6	0.2
	B+	38	69	12	58	55.5	406.7	211.1	0.42	39.6			-3.6	0.2
	SI1	40	41	4	37	14.9	152.6	40.7	0.00	1.9	-4.3	2.2	-3.6	0.2
	SI2	738	512	13	499	68.9	475.6	127.5	0.41	5.2	-2.34	10.9	-3.6	0.2
	SI3	1515	914	6	909	34.2	315.4	102.2	0.16	3.6	-1.96	9	-3.6	0.2
	SI4	760	791	15	776	121.0	950.8	481.9	4.34	6.6	-1.52	22.2	-3.6	0.2
	SI5	2152	2155	17	2138	1902.3	15417.8	8389.5	253.60	12.3	-1.7	37.2	-3.6	0.2
	SW0	21	15	2	12	3.1	52.5	156.9	1.09	33.7			-3.6	0.2
	SW5	21	17	2	14	1.3	55.1	176.3	0.07	33.6			-3.6	0.2
	SW10	20	15	2	13	0.4	35.9	192.7	0.01	33.3			-3.6	0.2
	SW15	43	46	3	43					33			-3.6	0.2
STN5	SNOW	101	47	7	40								-6.1	-3.7
	B-	117	109	0	109	69.4	665.7	322.1	0.13	38			-6.1	-3.7
	B+	73	63	5	58	47.2	391.7	235.3	0.40	35.1			-6.1	-3.7
	SI1	80	34	3	31	49.5	326.7	61.5	0.11	2.9	-5.2	2.8	-6.1	-3.7
	SI2	662	316	3	312	45.0	336.7	97.4	0.10	5.2	-2.22	11.5	-6.1	-3.7
	SI3	1285	1601	4	1597	34.3	267.1	100.5	0.10	4	-1.76	11.3	-6.1	-3.7
	SI4	461	397	11	386	67.1	726.6	588.0	1.08	5.9	-1.52	19.8	-6.1	-3.7
	SI5	3796	2357	22	2335	1594.5	12549.9	8656.8	189.00	11.5	-1.64	36.1	-6.1	-3.7
	SW0	33	27	3	25	1.1	93.3	259.7	0.05	33.4			-6.1	-3.7
	SW5	25	16	3	13	0.7	18.2	174.7	0.08	32.9			-6.1	-3.7
	SW10	31	24	2	22	0.7	32.8	148.0	0.06	33.5			-6.1	-3.7
	SW15	22	29	3	26					33			-6.1	-3.7
STN6	SNOW	79	21	1	20								-3.5	-0.1
	B-	170	141	8	133	92.0	657.7	216.9	0.28	36.6			-3.5	-0.1
	B+	67	56	3	53	31.8	271.7	155.8	0.71	34.1			-3.5	-0.1
	SI1	215	192	4	189	44.8	287.1	55.3	0.00	3.5	-2.8	6.1	-3.5	-0.1
	SI2	129	100	5	95	30.9	267.9	75.3	0.07	4.9	-2.12	11.4	-3.5	-0.1
	SI3	1298	1036	8	1027	42.1	332.2	115.5	0.12	3.8	-1.78	10.6	-3.5	-0.1
	SI4	489	476	23	453	69.1	794.7	450.0	1.01	5.8	-1.51	19.6	-3.5	-0.1
	SI5	3875	2258	28	2231	1441.2	12530.7	7150.7	134.00	11.1	-1.57	36.6	-3.5	-0.1
	SW0	18	13	2	11	4.2	75.7	215.1	1.21	33.8			-3.5	-0.1
	SW5	18	13	2	11	1.9	24.6	176.2	0.04	33.7			-3.5	-0.1
	SW10	21	20	2	18	1.4	26.3	133.7	0.04	33.4			-3.5	-0.1
	SW15	24	17	2	14					33			-3.5	-0.1
STN7	SNOW	2	10	1	9								0.2	2.2
	B-	103	105	5	100	30.7	202.0	113.9	0.10	33.2			0.2	2.2
	B+	85	128	4	124	69.7	487.1	145.5	0.43	31.4			0.2	2.2
	SI1	236	226	3	222	41.7	264.6	99.9	0.08	1.4	-1.4	5.1	0.2	2.2
	SI2	955	418	2	416	43.8	330.4	86.6	0.06	4.9	-1.68	14.6	0.2	2.2
	SI3	1083	782	5	777	37.3	299.0	82.8	0.12	4.1	-1.58	13.1	0.2	2.2
	SI4	348	449	8	441	75.4	790.5	874.5	1.47	6.4	-1.58	20.6	0.2	2.2
	SI5	2498	1504	21	1484	2097.8	18501.0	14483.4	231.00	12.6	-1.7	38.1	0.2	2.2
	SW0	50	48	1	46	1.9	27.4	291.4	0.27	33.7			0.2	2.2
	SW5	54	42	3	39	1.4	26.7	138.7	0.11	33.4			0.2	2.2
	SW10	60	44	2	42	1.4	22.7	258.2	0.02	33.6			0.2	2.2
	SW15	50	42	4	38	1.0	62.9	444.3	0.01	33.5			0.2	2.2

6. Global Summary and Future Work

This thesis has produced three peer-reviewed publications which have been or are to be published in high impact journals. Two articles based on the Sea Ice Physics and Ecosystem eXperiment (SIPEX) were published by van der Merwe et al (Accepted; 2009) (Chapters 3 and 4), with a third based on a physical and biogeochemical time series study at Casey Station (Australian Antarctic Territory) (van der Merwe et al., submitted; Chapter 5).

SIPEX was a research cruise in the region between the 110˚ – 130˚ E meridians off East Antarctica during austral spring (September and October 2007). Nine stations were surveyed that consisted of both land fast and pack ice, allowing a direct comparison of the ice types. Although this was not strictly a temporal study, as many of the sites were separated by hundreds of kilometres, the authors observed a significant change in average air temperature, sea ice temperature and brine volume fraction between the first three sampled sites and the last three sampled sites. Chapter 3 focused on dissolved iron (Fe) and its relationship to other physical and biogeochemical variables. Apparent Fe (i.e. dissolved Fe × brine volume fraction) together with estimates of cellular carbon-to-Fe ratios indicated that the sea ice algae were not limited by the micronutrient Fe, and that the availability of dissolved macronutrients silicate and nitrate were likely limiting production within the sea ice. However, the growth of phytoplankton in under ice seawater may have been limited by the availability of dissolved Fe, as the concentrations at this early stage of the melting season were quite low (range <0.19 – 2.6 nM, mean 0.63 nM). A significant inverse correlation ($R = -.458$, $P > 0.05$) was observed between Chl a and apparent dissolved Fe and the authors suggested that it implied active draw-down of the dissolved Fe fraction by the sea ice biota. However this result included some fraction of

dissolved Fe was lost to the water column through brine drainage, a quantity that is difficult to directly measure.

In Chapter 4, a more focused study was performed with a particular emphasis on the size fractionation of Fe between pack and land fast ice in samples also taken from the SIPEX expedition. Particulate Fe within the basal ice at the fast ice station was 31 × higher than in the pack ice mean. The underlying seawater at this site also had the highest pFe : dFe ratio. Furthermore, this basal ice pFe enrichment was only observed with a strong acid digestion treatment (involving concentrated acids HF, HCl and HNO_3 at 95 ^{o}C for 12 h; "pFe") and was not observed with a milder acid treatment (HCl at pH 1.8 for >6 months; "plFe"). Therefore, it was concluded that the pFe observed in the basal ice of the fast ice station was highly refractory in nature, and therefore most likely lithogenic material of sedimentary origin. This was confirmed by the high particulate Al and Mn concentrations in basal ice at the fast ice station compared to pack ice (Lannuzel et al., accepted). Conversely, the basal ice plFe at the pack ice stations was always comparable with the pFe indicating the easily exchangeable nature of this fraction.

An interesting finding that has been alluded to in both Grotti et al (2001) and Lannuzel et al (2008), without a full discussion of the implications, is that there seems to be a temporal decoupling between the release of the dissolved and particulate Fe fractions during the spring melt of sea ice. In Chapter 4 we observed high brine dFe concentrations relative to the associated sea ice and conversely, the brines contained relatively little pFe compared to the associated sea ice. Sampling brines with the sack hole method (drilling a hole part way through the sea ice and waiting for the brine to infiltrate) is indicative of natural brine drainage. The diffuse nature of the dFe fraction and the attached nature of the pFe fraction suggests that as sea ice becomes more permeable during the spring melt we would see a preferential release of dFe

first into the water column over the course of approximately 10 or more days (the duration depending on local temperature regimes, ice thickness and Fe distributions throughout the core profile) and then secondly a release of pFe as physical melting releases the larger aggregates from the ice.

Interestingly, Grotti et al (2001) observed surface particulate enrichment approximately 10 days before they observed surface dissolved Fe enrichment. The authors suggested that the particulate enrichment was from the melting sea ice but little time was spent discussing the absence of a dissolved Fe enrichment beforehand. Could the particulate enrichment have been derived from direct resuspension of sediments? Could the dissolved enrichment have been so efficiently converted to the biogenic particulate fraction that it was not observed in the dissolved fraction any more? Could the temporal resolution of one sampling site every ~15 days have missed some information? Further research is required to answer these questions more fully, but one agreed conclusion between these independent studies is that the release of the particulate and dissolved fraction may operate independently. This multi stage release would result in enriched water column concentrations over a sustained time frame. Due to the short residence time of Fe (soluble Fe and dFe in particular) in seawater, this would give phytoplankton more time to make efficient use of what Fe is available, before it is converted to less bioavailable particulate fractions and lost to depth.

In Chapter 5, we conducted a series of physical and biogeochemical observations at a coastal fast ice site off Casey Station in a period of rapid warming and associated ice melt during late austral spring (November 4 – December 2, 2010). We found that the ambient air temperature (primarily driven by local wind patterns) was clearly associated with large changes in brine volume fraction. This was particularly evident at sea ice section 2 (30-36 cm deep), which was thermally insulated from rapid changes from above and below. Macronutrient profiles revealed

the nitrate deficient state of the upper sea ice sections 1-4. This was most obvious in the brine concentrations which slowed a large excess of silicate and a deficit of nitrate. In the basal ice (SI5), relative to sea water, nitrate and silicate were drawn-down through time, but due to resupply from below, most likely did not lead to limiting conditions. Particulate organic carbon (POC) and Chl *a* fluctuated from one station to the next reflecting both the spatial heterogeneity, difficulties of complete sample homogenisation of an organic-rich media, and rapid melting and ice mass loss in the skeletal layer at the ice water interface.

Dissolved Fe was highly diffuse and readily transferred from the surface/interior to the bottom sea ice layers as the ice melting progressed. In contrast, pFe did not show this clear decreasing trend and correlated well with the POC and Chl *a* distributions. Indeed, a factor analysis revealed that 53% of the total variance of all the variables could be accounted for by one component most closely correlated with POC. Thus POC and all fractions of Fe measured were closely correlated. Furthermore, the macronutrients, in particularly phosphate and nitrate, were closely correlated to a separate component (component 2, 27.6 %), most likely due to active drawdown by the sea ice algal assemblage. The non-refractory plFe fraction did decrease through time in most sea ice sections and was deposited into the underlying seawater.

Using TDFe concentrations, we calculated the decrease in sea ice entrained Fe through time as the melting progressed. This deficit in Fe was released into the underlying water column and can completely explain the seawater enrichment observed over our study period. Over the 28 days of sampling, two distinct mean-air-temperature warming events were observed of -12.1 to -1.3 ˚C and then -6.4 to 0.8 ˚C. This resulted in the release of 41.9 mol of TDFe into the underlying seawater per m^2 of sea ice from our coastal fast ice station. This is 3 orders of magnitude higher than that observed in pack ice in the Western Weddell Sea (Lannuzel et al., 2008), and indicates the potential of coastal fast ice as a significant Fe store. Uncertainties

remain on how bio-available the Fe supplied by fast ice is compared to pack ice. Given the trace quantities of Fe required by typical Antarctic diatoms to bloom, this represents a fertilisation potential for 42,000 m^3 of typical Fe-limited surface Southern Ocean seawater (0.1 nmol l^{-1}), per m^2 of similar coastal fast ice.

6.1. Discussion and Perspectives

6.1.1. Bioavailability of sea ice derived Fe

Fe bioavailability is difficult to predict and is a function of its physical and chemical form, and the uptake strategies employed by the various biota to access the micronutrient (Hassler & Schoemann, 2009). A reciprocal interaction exists between trace metals and phytoplankton in seawater. Trace metals such as iron may limit microbial activity and have a major role in determining species composition or taxonomy. Conversely, phytoplankton assist in regulating the concentrations and speciation of many trace metals micronutrients through the exudation of high affinity, relatively specific complexing ligands and through cell-surface reactions, in an attempt to facilitate its acquisition or for the storage of excess concentrations of these elements. The dissolved fraction (dFe) consists of inorganic and organic complexes, ranging in different sizes (from the free ionic or 'truly soluble' form through to small colloids < 0.2 μm) which can be mobilised through photo-reduction or thermal dissolution (Rich & Morel, 1990). In oxic sea water dFe is present as FeII and FeIII, with the former being the most bioavailable but the latter the more thermodynamically favoured and therefore abundant (Croot et al., 2004; Rich & Morel, 1990). In seawater, the vast majority of Fe (>99 %) is bound to strong organic ligands (Macrellis et al., 2001; Rue & Bruland, 1995) and it appears that most phytoplankton and bacteria can access this pool via a reduction step to free the bound Fe at the cell surface (Hopkinson & Morel, 2009; Maldonado & Price, 1999). Organic complexation of dFe also

generally increases its solubility by slowing the formation of Fe oxyhydroxides (Boye et al., 2001; de Baar & de Jong, 2001). Particulate Fe (pFe) is the result of coalescence of colloidal oxyhydroxides which will generally become more insoluble with time through the formation of more stable Fe oxides (Sunda, 2001) and thus, theoretically less bioavailable.

Various studies have shown the importance of organic chelators and ligands in modifying the availability of trace metals (Boye et al., 2001; Hassler & Schoemann, 2009). Some studies show that marine phytoplankton and bacteria produce exoploysaccharides and siderophores capable of acting as trace metal chelators (Hassler & Schoemann, 2009). Furthermore, phytoplankton photosynthesis in the sea ice zone can be increased by the addition of basal sea ice extracts (Apollonio et al., 2002) and this was suggested to be due to the organic ligands and trace metals "conditioning" the meltwaters. Steigenberger et al. (2009) showed the importance of acid polysaccharides and more generally, diatom exudates, in stabilising Fe(II), which is the more biologically available but least thermodynamically favoured species of Fe. They found that the production of superoxide (O_2^-) in the presence of diatom exudates and UV radiation had an overall reducing effect on Fe(III) and resulted in higher than expected Fe(II) concentrations. This finding was based on coastal waters where high organic loading is common.

Sea ice also has very high organic loading especially at the ice water interface (Chapter 3). Snow cover and rafting of sea ice will greatly reduce UV levels at the ice water interface, although a small but significant fraction of UV light (~1%) is available to perform photo-oxidation in situ. More importantly, and in contrast to resuspended sediments, when Fe is released from melting sea ice, it is released in conjunction with high levels of particulate and dissolved organics including high levels of acid polysaccharides. In fact, particulate acid polysaccharides were found in basal ice to be as high as 2690 - 3071 μg xanthan gum equivalent L^{-1} in Antarctic pack ice (Dumont et al., 2009; Chapter 3). The mean basal ice acid

polysaccharide concentration during SIPEX was 532 μg xanthan gum equivalent L^{-1} in the pack ice (excluding one fast ice station) and the mean basal ice total Fe concentration (dFe + pFe) in the same ice was 20 nM. This equates to approximately 475000 × more acid polysaccharide than total Fe. Likewise, in the under ice seawater (0 and 1 m depth), mean total Fe was 1.6 nM and mean particulate acid polysaccharide was 18.4 μg xanthan gum equivalent L^{-1} which equates to approximately 200000 × more acid polysaccharide than total Fe (w:w). Thus, this surplus of organics, released together with Fe into stratified surface waters and in conjunction with maximum solar radiation would likely result in more bioavailable Fe(II) than if an equal amount of Fe was supplied via sediment resuspension or aeolian dust. Thus, a simple calculation of Fe added vs productivity may not be applicable to the sea ice environment as the bioavailability of this source may be significantly higher than purely lithogenic sources supplied through other mechanisms. To date there are no direct measurements of Fe speciation in meltwaters from Antarctic sea ice and we suggest that urgent attention be paid to this area of research to better elucidate the bioavailability of this source and therefore, get a better understanding of the role of ice edge blooms in Antarctic productivity.

6.1.2. Incorporation of sea ice Fe in global biogeochemical models

Currently only one model takes into account sea ice derived Fe for the Southern Ocean (Lancelot et al., 2009), and no global biogeochemical models take into account the affect of sea ice derived Fe. Studies have attempted to elucidate the role of ligand complexed Fe in stimulating the observed phytoplankton blooms of the Ross Sea (Tagliabue & Arrigo, 2006), but only Lancelot et al (2009) actually include the spatial and temporal effect of sea ice on Fe distributions over the whole Southern Ocean. While sea ice is not a new source of Fe, it acts like a 'capacitor' and is a significant temporal storage of this important trace micronutrient element. The concentrating ability of sea ice means that Fe, which has a very short residence

time, can be retained near the surface waters throughout the entire winter season. Without sea ice, this Fe advected off the shelf or delivered as dust during winter would be lost to depth with little biologically mediated recycling or complexation due to light limitation at this time of the year. When this store is released in a pulse, it is done so together with a vast array of complexing organics and seeding algae and into well stratified waters during times of maximum solar radiation. This coincidental sequence of events presumably makes the supplied Fe highly bioavailable and efficiently recycled. Furthermore, the sea ice may act to affect the spatial distribution of Fe, as movement and break out of fast ice may transport significant quantities of Fe from the Fe-rich shelf waters to the Fe-deficient open ocean waters. During SIPEX, fast ice containing 10 × the dFe in the brines relative to the underlying sea water and 100 × the pFe in the basal ice relative to the underlying seawater was found approximately 75 km from the coast (Chapter 4). Considering that the sea water dFe concentration at this site was only 0.3 – 0.4 nM (at 0 m and 1 m depth) the sea ice would have provided Fe to Fe limited waters that would otherwise not allow significant production.

Arrigo et al (2008b) developed a model to determine Southern Ocean production based primarily on sea surface temperature, sea ice concentration and Chl a distributions (derived from SeaWiFS). With the caveat that SeaWiFS only determines Chl *a* from the surface waters, they noted that inter-annual variability in production was most closely related to changes in sea ice cover which the authors suggested was primarily the result of associated changes in photosynthetically active radiation (PAR) reaching the water column. However, the effect of Fe input from melting sea ice was not parameterised and therefore its effect in this correlation is unknown. Lancelot et al (2009) showed that the largest source of Fe to the Southern Ocean was sediment derived. Their modelling study suggested that the temporal storage of this sediment derived Fe in sea ice resulted in a net source of Fe to oceanic waters at the ice edge during the summer melt, so long as the area of its formation had significant amounts of dFe. Some areas,

having low seawater dFe concentrations at the time of formation resulted in very low fluxes during sea ice melting and help explain the highly heterogeneous distribution of Chl *a* around the receding ice edge as evidenced from SeaWiFS data (Lannuzel et al., 2010). They also found that sea ice formation during winter resulted in lowering of surface water dFe, and when averaged over the year actually resulted in a lowering of Chl *a* in certain regions of the Ross, Belingshausen and Amundsen Seas. Thus, the timing of sea ice formation as well as the sources of Fe available to entrain in the sea ice upon formation is fundamental to predicting marginal ice zone (MIZ) production.

If biogeochemical models are to truly constrain the spatial and temporal distribution of productivity in the Southern Ocean, then the incorporation of sea ice derived Fe must be included. Essential information on the relative bioavailability of this source should be a priority for future research to truly understand its impact in driving productivity in the Southern Ocean.

6.1.3. Climate change induced reduction of sea ice and implications for Southern Ocean productivity/carbon sequestration

Although it is difficult to measure over time scales relevant to climate, sea ice extent and thickness is predicted to decrease in the Antarctic with all "special report on emission scenarios" (SRES) in the latest intergovernmental panel on climate change (IPCC) report (IPCC, 2007). Climate models predict, on average, that Antarctic sea ice will, by the end of this century, reduce by 24% in extent and 34% in volume (Arzel et al., 2006). A decrease in Antarctic sea ice thickness would result in presumably lower Fe flux to the surface ocean as Fe does not accumulate solely at the ice water horizon, rather it is distributed throughout the full core profile and as such a lower volume would result in a lower overall Fe flux. Conversely, if thinning resulted in reduced solar attenuation through sea ice, then productivity may actually be

increased by alleviating some degree of light limitation. However, this may be unlikely due to the fact that precipitation is forecast to increase in Antarctica leading to more snow accumulation on sea ice and therefore increased light attenuation, possibly resulting in light limitation for the sea ice autotrophs. A contracted sea ice boundary associated with a reduction in overall extent would result in less Fe delivered to the marginal ice zone at maximum sea ice extent, which includes the waters most deficient in Fe (i.e. furthest from the continent) and therefore could result in an overall lowering of open Southern Ocean productivity and thus carbon drawdown.

Tagliabue and Arrigo (2006) noted that if warming trends resulted in increased stratification of the water column, then productivity may actually be increased regardless of Fe supply due to reduced light limitation. However, in a somewhat contradictory statement, Arrigo et al (2008b) suggested that production in the Southern Ocean may increase as a result of increased wind mixing resulting in increased nutrient supply. Unless significant regional differences occur, these two statements cannot both be true since increased wind mixing would result in decreased stratification. This highlights the significant uncertainty associated with attributing consequences resulting from global warming within this complex system. While overall Southern Ocean primary production may increase, MIZ primary production is predicted to decrease (Arrigo & Thomas, 2004). In addition, ice edge blooms provide ecological hotspots and are crucially important as foraging grounds for higher trophic levels. Thus, decrease in MIZ primary production may have a disproportionately strong effect on ecosystem health. Further work is required, particularly in the development of regional or global biogeochemical models that incorporate sea ice mediated Fe delivery to the high nutrient low chlorophyll Southern Ocean, and to place these models within a framework of a changing Earth's climate.

7. References

Alexander, V., & Niebauer, H. J. (1981). Oceanography of the Eastern Bering Sea Ice-Edge Zone in Spring. *Limnol. Oceanogr., 26*(6), 1111-1125.

Apollonio, S., Pennington, M., & Cota, G. F. (2002). Stimulation of phytoplankton photosynthesis by bottom-ice extracts in the Arctic. *Polar Biol., 25*(5), 350-354.

Archer, S. D., Leakey, R. J. G., Burkill, P. H., Sleigh, M. A., & Appleby, C. J. (1996). Microbial ecology of sea ice at a coastal Antarctic site: Community composition, biomass and temporal change. *Mar. Ecol. Prog. Ser., 135*(1-3), 179-195.

Arrigo, K. R., & Thomas, D. N. (2004). Large scale importance of sea ice biology in the Southern Ocean. *Antarct. Sci., 16*(4), 471-486.

Arrigo, K. R., van Dijken, G., & Long, M. (2008a). Coastal Southern Ocean: A strong anthropogenic CO2 sink. *Geophys. Res. Lett., 35*(21).

Arrigo, K. R., van Dijken, G. L., & Bushinsky, S. (2008b). Primary production in the Southern Ocean, 1997-2006. *J.Geophys. Res., [Oceans], 113*(8).

Arrigo, K. R., Worthen, D. L., Lizotte, M. P., Dixon, P., & Dieckmann, G. (1997). Primary production in Antarctic sea ice. *Science, 276*(5311), 394-397.

Arzel, O., Fichefet, T., & Goosse, H. (2006). Sea ice evolution over the 20th and 21st centuries as simulated by current AOGCMs. *Ocean Modelling, 12*(3-4), 401-415.

Becquevort, S., Dumont, I., Tison, J. L., Lannuzel, D., Sauvee, M. L., Chou, L., & Schoemann, V. (2009). Biogeochemistry and microbial community composition in sea ice and underlying seawater off East Antarctica during early spring. *Polar Biol.*, 1-17.

Blain, S., Queguiner, B., Armand, L., Belviso, S., Bombled, B., Bopp, L., et al. (2007). Effect of natural iron fertilization on carbon sequestration in the Southern Ocean. *Nature, 446*(7139), 1070-1074.

Bowie, A., Lannuzel, D., Remenyi, T., Wagener, T., Lam, P., Boyd, P., et al. (2009). Biogeochemical iron budgets of the Southern Ocean south of Australia: Decoupling of iron and nutrient cycles in the subantarctic zone by the summertime supply. *Global Biogeochem. Cycles, 23*(4), GB4034.

Bowie, A., & Lohan, M. C. (2009). Analysis of Iron in Seawater. In O. Wurl (Ed.), *Practical Guidelines for the Analysis of Seawater* (Vol. in press). Boca Raton (USA): Taylor and Francis.

Bowie, A., Townsend, A. T., Lannuzel, D., Remenyi, T., & van der Merwe, P. (2010). Modern sampling and analytical methods for the determination of trace elements in marine particulate material using magnetic sector ICP-MS. *Anal. Chim. Acta, 676*(1-2), 15-27.

Bowie, A. R., Maldonado, M. T., Frew, R. D., Croot, P. L., Achterberg, E. P., Mantoura, R. F. C., et al. (2001). The fate of added iron during a mesoscale fertilisation experiment in the Southern Ocean. *Deep-Sea Res. Part II Top. Stud. Oceanog., 48*(11-12), 2703-2743.

Bowie, A. R., Sedwick, P. N., & Worsfold, P. J. (2004). Analytical intercomparison between flow injection-chemiluminescence and flow injection-spectrophotometry for the determination of picomolar concentrations of Iron in seawater. *Limnology and Oceanography: Methods, 2*(FEB.), 42-54.

Boyd, P. W. (2007). Biogeochemistry: Iron findings. *Nature, 446*(7139), 989-991.

Boyd, P. W., Jickells, T., Law, C. S., Blain, S., Boyle, E. A., Buesseler, K. O., et al. (2007). Mesoscale iron enrichment experiments 1993-2005: Synthesis and future directions. *Science, 315*(5812), 612-617.

Boyd, P. W., Watson, A. J., Law, C. S., Abraham, E. R., Trull, T., Murdoch, R., et al. (2000). A mesoscale phytoplankton bloom in the polar Southern Ocean stimulated by iron fertilization. *Nature, 407*(6805), 695-702.

Boye, M., Van Den Berg, C. M. G., De Jong, J. T. M., Leach, H., Croot, P., & De Baar, H. J. W. (2001). Organic complexation of iron in the Southern Ocean. *Deep-Sea Res. Part I Oceanogr. Res. Pap., 48*(6), 1477-1497.

Brzezinski, M. A. (1985). THE Si:C:N RATIO OF MARINE DIATOMS: INTERSPECIFIC VARIABILITY AND THE EFFECT OF SOME ENVIRONMENTAL VARIABLES¹. *J. Phycol., 21*(3), 347-357.

Chisholm, S. W. (2000). Stirring times in the Southern Ocean. *Nature, 407*(6805), 685-687.

Constable, A. J., Nicol, S., & Strutton, P. G. (2003). Southern Ocean productivity in relation to spatial and temporal variation in the physical environment. *J. Geophys. Res., [Oceans], 108*(4).

Cox, G. F. N., & Weeks, W. F. (1988). Numerical simulations of the profile properties of undeformed first year sea ice during the growth season. *J. Geophys. Res., [Oceans], C10*, 12449-12460.

Croot, P. L., Andersson, K., Ozturk, M., & Turner, D. R. (2004). The distribution and speciation of iron along 6°E in the Southern Ocean. *Deep-Sea Res. Part II Top. Stud. Oceanog., 51*(22-24), 2857-2879.

Cullen, J. T., & Sherrell, R. M. (1999). Techniques for determination of trace metals in small samples of size-fractionated particulate matter: Phytoplankton metals off central California. *Mar. Chem., 67*(3-4), 233-247.

de Baar, H. J. W., & de Jong, J. (2001). Distribution, sources and sinks of iron in seawater. In D. R. Turner & K. A. Hunter (Eds.), *The Biogeochemistry of Iron in Seawater* (Vol. 7, pp. 123-253): IUPAC Series on Analytical and Physical Chemistry of Environmental Systems.

de Baar, H. J. W., de Jong, J. R. M., Bakker, D. C. E., Loscher, B. M., Veth, C., Bathmann, U., & Smetacek, V. (1995). Importance of iron for plankton blooms and carbon dioxide drawdown in the Southern Ocean. *Nature, 373*(6513), 412-415.

de Baar, H. J. W., Gerringa, L. J. A., Laan, P., & Timmermans, K. R. (2008). Efficiency of carbon removal per added iron in ocean iron fertilization. *Mar. Ecol. Prog. Ser., 364*, 269-282.

de Jong, J. T. M., Den Das, J., Bathmann, U., Stoll, M. H. C., Kattner, G., Nolting, R. F., & de Baar, H. J. W. (1998). Dissolved iron at subnanomolar levels in the Southern Ocean as determined by ship-board analysis. *Anal. Chim. Acta, 377*(2-3), 113-124.

Dubois, M., Gilles, K. A., Hamilton, J. K., Rebers, P. A., & Smith, F. (1956). Colorimetric method for determination of sugars and related substances. *Anal. Chem., 28*(3), 350-356.

Dumont, I., Schoemann, V., Lannuzel, D., Chou, L., Tison, J. L., & Becquevort, S. (2009). Distribution and characterization of dissolved and particulate organic matter in Antarctic pack ice. *Polar Biol.*, 1-18.

Edwards, R., & Sedwick, P. (2001). Iron in east Antarctic snow: Implications for atmospheric iron deposition and algal production in Antarctic waters. *Geophys. Res. Lett., 28*(20), 3907-3910.

Eicken, H. (2003). From the microscopic, to the macroscopic, to the regional scale: growth microstructure, and properties of sea ice. In D. N. Thomas & G. S. Dieckmann (Eds.), *Sea Ice - An introduction to its physics, chemistry, biology and geology.* (pp. 22-83). Oxford: Blackwell Science.

Eicken, H., & Lange, M. (1989). Development and properties of sea ice in the coastal regime of the southeastern Weddell Sea. *J. Geophys. Res., 94*, 8193-8206.

El-Sayed, S. Z., & Taguchi, S. (1981). Primary production and standing crop of phytoplankton along the ice-edge in the Weddell Sea. *Deep Sea Research Part A, Oceanographic Research Papers, 28*(9), 1017-1032.

Engel, A., & Passow, U. (2001). Carbon and nitrogen content of transparent exopolymer particles (TEP) in relation to their Alcian Blue adsorption. *Mar. Ecol. Prog. Ser., 219*, 1-10.

Fitch, D. T., & Moore, J. K. (2007). Wind speed influence on phytoplankton bloom dynamics in the Southern Ocean Marginal Ice Zone. *J.Geophys. Res., [Oceans], 112*(8).

Fitzwater, S. E., Johnson, K. S., Gordon, R. M., Coale, K. H., & Smith W.O, Jr. (2000). Trace metal concentrations in the Ross Sea and their relationship with nutrients and phytoplankton growth. *Deep-Sea Res. Part II Top. Stud. Oceanog., 47*(15-16), 3159-3179.

Garrison, D. L., Ackley, S. F., & Buck, K. R. (1983). A physical mechanism for establishing algal populations in frazil ice. *Nature, 306*(5941), 363-365.

Geider, R. J. (1999). Complex lessons of iron uptake. *Nature, 400*(6747), 815-816.

Geider, R. J., MacIntyre, H. L., & Kana, T. M. (1996). A dynamic model of photoadaptation in phytoplankton. *Limnol. Oceanogr., 41*(1), 1-15.

Gibson, J. A. E., & Trull, T. W. (1999). Annual cycle of fCO2 under sea-ice and in open water in Prydz Bay, East Antarctica. *Mar. Chem., 66*(3-4), 187-200.

Gledhill, M., Van Den Berg, C. M. G., Nolting, R. F., & Timmermans, K. R. (1998). Variability in the speciation of iron in the northern North Sea. *Mar. Chem., 59*(3-4), 283-300.

Golden, K. M., Ackley, S. F., & Lytle, V. I. (1998). The percolation phase transition in sea ice. *Science, 282*(5397), 2238-2241.

Gordon, R. M., Coale, K. H., & Johnson, K. S. (1997). Iron distributions in the equatorial Pacific: Implications for new production. *Limnol. Oceanogr., 42*(3), 419-431.

Grasshoff, K., Ehrhardt, M., & Kremling, K. (1983). Methods of sea water analysis. *Verlag Chem., 63-97*, 127-187.

Grotti, M., Soggia, F., Abelmoschi, M. L., Rivaro, P., Magi, E., & Frache, R. (2001). Temporal distribution of trace metals in Antarctic coastal waters. *Mar. Chem., 76*(3), 189-209.

Grotti, M., Soggia, F., Ianni, C., & Frache, R. (2005). Trace metals distributions in coastal sea ice of Terra Nova Bay, Ross Sea, Antarctica. *Antarct. Sci., 17*(2), 289-300.

Hales, B., van Geen, L., & Takahashi, T. (2004). High-frequency measurement of seawater chemistry: Flow-injection analysis of macronutrients. *Limnol. Oceanog., [Methods], 2*, 91-101.

Hassler, C. S., & Schoemann, V. (2009). Bioavailability of organically bound Fe to model phytoplankton of the Southern Ocean. *Biogeosciences Discussions, 6*(1), 1677-1712.

Holm-Hansen, O., Lorenzen, C. J., Holmes, R. W., & Strickland, J. D. H. (1965). Fluorometric determination of chlorophyll a. *J Cons Perm Int Explor Mer, 30*, 3-15.

Hopkinson, B. M., & Morel, F. M. M. (2009). The role of siderophores in iron acquisition by photosynthetic marine microorganisms. *Biometals, 22*(4), 659-669.

Hunter, K. A., & Boyd, P. W. (2007). Iron-binding ligands and their role in the ocean biogeochemistry of iron. *Environ. Chem., 4*(4), 221-232.

IPCC. (2007). Climate Change 2007: Synthesis Report. Contribution of Working Groups I, II and III to the Fourth Assessment Report of the Intergovernmental Panel on Climate Change. In P. Core Writing Team, R.K and Reisinger, A. (Ed.), (pp. 104). Geneva, Switzerland: IPCC.

Jeffries, M. O., & Adolphs, U. (1997). Early winter ice and snow thickness distribution, ice structure and development of the western Ross Sea pack ice between the ice edge and the Ross Ice Shelf. *Antarct. Sci., 9*(2), 188-200.

Johnson, K. S. (2001). Iron supply and demand in the upper ocean: Is extraterrestrial dust a significant source of bioavailable iron? *Global Biogeochem. Cycles, 15*(1), 61-63.

Kim, K., Choi, W., Hoffmann, M. R., Yoon, H. I., & Park, B. K. (2010). Photoreductive dissolution of iron oxides trapped in ice and its environmental implications. *Environ. Sci. Technol., 44*(11), 4142-4148.

Krembs, C., & Deming, J. W. (2008). The role of exopolymers in microbial adaptations to sea ice. In R. Margesin, F. Schinner, J. Marx, & C. Gerday (Eds.), *Psychrophiles: from Biodiversity to Biotechnology* (pp. 247-264). Berlin: Springer.

Krembs, C., Eicken, H., Junge, K., & Deming, J. W. (2002a). High concentrations of exopolymeric substances in Arctic winter sea ice: Implications for the polar ocean carbon cycle and cryoprotection of diatoms. *Deep-Sea Res. Part I Oceanogr. Res. Pap., 49*(12), 2163-2181.

Krembs, C., Gradinger, R., & Spindler, M. (2000). Implications of brine channel geometry and surface area for the interaction of sympagic organisms in Arctic sea ice. *J. Exp. Mar. Biol. Ecol., 243*(1), 55-80.

Krembs, C., Mock, T., & Gradinger, R. (2001). A mesocosm study of physical-biological interactions in artificial sea ice: Effects of brine channel surface evolution and brine movement on algal biomass. *Polar Biol., 24*(5), 356-364.

Krembs, C., Tuschling, K., & Juterzenka, K. V. (2002b). The topography of the ice-water interface - Its influence on the colonization of sea ice by algae. *Polar Biol., 25*(2), 106-117.

Lancelot, C., De Montety, A., Goosse, H., Becquevort, S., Schoemann, V., Pasquer, B., & Vancoppenolle, M. (2009). Spatial distribution of the iron supply to phytoplankton in the Southern Ocean: A model study. *Biogeosciences, 6*(12), 2861-2878.

Langway, C. C. (1958). Ice fabrics and the universal stage. *CRREL Technical, 62*.

Lannuzel, D., Bowie, A., van der Merwe, P., Townsend, A. T., & Schoemann, V. (accepted). Distribution of dissolved and particulate metals in Antarctic sea ice. *Mar. Chem.*

Lannuzel, D., De Jong, J., Schoemann, V., Trevena, A., Tison, J. L., & Chou, L. (2006). Development of a sampling and flow injection analysis technique for iron determination in the sea ice environment. *Anal. Chim. Acta, 556*(2), 476-483.

Lannuzel, D., Schoemann, V., de Jong, J., Chou, L., Delille, B., Becquevort, S., & Tison, J. L. (2008). Iron study during a time series in the western Weddell pack ice. *Mar. Chem., 108*(1-2), 85-95.

Lannuzel, D., Schoemann, V., de Jong, J., Pasquer, B., Masson, F., van der Merwe, P., et al. (2010). What controls the distribution of dissolved iron in Antarctic sea ice: spatial, seasonal or inter-annual variability? *J. Geophys. Res., [Biogeoscience], 115*(3), G03022.

Lannuzel, D., Schoemann, V., de Jong, J. T. M., Tison, J.-L., & Chou, L. (2007). Distribution and biogeochemical behaviour of iron in the East Antarctic sea-ice. *Mar. Chem., 106*(1-2 spec. iss.), 18-32.

Legendre, L., Ackley, S. F., Dieckmann, G. S., Gulliksen, B., Horner, R., Hoshiai, T., et al. (1992). Ecology of sea ice biota - 2. Global significance. *Polar Biol., 12*(3-4), 429-444.

Leventer, A. (2003). Particulate Flux from Sea Ice in Polar Waters. In D. N. Thomas & G. S. Dieckmann (Eds.), *Sea Ice: An introduction to its Physics, Chemistry, Biology and Geology*. Oxford: Blackwell publishing.

Loaec, M., Olier, R., & Guezennec, J. (1997). Uptake of lead, cadmium and zinc by a novel bacterial exopolysaccharide. *Water Res., 31*(5), 1171-1179.

Loscher, B. M., De Baar, H. J. W., De Jong, J., Veth, C., & Dehairs, F. (1997). The distribution of Fe in the Antartic Circumpolar Current. *Deep-Sea Res. Part II Top. Stud. Oceanog., 44*, 143-187.

Lowe, I. (1997). Antipodes : Core of controversy. *New Sci., 156*(2107), 58.

Macrellis, H. M., Trick, C. G., Rue, E. L., Smith, G., & Bruland, K. W. (2001). Collection and detection of natural iron-binding ligands from seawater. *Mar. Chem., 76*(3), 175-187.

Maldonado, M. T., & Price, N. M. (1999). Utilization of iron bound to strong organic ligands by plankton communities in the subarctic Pacific Ocean. *Deep-Sea Res. Part II Top. Stud. Oceanog., 46*(11-12), 2447-2473.

Mancuso Nichols, C., Lardiere, S. G., Bowman, J. P., Nichols, P. D., Gibson, J., & Guezennec, J. (2005a). Chemical characterization of exopolysaccharides from Antarctic marine bacteria. *Microb. Ecol., 49*(4), 578-589.

Mancuso Nichols, C. A., Garon, S., Bowman, J. P., Raguenes, G., & Guezennec, J. (2004). Production of exopolysaccharides by Antarctic marine bacterial isolates. *J. Appl. Microbiol., 96*(5), 1057-1066.

Mancuso Nichols, C. A., Guezennec, J., & Bowman, J. P. (2005b). Bacterial exopolysaccharides from extreme marine environments with special consideration of the Southern Ocean, sea ice, and deep-sea hydrothermal vents: A review. *Mar. Biotechnol., 7*(4), 253-271.

Martin, J. H. (1990). Glacial-interglacial CO2 change: the iron hypothesis. *Paleoceanography, 5*(1), 1-13.

Martin, J. H., Fitzwater, S. E., & Gordon, R. M. (1990a). Iron deficiency limits phytoplankton growth in Antarctic waters. *Global Biogeochem. Cycles, 4*(1), 5-12.

Martin, J. H., Gordon, R. M., & Fitzwater, S. E. (1990b). Iron in Antarctic waters. *Nature, 345*(6271), 156-158.

Martin, J. H., Gordon, R. M., & Fitzwater, S. E. (1991). The case for iron. *Limnology & Oceanography, 36*(8), 1793-1802.

McConville, M. J., Mitchell, C., & Wetherbee, R. (1985). Patterns of carbon assimilation in a microalgal community from annual sea ice, east Antarctica. *Polar Biol., 4*(3), 135-141.

McConville, M. J., & Wetherbee, R. (1983). THE BOTTOM-ICE MICROALGAL COMMUNITY FROM ANNUAL ICE IN THE INSHORE WATERS OF EAST ANTARCTICA. *J. Phycol., 19*(4), 431-439.

Meiners, K., Brinkmeyer, R., Granskog, M. A., & Lindfors, A. (2004). Abundance, size distribution and bacterial colonization of exopolymer particles in Antarctic sea ice (Bellingshausen Sea). *Aquat. Microb. Ecol., 35*(3), 283-296.

Meiners, K., Gradinger, R., Fehling, J., Civitarese, G., & Spindler, M. (2003). Vertical distribution of exopolymer particles in sea ice of the Fram Strait (Arctic) during autumn. *Mar. Ecol. Prog. Ser., 248*, 1-13.

Meiners, K., Norman, L., Granskog, M. A., Krell, A., Heil, P., & Thomas, D. (this volume). Physico-ecobiogeochemistry of East Antarctic pack ice during the winter spring transition. *Deep-Sea Res. Part II Top. Stud. Oceanog.*

Morillo Perez, J. A., Garcia-Ribera, R., Quesada, T., Aguilera, M., Ramos-Cormenzana, A., & Monteoliva-Sanchez, M. (2008). Biosorption of heavy metals by the exopolysaccharide produced by Paenibacillus jamilae. *World Journal of Microbiology and Biotechnology, 24*(11), 2699-2704.

Muñoz, R., Alvarez, M. T., Muñoz, A., Terrazas, E., Guieysse, B., & Mattiasson, B. (2006). Sequential removal of heavy metals ions and organic pollutants using an algal-bacterial consortium. *Chemosphere, 63*(6), 903-911.

Nicol, S., Bowie, A., Jarman, S., Lannuzel, D., Meiners, K. M., & van der Merwe, P. (2010). Southern Ocean iron fertilization by baleen whales and Antarctic krill. *Fish and Fisheries, 11*(2), 203-209.

Obata, H., Karatani, H., & Nakayama, E. (1993). Automated determination of iron in seawater by chelating resin concentration and chemiluminescence detection. *Anal. Chem., 65*(11), 1524-1528.

Passow, U., & Alldredge, A. L. (1995). A dye-binding assay for the spectrophotometric measurement of transparent exopolymer particles (TEP). *Limnol. Oceanogr., 40*(7), 1326-1335.

Qian, J., & Mopper, K. (1996). Automated High-Performance, High-Temperature Combustion Total Organic Carbon Analyzer. *Anal. Chem., 68*(18), 3090-3097.

Raiswell, R., Benning, L. G., Davidson, L., & Tranter, M. (2008a). Nanoparticulate bioavailable iron minerals in icebergs and glaciers. *Mineral. Mag., 72*(1), 345-348.

Raiswell, R., Benning, L. G., Tranter, M., & Tulaczyk, S. (2008b). Bioavailable iron in the Southern Ocean: The significance of the iceberg conveyor belt. *Geochem. Trans., 9*, article no. 7.

Raiswell, R., Tranter, M., Benning, L. G., Siegert, M., De'ath, R., Huybrechts, P., & Payne, T. (2006). Contributions from glacially derived sediment to the global iron (oxyhydr)oxide cycle: Implications for iron delivery to the oceans. *Geochim. Cosmochim. Acta, 70*(11), 2765-2780.

Redfield, A. C. (1958). The biological control of chemical factors in the environment. *Am. Sci., 46*, 205-221.

Rich, H. W., & Morel, F. M. M. (1990). Availability of well-defined iron colloids to the marine diatom Thalassiosira weissflogii. *Limnology & Oceanography, 35*(3), 652-662.

Riedel, A., Michel, C., & Gosselin, M. (2006). Seasonal study of sea-ice exopolymeric substances on the Mackenzie shelf: Implications for transport of sea-ice bacteria and algae. *Aquat. Microb. Ecol., 45*(2), 195-206.

Riedel, A., Michel, C., Gosselin, M., & LeBlanc, B. (2007). Enrichment of nutrients, exopolymeric substances and microorganisms in newly formed sea ice on the Mackenzie shelf. *Mar. Ecol. Prog. Ser., 342*, 55-67.

Rijkenberg, M. J. A., Gerringa, L. J. A., Timmermans, K. R., Fischer, A. C., Kroon, K. J., Buma, A. G. J., et al. (2008). Enhancement of the reactive iron pool by marine diatoms. *Mar. Chem., 109*(1-2), 29-44.

Rue, E. L., & Bruland, K. W. (1995). Complexation of iron(III) by natural organic ligands in the Central North Pacific as determined by a new competitive ligand equilibration/adsorptive cathodic stripping voltammetric method. *Mar. Chem., 50*(1-4), 117-138.

Russell, R. (2007). Windows to the Universe: Compare Images of Antarctic Sea Ice Extent Side-by-side. Retrieved from http://www.windows.ucar.edu/tour/link=/earth/polar/sea_ice/sea_ice_compare_south.html

Schoemann, V., De Jong, J. T. M., Lannuzel, D., Tison, J. L., Dellile, B., Chou, L., et al. (2008). Microbiological control on the cycling of Fe and its isotopes in Antarctic sea ice. *Geochim. Cosmochim. Acta, 72*(12), A837 Suppl. S.

Schoemann, V., Wollast, R., Chou, L., & Lancelot, C. (2001). Effects of photosynthesis on the accumulation of Mn and Fe by Phaeocystis colonies. *Limnol. Oceanogr., 46*(5), 1065-1076.

Scott, F. J., & Marchant, H. J. (Eds.). (2005). *Antarctic Marine Protists*. Canberra: Australian Biological Resources Study.

Sedwick, P. N., & Ditullio, G. R. (1997). Regulation of algal blooms in Antarctic shelf waters by the release of iron from melting sea ice. *Geophys. Res. Lett., 24*(20), 2515-2518.

Sedwick, P. N., DiTullio, G. R., & Mackey, D. J. (2000). Iron and manganese in the Ross Sea, Antarctica: Seasonal iron limitation in Antarctic shelf waters. *J.Geophys. Res., [Oceans], 105*(C5), 11321-11336.

Sedwick, P. N., Edwards, P. R., Mackey, D. J., Griffiths, F. B., & Parslow, J. S. (1997). Iron and manganese in surface waters of the Australian subantarctic region. *Deep-Sea Res. Part I Oceanogr. Res. Pap., 44*(7), 1239-1253.

Shanks, A. L., & Trent, J. D. (1980). Marine snow: sinking rates and potential role in vertical flux. *Deep-Sea Res. Part I Oceanogr. Res. Pap., 27*(2), 137-143.

Smith, K. L., Robison, B. H., Helly, J. J., Kaufmann, R. S., Ruhl, H. A., Shaw, T. J., et al. (2007). Free-drifting icebergs: Hot spots of chemical and biological enrichment in the Weddell Sea. *Science, 317*(5837), 478-482.

Smith, W. O., & Nelson, D. M. (1985). Phytoplankton bloom produced by a receding ice edge in the ross sea: Spatial coherence with the density field. *Science, 227*(4683), 163-166.

Steigenberger, S., Statham, P. J., Volker, C., & Passow, U. (2009). The role of polysaccharides and diatom exudates in the redox cycling of Fe and the photoproduction of hydrogen peroxide in coastal seawaters. *Biogeosciences, 7*(1), 109-119.

Sunda, W. G. (2001). Bioavailability and Bioaccumulation of Iron in the Sea. In D. R. Turner & K. H. hunter (Eds.), *The Biogeochemistry of Iron in Seawater* (Vol. 7, pp. 41-84): IUPAC Series on Analytical and Physical Chemistry of Environmental Systems.

Sunda, W. G. (2003). Bioavailability and Bioaccumulation of Iron in the Sea. In D. N. Thomas & G. S. Dieckmann (Eds.), *Sea Ice: An introduction to its Physics, Chemistry, Biology and Geology*: Blackwell publishing.

Tagliabue, A., & Arrigo, K. R. (2006). Processes governing the supply of iron to phytoplankton in stratified seas. *J.Geophys. Res., [Oceans], 111*(6), Article no. C06019.

Tagliabue, A., Bopp, L., & Aumont, O. (2009a). Evaluating the importance of atmospheric and sedimentary iron sources to Southern Ocean biogeochemistry. *Geophys. Res. Lett., 36*(13).

Tagliabue, A., Bopp, L., Aumont, O., & Arrigo, K. R. (2009b). Influence of light and temperature on the marine iron cycle: From theoretical to global modeling. *Global Biogeochem. Cycles, 23*(2).

Tagliabue, A., Bopp, L., Dutay, J. C., Bowie, A. R., Chever, F., Jean-Baptiste, P., et al. (2010). Hydrothermal contribution to the oceanic dissolved iron inventory. *Nat Geosci, 3*(4), 252-256.

Takahashi, T., Sutherland, S. C., Sweeney, C., Poisson, A., Metzl, N., Tilbrook, B., et al. (2002). Global sea-air CO_2 flux based on climatological surface ocean pCO_2, and seasonal biological and temperature effects. *Deep-Sea Res. Part II Top. Stud. Oceanog., 49*(9-10), 1601-1622.

Thomas, D. N., & Dieckmann, G. S. (2002). Antarctic Sea Ice--a Habitat for Extremophiles. *Science, 295*, 641-644.

Thomas, D. N., & Papadimitriou, S. (2003). Biogeochemistry of sea ice. In D. N. Thomas & G. S. Dieckmann (Eds.), *Sea Ice: An introduction to its Physics, Chemistry, Biology and Geology*. Oxford: Blackwell publishing.

Timmermans, K. R., Gerringa, L. J. A., De Baar, H. J. W., Van der Wagt, B., Veldhuis, M. J. W., De Jong, J. T. M., & Croot, P. L. (2001). Growth rates of large and small Southern Ocean diatoms in relation to availability of iron in natural seawater. *Limnol. Oceanogr., 46*(2), 260-266.

Timmermans, K. R., Van Der Wagt, B., & De Baar, H. J. W. (2004). Growth rates, half-saturation constants, and silicate, nitrate, and phosphate depletion in relation to iron availability of four large, open-ocean diatoms from the Southern Ocean. *Limnol. Oceanogr., 49*(6), 2141-2151.

Tison, J. L., Worby, A., Delille, B., Brabant, F., Papadimitriou, S., Thomas, D., et al. (2008). Temporal evolution of decaying summer first-year sea ice in the Western Weddell Sea, Antarctica. *Deep-Sea Res. Part II Top. Stud. Oceanog., 55*(8-9), 975-987.

Townsend, A. T. (2000). The accurate determination of the first row transition metals in water, urine, plant, tissue and rock samples by sector field ICP-MS. *J. Anal. At. Spectrom., 15*(4), 307-314.

Toyota, T., Kawamura, T., Ohshima, K. I., Shimoda, H., & Wakatsuchi, M. (2004). Thickness distribution, texture and stratigraphy, and a simple probabilistic model for dynamical thickening of sea ice in the southern Sea of Okhotsk. *J. Geophys. Res., [Oceans], 109*(6), C06001.

van den Berg, C. M. G. (1995). Evidence for organic complexation of iron in seawater. *Mar. Chem., 50*(1-4), 139-157.

van der Merwe, P., Lannuzel, D., Bowie, A., Mancuso Nichols, C., & Meiners, K. (Accepted). Iron fractionation in pack and fast ice in East Antarctica: temporal decoupling between

the release of dissolved and particulate iron during spring melt. *Deep-Sea Research Part II Oceanographic Research Papers*.

van der Merwe, P., Lannuzel, D., Bowie, A., Mancuso Nichols, C., & Meiners, K. (in Press). Iron fractionation in pack and fast ice in East Antarctica: temporal decoupling between the release of dissolved and particulate iron during spring melt. *Deep-Sea Res. Part II Top. Stud. Oceanog.*

van der Merwe, P., Lannuzel, D., Mancuso Nichols, C., Meiners, K., Heil, P., Norman, L., et al. (2009). Biogeochemical observations during the winter-spring transition in East Antarctic sea ice: evidence of iron and exopolysaccharide controls. *Mar. Chem., 115*, 163-175.

Vancoppenolle, M., Goosse, H., De Montety, A., Fichefet, T., Tremblay, B., & Tison, J. L. (2010). Modeling brine and nutrient dynamics in Antarctic sea ice: The case of dissolved silica. *J.Geophys. Res., [Oceans], 115*(2).

Wagener, T., Guieu, C., Losno, R., Bonnet, S., & Mahowald, N. (2008). Revisiting atmospheric dust export to the Southern Hemisphere ocean: Biogeochemical implications. *Global Biogeochem. Cycles, 22*(2).

Weinelt, M. (1996, 2006). Online Map Creation (OMC). Retrieved from http://www.aquarius.ifm-geomar.de

Weinelt, M. (2006). Online Map Creation (OMC). Retrieved from http://www.aquarius.ifm-geomar.de

Wells, M. L. (1998). A neglected dimension. *Nature, 391*(6667), 530-531.

Worby, A. P., Massom, R. A., Allison, I., Lytle, V. I., & Heil, P. (1998). East Antarctic Sea Ice: A review of its Structure, Properties and Drift. In M. O. Jeffries (Ed.), *Antarctic Sea Ice Properties, Processes and Variability* (Vol. 74, pp. 41-67): AGU Antarctic Research Series.